THE UNIVERSITY OF CALGARY

Seismic Modeling of Thrust Sheets in the Wildcat Hills Area, Southern Alberta Foothills

by

Eric Wesely Pearson

A THESIS

SUBMITTED TO THE FACULTY OF GRADUATE STUDIES

IN PARTIAL FULFILMENT OF THE REQUIREMENTS FOR THE

DEGREE OF MASTER OF SCIENCE

DEPARTMENT OF GEOLOGY AND GEOPHYSICS

CALGARY, ALBERTA

APRIL, 1997

ABSTRACT

Thrust sheets of Mississippian strata in the Wildcat Hills area, delineated using 3-dimensional (3-D) seismic data, form an imbricate thrust structure that varies along strike via displacement transfer between two faults. A 3-D numerical depth model of this structure allowed analysis of out-of-plane imaging effects on 2-dimensional (2-D) seismic data through ray-tracing. Synthetic 2-D seismic data collected in the dip direction display time structure errors (related to out-of-plane imaging) typically ranging between 5 and 10 ms (up to 30 ms) for the Top Mississippian horizon in the hangingwall of the structure. Similar analysis of data collected at 45° to the dip direction indicates typically higher time-structure errors (up to 50 ms). Out-of-plane reflections (up to 1000 m from the line) are common in these 2-D seismic data, but do not severely affect delineation of the hangingwall using dip-lines.

ACKNOWLEDGEMENTS

I would like to thank my supervisor, Don Lawton, for his guidance and support over the last three years, especially during the frantic final stages of thesis production. The Foothills Research Project supported this research with funds provided to the project by the Natural Sciences and Engineering Research Council of Canada and numerous industry sponsors. Canadian Hunter and Petrofina S.A. provided the Wildcat Hills 3-D data to the University of Calgary. Too many people were involved in the production of this thesis to list here, but I must thank Darren Foltinek and Henry Bland for their help with all the computer-related problems I discovered (or created), and Susan Collins at GX Technologies for her technical support of the modeling software. I thank my wife Krista for her patience through all of this and for supporting (or at least not questioning) my academic pursuits. Thanks also to my parents for all of their support throughout my academic career. Finally, I owe what remains of my sanity to my friends who made the stay here so enjoyable, you all know who you are. It's been an interesting few years, and I know I'll miss the place...eventually.

TABLE OF CONTENTS

LIST OF TABLES

LIST OF FIGURES

GLOSSARY OF TERMS

Allochthonous: Refers to material with a foreign origin, in this case rocks that have been transported tectonically from their place of origin.

Autochthonous: Refers to something formed where it is currently found, and in this case refers to rocks that have not been transported tectonically from their original location of deposition.

Automatic Gain Control: A process that uses the output amplitude of a signal to automatically control amplification.

Band-pass filter: In seismic data processing refers to a filter which preserves frequencies within the "pass band" and attenuates all other frequencies.

Carbonate rocks: Lithified sediments containing mainly carbonates of calcium and magnesium (i.e. limestone and dolomite), normally produced organically in situ.

CDP/CMP: Equivalent for horizontally-layered media, these terms (common depth or reflection point, and common midpoint) refer to the the midpoint between a source and a receiver. Multi-offset seismic data can be sorted to common midpoint (CMP), NMO-corrected, and stacked together (combined) to improve signal to noise ratios.

Clastic rock: A sedimentary rock composed mainly of fragments derived from pre-existing rocks and transported mechanically to the location of deposition (e.g. conglomerate, sandstone, or shale).

Detachment: or decollement; a surface separating independent styles of deformation above and below.

Diffraction: An event present on a seismic section, normally hyperbolic in character, produced by diffracted energy from a point source (discontinuity) in the subsurface. When properly migrated a simple diffraction will collapse to the point of origin for the diffracted energy.

Dip direction: Perpendicular to the strike direction, more specifically, orthogonal to the line-of-intersection between the dipping plane and the horizontal plane.

DMO (dip moveout): A seismic data processing scheme that, for dipping reflectors, attempts to correct for the fact that traces in the CMP stack do not have a common reflection point.

En echelon: An overlapping or staggered arrangement of geological features.

Fault cutoffs: Intersection of a horizon and a fault plane.

Fault displacement: The amount of relative movement of between two sides of a fault, measured in any chose direction. In this case displacement is measured in the dip direction, along the fault plane between fault cutoffs.

Flexural Slip: or bedding plane slip, describes the movement of strata along bedding planes during folding. The flexural slip structural restoration algorithm uses this principal to calculate the position of surfaces prior to deformation.

Footwall: The mass of rock below a dipping fault surface.

Foreland: A tectonically stable area adjacent to an orogenic belt toward which compressional structures propagate. A foreland basin may form in response to tectonic loading of the crust.

Hangingwall: The mass of rock above a dipping fault surface.

Interval velocity: Velocity value (or function) between two horizons in the subsurface.

Migration: As it refers to seismic data, is an inversion procedure that attempts to move reflections and diffractions to their true subsurface locations. Reflections deviate from their true subsurface locations in response to velocity variations and structural dip on the reflecting surface. Post-stack migration refers to those procedures which operate on a stacked section.

NMO (normal moveout): Describes the increase in reflection arrival time related to increasing distance between sources and a receivers (offset).

Normal fault: A fault on which the hangingwall appears to move down relative to the footwall.

Plunge: The inclination of a linear feature in the vertical plane. Plunge in this case refers to the inclination of the axis of a broad fold created in the hangingwall of the thrust faults.

Pull-up anomaly: Local uplift on a horizon related to the presence of a higher-velocity region above, which reduces two-way traveltime to this horizon.

Push-down anomaly: Negative time structure anomaly related to an overlying region of lower velocity strata, increasing two-way traveltime.

RMS velocity: The square root of the average of the squared velocities over a particular interval

Shot record: A seismic recording for a single shot, measured in a number of receivers.

Snell's Law: The relationshp that describes the change in direction of a wave as it crosses the boundary between two isotropic media.

Sonic log: A well log that measures seismic traveltime over a given distance (reciprocal velocity). The interval traveltimes are integrated to produce total traveltime, and reflection coefficients are convolved with a wavelet similar in character to an adjacent seismic line, producing a synthetic seismogram to correlate the well and seismic information.

Source-Receiver offset: Distance between a given source and receiver.

Stacked seismic data: A composite seismic section created by combining traces from different records in an effort to improve signal to noise ratios. In this study stacking refers specifically to combining the traces on common midpoint (CMP) gathers following normal moveout (NMO) correction.

Strike direction: The orientation of the line-of-intersection between the a dipping surface and a horizontal plane.

Structural balancing (palinspastic restoration): The process of restoring structural features to their original geographic locations, often in an iterative process in an effort to produce an acceptable result which demonstrates conservation of mass during deformation.

Structural shortening: A method for reporting the extent of deformation in a given section. Shortening is expressed as a percentage of the restored section length.

Thrust fault: A fault on which the hangingwall appears to have moved up relative to the footwall.

Thrust sheet: A body of rock carried in the hangingwall of a thrust fault.

Triangle zone: A term used to describe the wedge-like geometry observed in cross-sections at the leading edge of deformation in many fold and thrust belts.

Unconformity: A gap in the geological record related to an interruption of the normal depositional sequence or the uplift and erosion of strata.

CHAPTER 1: INTRODUCTION

1.1 Opening Statement

Thrust sheets of Mississippian strata in the Wildcat Hills area of the southern Alberta Foothills, delineated using 3-dimensional (3-D) seismic data, form a structure that varies along-strike. Displacement transfer between two thrust faults with a common detachment creates this along-strike variation in structural geometry. A 3-D numerical depth model of this structure, built using the seismic data interpretation for geometric constraint, allows ray tracing experiments designed to study out-of-plane imaging effects on 2-dimensional (2-D) seismic data collected over this structure.

Seismic data collected using a single line of receivers and colinear sources (2-D seismic data) are processed and often interpreted assuming that events in the resulting seismic section are derived from reflectors that lie directly below the line. This assumption is not valid for complex 3-D subsurface structure where reflections may originate outside of the vertical plane below the 2-D seismic line (out-of-plane events). Collection of seismic data using receivers and sources distributed over an area (3-D seismic data) allows processing and interpretation of these data without the assumptions inherent in the 2-D seismic imaging technique. The increased acquisition and processing costs for 3-D seismic data, especially in areas with difficult surface conditions, normally restrict the use of these data to enhancing the interpretation of subsurface structures first

delineated using 2-D seismic data. Understanding the effects of complex subsurface structure on 2-D seismic data allows critical evaluation of structures delineated using these data.

1.2 Research Objectives

The objectives of this thesis include:

- definition of the 3-D geometry of thrust sheets involving Mississippian strata in the Wildcat Hills area through the interpretation of 3-D seismic data,
- analysis of along-strike variations in displacement on thrust faults carrying Mississippian strata to elucidate displacement transfer relationships in this area,
- creation of a 3-D numerical depth model of this structure using the 3-D seismic data interpretation to constrain the geometry, and
- collection of 2-D synthetic seismic data over the 3-D numerical depth model (via ray tracing) to illustrate the effects of out-of-plane imaging on 2-D seismic data and quantify structural imaging errors.

1.3 Study Area

1.3.1 Location

This study focuses on a 3-D seismic survey in the Wildcat Hills area, located near the Ghost Reservoir, approximately 50 km northwest of Calgary, Alberta (Figure 1.1). The study area lies within the southern Alberta Rocky Mountain Foothills, near the surface expression of the leading edge of deformation (Figure 1.2).

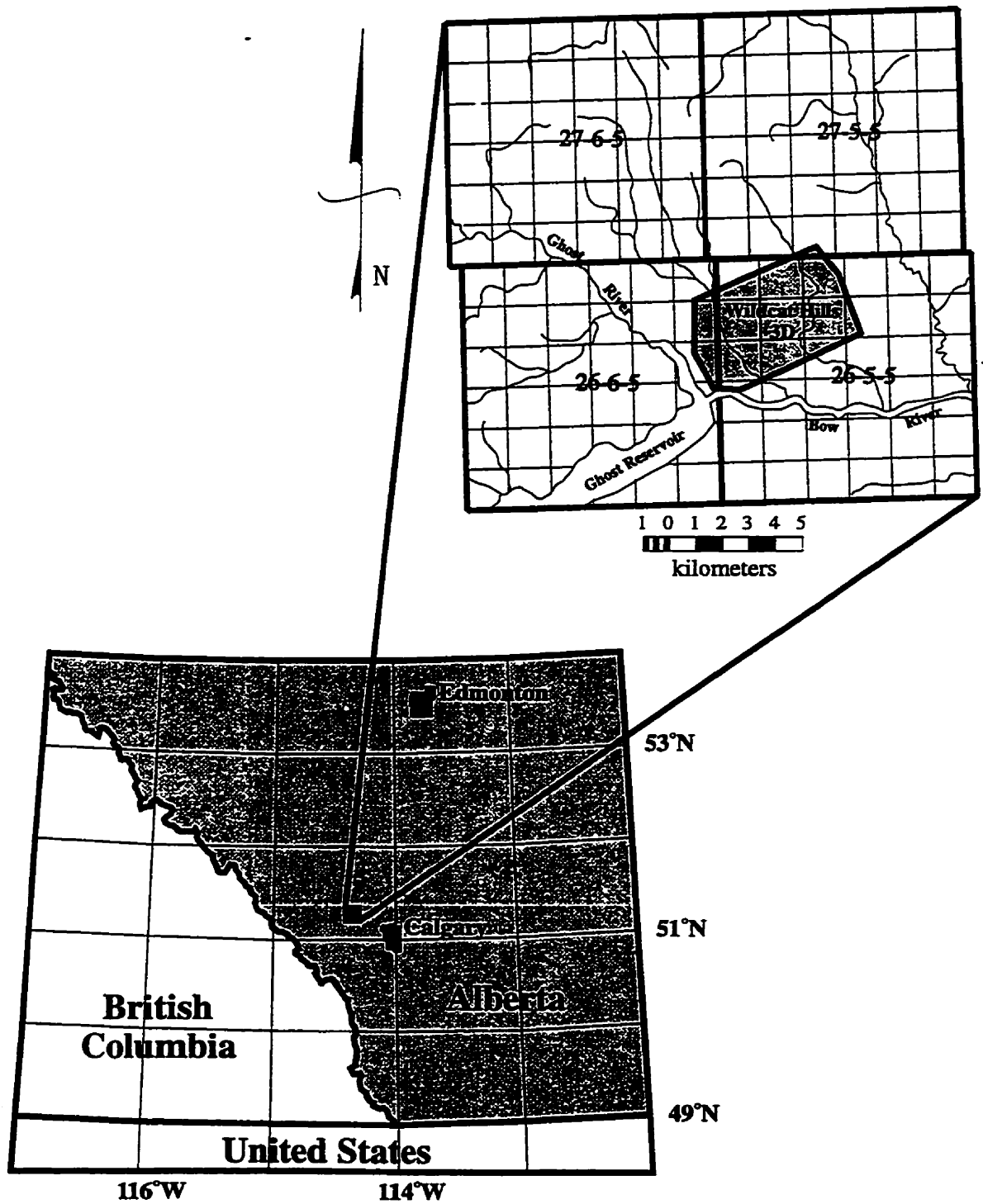

Figure 1.1. Location map for the study area showing the location of the Wildcat Hills 3-D seismic survey. The survey lies mostly within Township 27, Range 5W5 (27-5-5), northeast of the Ghost Reservoir.

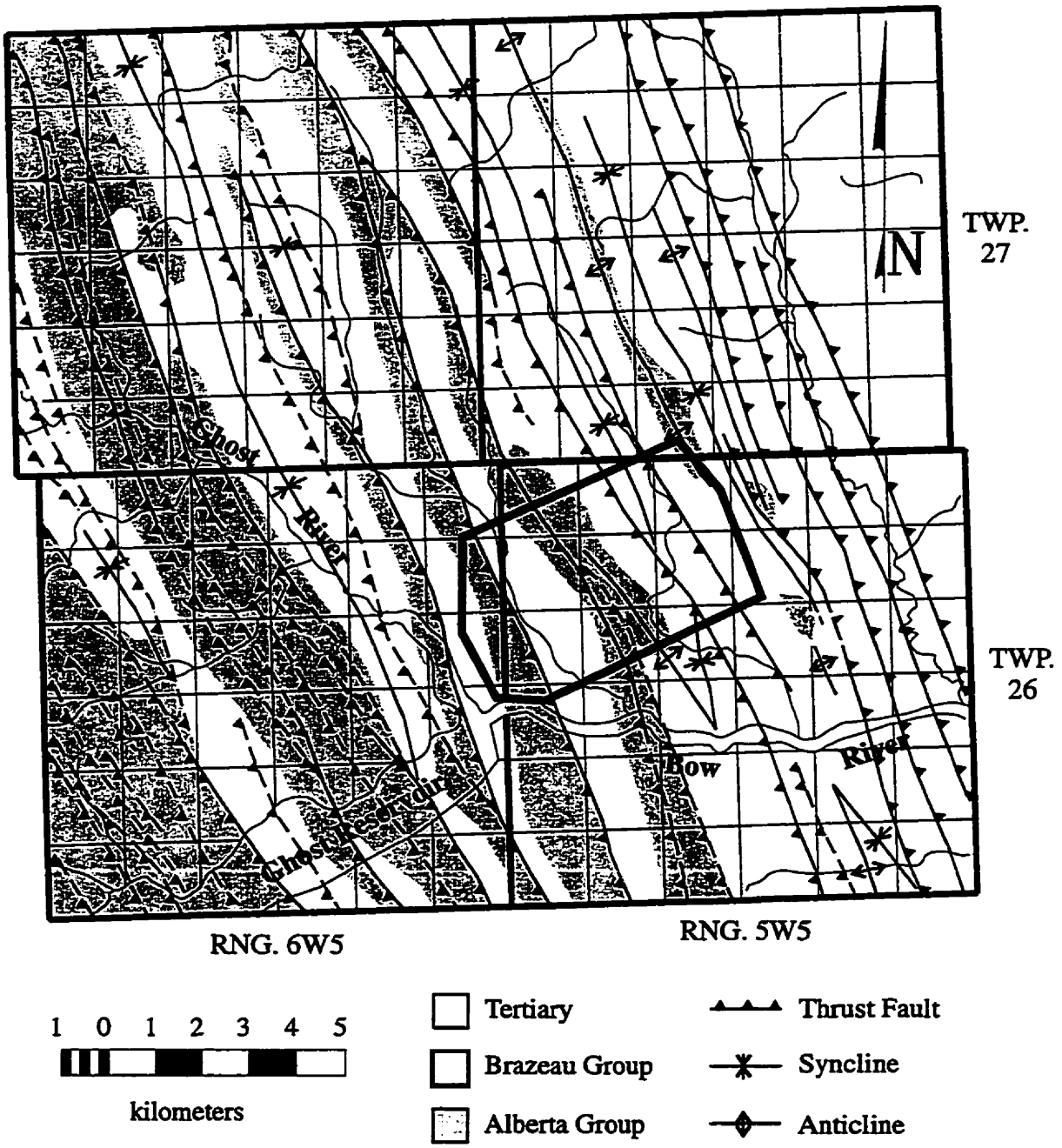

Figure 1.2. Surface geology map for the study area showing the location of the Wildcat Hills 3-D survey (dark outline). Geology as published by Ollerenshaw (1975), modified near the leading edge of deformation after Spratt et al. (1993), and Lawton et al. (1994). Surface expression of the leading edge of deformation is the easternmost thrust fault in this figure. Dashed thrust faults indicate inferred surface traces.

The Wildcat Hills area hosts natural gas production from structural traps involving Mississippian-aged carbonate reservoir rocks. This type of hydrocarbon trap has long been the focus of petroleum exploration efforts in the southern Alberta Foothills, and continues as a prolific hydrocarbon producer and exploration target (Bally et al., 1966; Dahlstrom, 1970; MacKay, 1991).

1.3.2 Structure

Fold and thrust structures in the southern Alberta Foothills formed in response to terrane accretion on the western margin of the North American continent during the late Cretaceous/Paleocene (Monger et al., 1982). East-vergent thrust faults and related folds are the dominant structures in the southern Alberta Foothills (Bally et al., 1966; Dahlstrom, 1970; Price, 1986). The McConnell thrust fault delineates the western boundary of the Foothills belt in the Wildcat Hills area (Bally et al., 1966). The eastern boundary of the Foothills in southern Alberta is the leading edge of Cordilleran deformation, normally delineated by the surface trace of an east-dipping, west-vergent thrust fault (the upper detachment). The leading edge of deformation in the southern Alberta Foothills is a triangle zone which includes significant subsurface structure east of the surface trace of the upper detachment (e.g. Price, 1986; MacKay, 1991; Lawton et al., 1996; MacKay, 1996; Skuce, 1996; Soule and Spratt, 1996; Stockmal et al., 1996). Lawton et al. (1994) describe the triangle zone at Wildcat Hills as a thinly-tapered wedge

of deformed rocks extending more than 8 km into the foreland. The thickest region of the triangle zone in this area consists of several stacked thrust slices (up to 500 m thick) of lower to mid-upper Cretaceous strata (Lawton et al., 1994).

1.3.3 Stratigraphy

Two main lithotectonic units define the stratigraphy in the southern Alberta Foothills: (i) a carbonate-dominated passive margin sequence, and (ii) a clastic-dominated foreland basin sequence. In this study these sequences are referred to as the Paleozoic and Mesozoic sections, respectively (Figure 1.3).

1.3.3.1 *The Paleozoic section*

The Paleozoic section preserves strata deposited on the passive western margin of the North American craton. This section contains predominantly carbonate rocks, with minor shale intervals that generally thicken toward the west (Bally et al. 1966). This interval includes several unconformities that record gentle tilting of the craton throughout the Paleozoic (Bally et al., 1966). The shale intervals act as detachments between the more competent carbonate units during deformation (Dahlstrom, 1970).

1.3.3.2 *The Mesozoic section*

The lower Mesozoic section (Fernie and Kootenay groups, Figure 1.3) consists mainly of shales with some coarse clastics and rare carbonates (Bally et al., 1966). This interval hosts an important detachment in the southern Alberta Foothills which separates deformation (and structures) in the Mesozoic section from deformation in the Paleozoic section (e.g. Dahlstrom, 1970; MacKay, 1991).

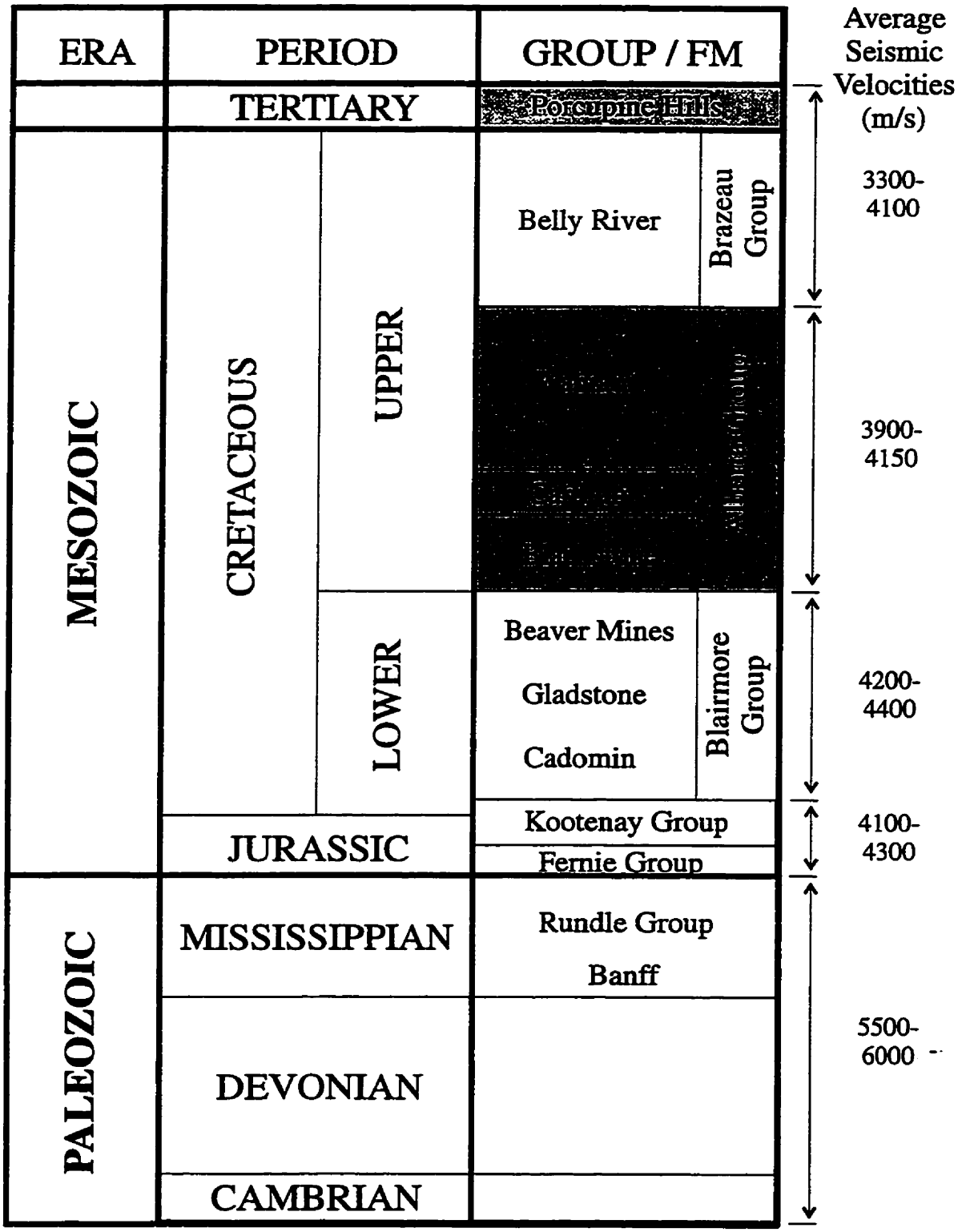

Figure 1.3. Stratigraphic chart for the southern Alberta foothills region, scaled vertically with respect to average regional thicknesses (after MacKay 1991). Shaded regions correspond to stratigraphic intervals shaded on the surface geology map (Figure 1.2). Regional interval velocities also shown (after Slotboom et al., 1996).

The upper Mesozoic (above the Kootenay group, Figure 1.3) and Tertiary sections contain a variety of clastic rocks of mixed continental and marine affinity, and record foreland basin sedimentation during the evolution of the Cordillera (Bally et al., 1966). The upper Mesozoic and Tertiary sections have several detachment horizons which produce complex fold and thrust structures (e.g. Dahlstrom, 1970; MacKay, 1991; Lawton et al., 1994; Lawton et al., 1996; Lebel et al., 1996; Liu et al., 1996; MacKay, 1996; Skuce, 1996; Soule and Spratt, 1996; Stockmal et al., 1996).

1.4 Fault Displacement Transfer

Thrust faults in the southern Alberta Foothills typically display a flat-ramp-flat geometry that facilitates imbrication of various units between detachment surfaces (flats) (Bally et al., 1966; Dahlstrom, 1970). Lateral variations in thrust structures are generated by: (i) lateral changes in detachment levels (lateral ramps), (ii) high-angle tear faults, and (iii) displacement transfer between discrete structures (which may share a common lower detachment). Displacement transfer between thrust faults can create significant lateral structural variations, and recognition of the three-dimensional nature of Foothills structures is critical in the treatment of 2-D seismic data from this region.

The existence of a basic fault displacement transfer mechanism for the Canadian Rocky Mountain Foothills was suggested by Dahlstrom (1970) to explain the general observation that the extent and amount of shortening observed over the entire Foothills belt is more constant than that of individual structures. Displacement transfer between en échelon thrust faults (at various scales) is documented for several locations within the

Rocky Mountain Foothills (e.g. Dahlstrom, 1970; Sanderson and Spratt, 1992; Liu et al., 1996). This observation is not restricted to compressional regimes, with similar fault displacement patterns reported for en échelon normal faults (e.g. Nicol et al., 1996).

Physical modeling studies suggest that variations in displacement along strike on large thrust faults (with local maxima and minima) are likely the result of separate, coplanar faults linking together as they propagate along strike (Liu and Dixon, 1991). Ellis and Dunlap (1988) used the idea of linking of colinear thrusts to explain similar displacement patterns observed on individual faults in natural systems. Liu et al. (1996) also used this idea to explain displacement variations along a single thrust fault carrying allochthonous Mississippian strata in the central Alberta Foothills. Liu et al. (1996) observed several displacement maxima and minima along the fault (similar to patterns observed in physical models), and proposed that the coalescence of several small thrusts was the mechanism for creation of the larger thrust.

1.5 Numerical Seismic Modeling

Forward numerical seismic modeling, used in this study, involves the computation of synthetic seismic data over a model describing subsurface geometry and physical properties. The two numerical seismic modeling techniques are: (i) wave equation modeling, which attempts to model wavefront propagation directly; and (ii) ray tracing, which attempts to model the wavefront indirectly using ray theory. The ray tracing method assumes that a propagating wavefront can be represented by the propagation of rays traveling normal to that wavefront from the source point. Three rules control the

trajectory of rays in the subsurface: (i) rays are unbent in constant velocity media, (ii) rays bend according to Snell's Law where they cross velocity boundaries, and (iii) rays reflect at an angle equal to the incidence angle at impedance boundaries.

Forward seismic modeling helps constrain the interpretation of seismic data through comparison of real and synthetic data, and by providing examples of synthetic data collected over known geologic models. Several forward seismic modeling studies in structurally complex areas using 2-D models demonstrate the utility of this technique (e.g. May and Hron, 1978; Skeen and Ray, 1983; Lingrey, 1991; Morse et al., 1991; Johansen et al., 1994). Using 2-D geologic models in forward seismic modeling requires the assumption of no out-of-plane reflections in the seismic data. Complete seismic modeling of complex structures, including out-of-plane effects, requires the use of 3-D geologic models. Several numerical seismic modeling studies using 3-D geologic models demonstrate the effects of out-of-plane imaging on 2-D seismic data, and the utility of 3-D forward seismic modeling techniques in the solution of interpretation problems (e.g. Fagin, 1991a; Morse et al., 1991; Rudolph and Greenlee, 1991). Scaled physical seismic modeling experiments using 3-D geologic models represent another approach to the problem but are not used in this study (e.g. French, 1974; Zimmerman, 1991)

Morse et al. (1991) show a series of synthetic zero-offset 2-D seismic sections collected over a 3-D geologic model of a thrust structure (constructed using structural theory). Comparison of vertical depth sections and these synthetic seismic data illustrates out-of-plane effects on 2-D seismic data collected over 3-D structure. Morse et al. (1991) suggest that 2-D seismic data collected in the dip direction are insufficient for structural

imaging based on these forward seismic modeling results, collected over a 3-D geologic model that varies radically along strike.

The potential for out-of-plane imaging (sideswipe) requires that 2-D seismic sections from structurally complex areas must always be treated as a composite of reflections rather than a direct image of structure below the line of section (Fagin 1991b). The interpreter in these situations must appreciate the 3-D nature of the subsurface, and the possible origins of reflections present in the 2-D seismic section (e.g. Fagin, 1991b; Houck et al., 1996).

1.6 Thesis Structure

The material discussed above serves to introduce the reader to the objectives of this thesis, and to provide some background information on topics presented. Chapter 2 describes the geometry of structures involving Mississippian strata in the Wildcat Hills area interpreted using 3-D seismic data, and presents an analysis of along-strike variations in thrust fault displacement. The procedure for construction of a 3-D numerical depth model, outlined in Chapter 3, describes the use of horizons interpreted in the 3-D seismic data to constrain the structural geometry of the model. Chapter 4 describes a ray-tracing experiment designed to illustrate and quantify out-of-plane imaging effects on structural interpretation using synthetic 2-D seismic data collected over this model. Finally, Chapter 5 presents an integrated discussion of results presented throughout the thesis, and outlines the conclusions drawn from them.

CHAPTER 2: SUBSURFACE STRUCTURE IN THE WILDCAT HILLS AREA

2.1 Seismic Data

2.1.1 Wildcat Hills 3-D seismic data

Interpretation of a 3-D seismic data volume from the Wildcat Hills area, donated to the University of Calgary by Canadian Hunter Petroleum and Petrofina S.A., allowed delineation of thrust sheets of Mississippian strata within the survey area. The 3-D survey is approximately 6 km x 4 km, with the long dimension oriented in the dip direction, approximately northeast (Figures 1.1, 2.1). Table 2.1 lists the acquisition parameters for this survey. Processing of these data, outlined in Table 2.2, included dip moveout (DMO) correction and a one-pass finite-difference post-stack time migration.

2.1.2 Interpretation

Figures 2.2 to 2.4 show examples of three dip lines (raw and interpreted sections) extracted from the 3-D data volume (marked A, B, and C in Figure 2.1). Figure 2.5 shows a sample strike line extracted from the 3-D data volume (section D in Figure 2.1). Reliable interpretation of the Mesozoic section was not possible using these data because of low signal to noise ratios. Limiting the scope of this study to the delineation of Paleozoic-involved structures focused the interpretation effort. SEISX interpretation software (Photon Systems Ltd.) was used to interpret dip lines (every 100 m) and strike lines (every 200 m) throughout the seismic data volume. The auto-picking facility in

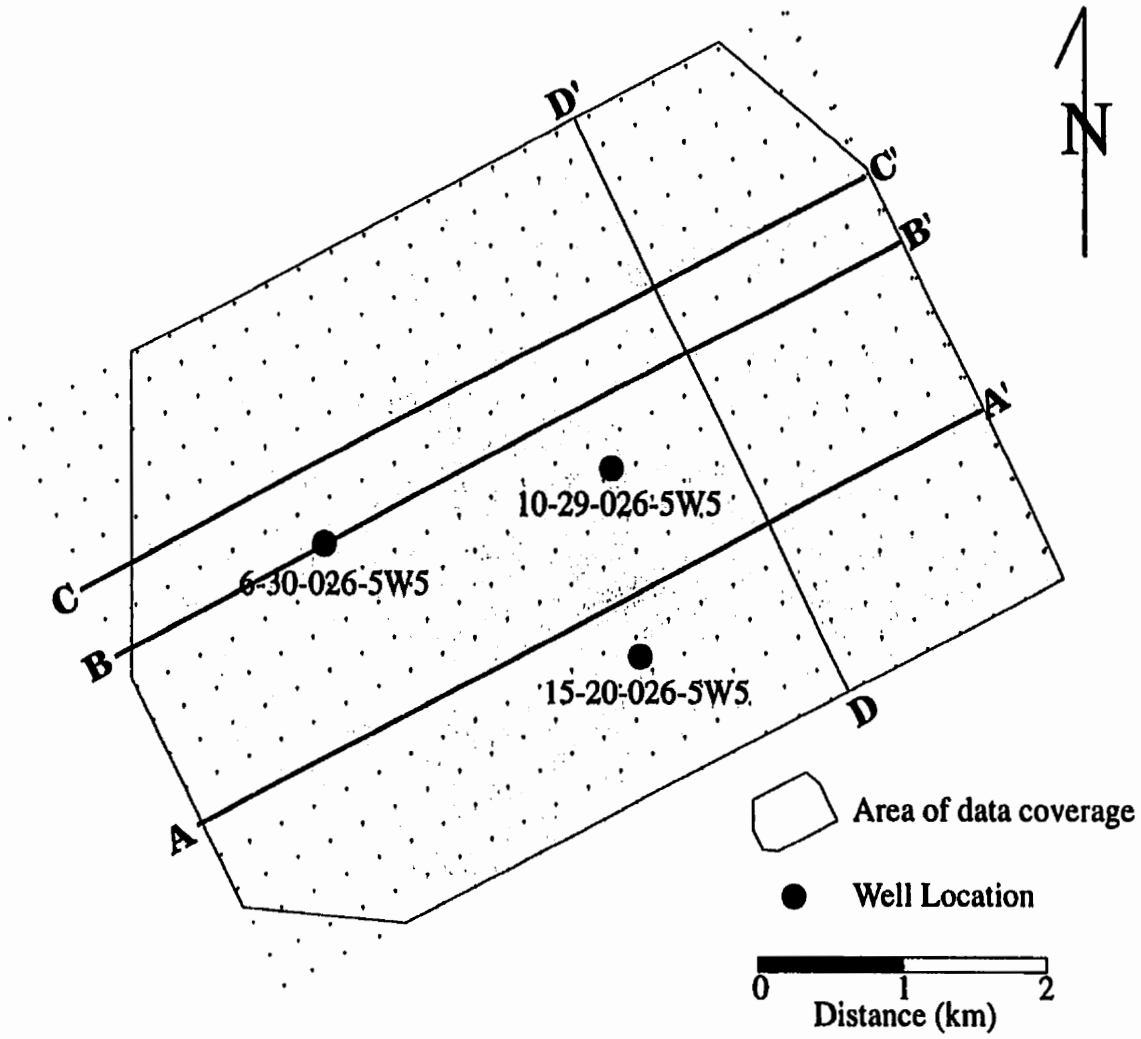

Figure 2.1. Map of Wildcat Hills 3-D seismic survey (grid node separation = 250 m). Shaded area represents the actual area of seismic data coverage. Lines A-A', B-B', C-C', and D-D' indicate the location of seismic lines presented in Figures 2.2 - 2.5. Locations shown for wells within the survey area with available sonic logs.

Table 2.1: Acquisition Parameters for the Wildcat Hills 3-D Survey

Acquisition Date:	October, 1991
Source Parameters:	
Type:	Vibroseis (10-70Hz sweep)
Array:	4
Shot Interval:	50 m
Recording Parameters:	
Receiver Type:	LRS 1016 (14 Hz)
Array:	8 phones over 25 m
Group Interval:	50 m
Recording Instrument:	Sercel 368
Time Sample Rate:	2 ms
Recording Time:	3 s
Recording Geometry:	
Receiver line Spacing:	600 m
Number of Receiver lines (NW-SE):	11
Source line Spacing:	800 m
Number of Source lines (NE-SW):	6
Receiver lines Active/Shot:	9
Total Number of Shots:	705
Nominal Fold:	13

Table 2.2: Processing History for the Wildcat Hills 3-D Survey
(1991 processing by HGS Incorporated)

Demultiplex and conversion
to minimum phase
↓
3D Geometry and Binning (25m x 25m)
↓
Refraction Statics (GLI)
(2 layer model from first break analysis)
↓
True Amplitude Recovery
(5 db/s from 0 - 2 s)
↓
First Break Mute
↓
Trace Editing
↓
Designature (shot domain)
Zero Phase Output
↓
Deconvolution (zero phase)
↓
Trace Equalization
↓
Surface-Consistent Residual Statics
↓
Velocity Analysis
(surface referenced)
↓
3-D Velocity Model Building
↓
Surface-Consistent Residual Statics
↓
Dip Moveout
↓
CDP Stack (25m x 25m bins)
↓
One-Pass Finite-Difference Migration
↓
Time Invariant Filter
(8/12 - 55/65)
↓
Time Variant Scaling

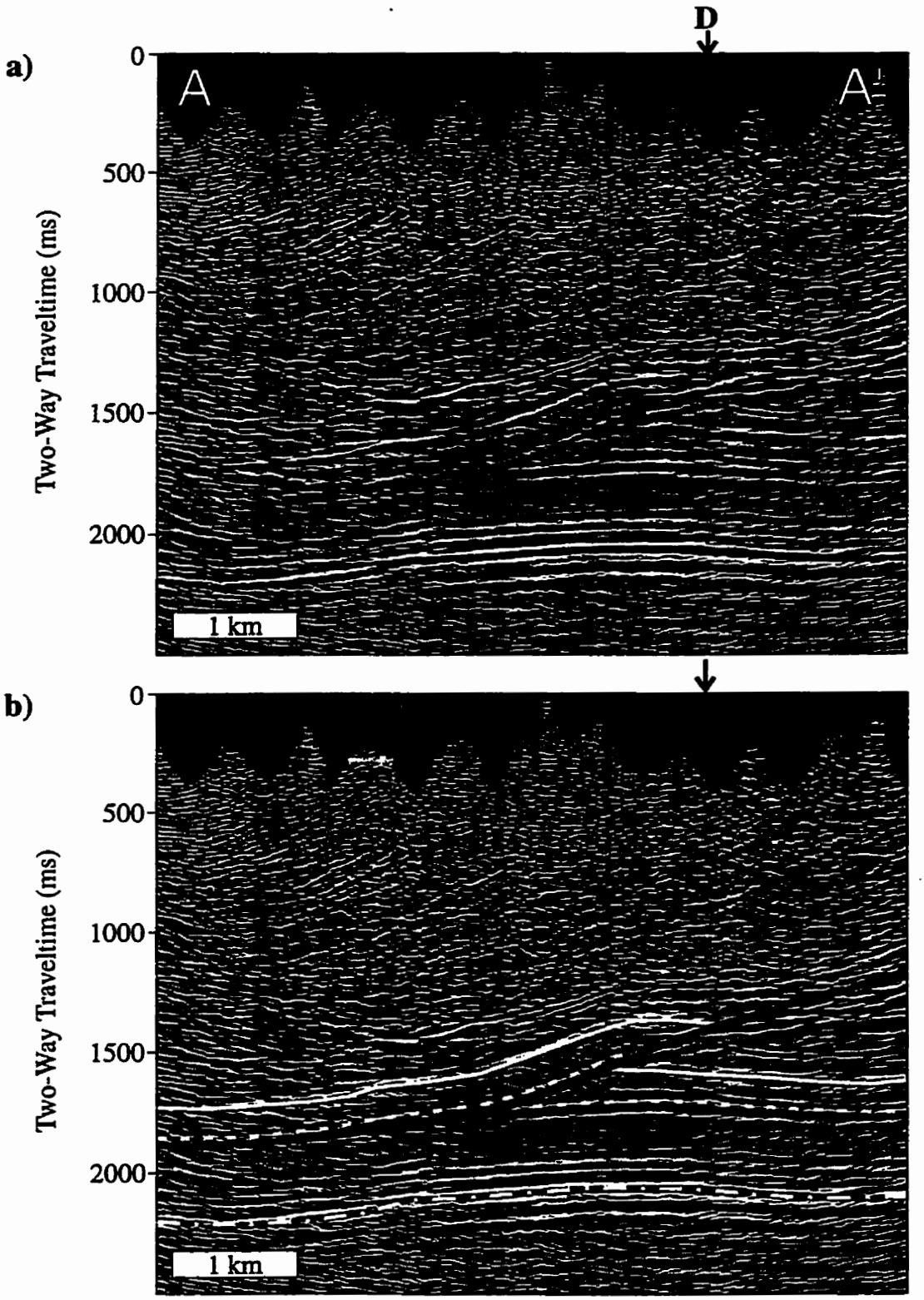

Figure 2.2. Dip line A-A' through the Wildcat Hills 3-D seismic data: a) uninterpreted, b) interpreted (see Figure 2.1 for location). Section (b) illustrates the Mississippian structure interpreted in the southeastern part of the survey area. Solid white = Top Mississippian marker, dashed white = Base Mississippian marker, dot-dashed white = Near Basement marker, solid black = fault. Section 1:1 at 4000 m/s.

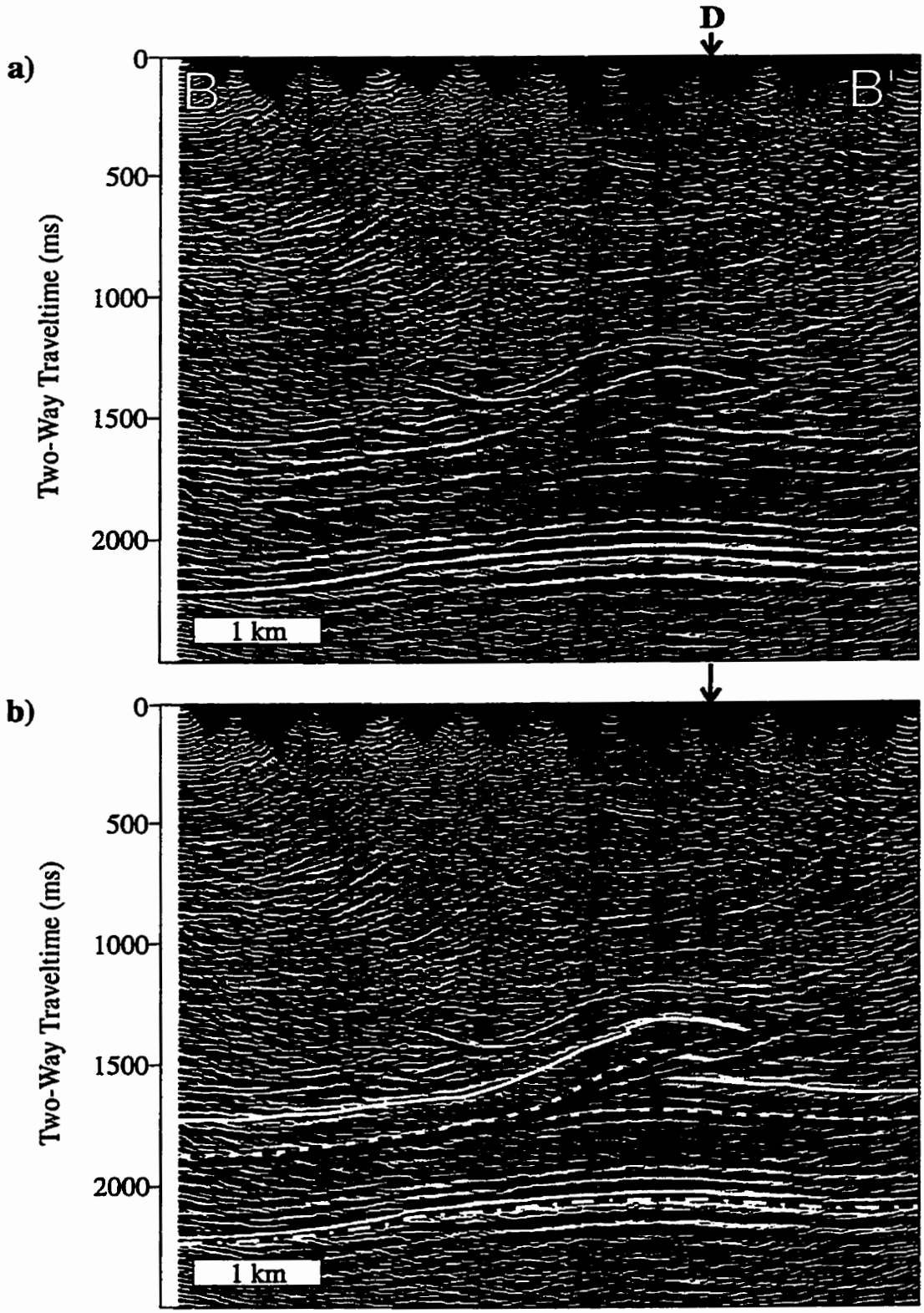

Figure 2.3. Dip line B-B' through the Wildcat Hills 3-D seismic data: a) uninterpreted, b) interpreted (see Figure 2.1 for location). Section (b) illustrates the Mississippian structure interpreted in the central part of the survey area where a second, lower thrust fault is initiated. Horizons as outlined in Figure 2.2. Section 1:1 at 4000 m/s.

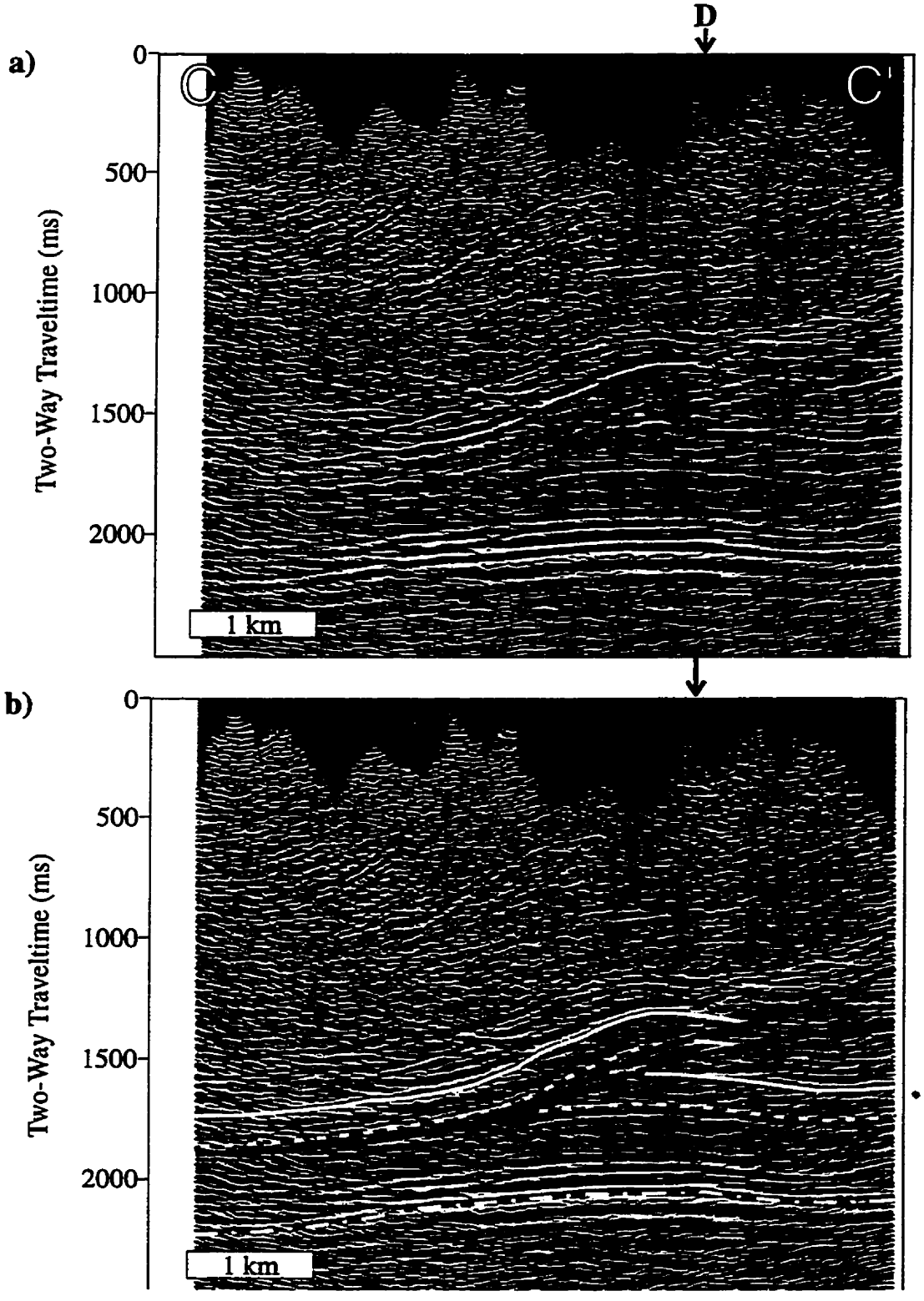

Figure 2.4. Dip line C-C' through the Wildcat Hills 3-D seismic data: a) uninterpreted, b) interpreted (see Figure 2.1 for location). Section (b) illustrates the Mississippian structure interpreted in the northwestern part of the survey area where displacement increases on the lower thrust fault, and decreases on the upper thrust fault. Horizons as outlined in Figure 2.2. Section 1:1 at 4000 m/s.

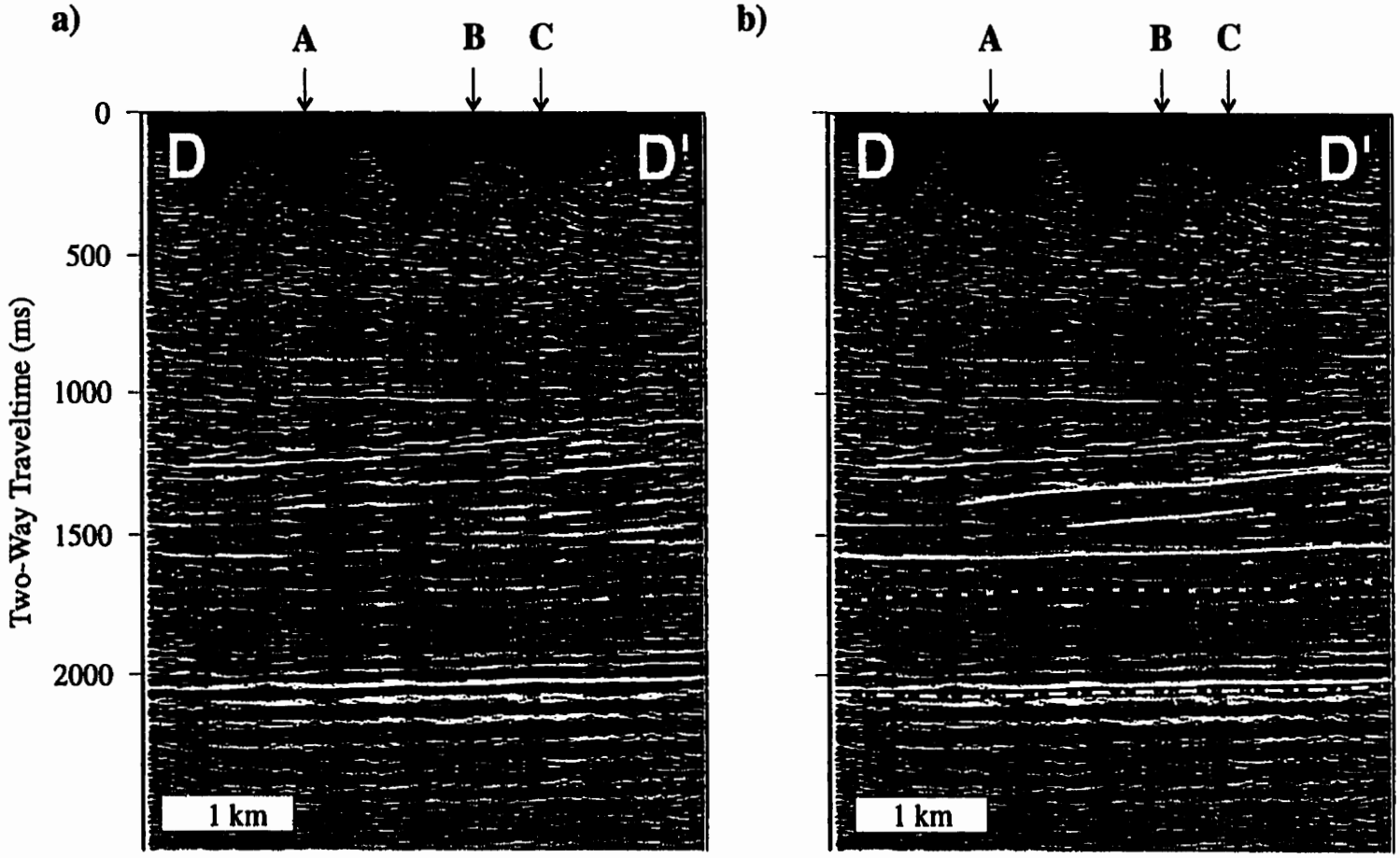

Figure 2.5. Strike line D-D' through the Wildcat Hills 3-D seismic data: a) uninterpreted, b) interpreted (see Figure 2.1 for location). Interpreted section (b) illustrates the along-strike changes in the Mississippian-involved thrust structure from a single thrust sheet in the southeast to a stack of two thrust sheets in the northwest. Horizons as outlined in Figure 2.2. Section 1:1 at 4000 m/s.

SEISX, using the interpreted lines as control, created tightly constrained time surfaces for map analysis. The final interpretation presented here is the result of several iterations.

The interpretation of the 3-D seismic data volume involved picking three horizons: (i) Top Mississippian, (ii) Base Mississippian, and (iii) Near Basement. A number of wells intersect the Mississippian section in the survey area, but only three of these wells have sonic log data available (see Figure 2.1 for locations). Sonic log data are used to create synthetic seismograms, which provide a character tie between the seismic data and the subsurface geology. Figure 2.6 shows an example of the character tie between the seismic data and the synthetic seismogram generated from the sonic log for well 15-20-026-5W5.

The Top Mississippian marker chosen for the seismic data interpretation appears to correspond approximately to the top of the Shunda Formation, 60 to 90 m (50 - 75 ms) below the actual top of the Mississippian interval (Figure 2.6). The Top Mississippian horizon interpreted in the seismic data is a stronger, more coherent reflection than that from the actual top of the Mississippian interval and provides a more reliable marker to constrain interpretation of the structure (Figures 2.2 - 2.5). The Base Mississippian horizon, picked to help constrain the structural interpretation, is a coherent seismic marker above a detachment carrying allochthonous Mississippian strata. The name for this horizon is based on the assumption that the detachment runs within the Banff Formation, a shaly interval at the base of the Mississippian (Slotboom et al., 1996). The Near Basement horizon, picked to evaluate time structure below the thrust sheets of Mississippian strata, is the most coherent event near the base of the section.

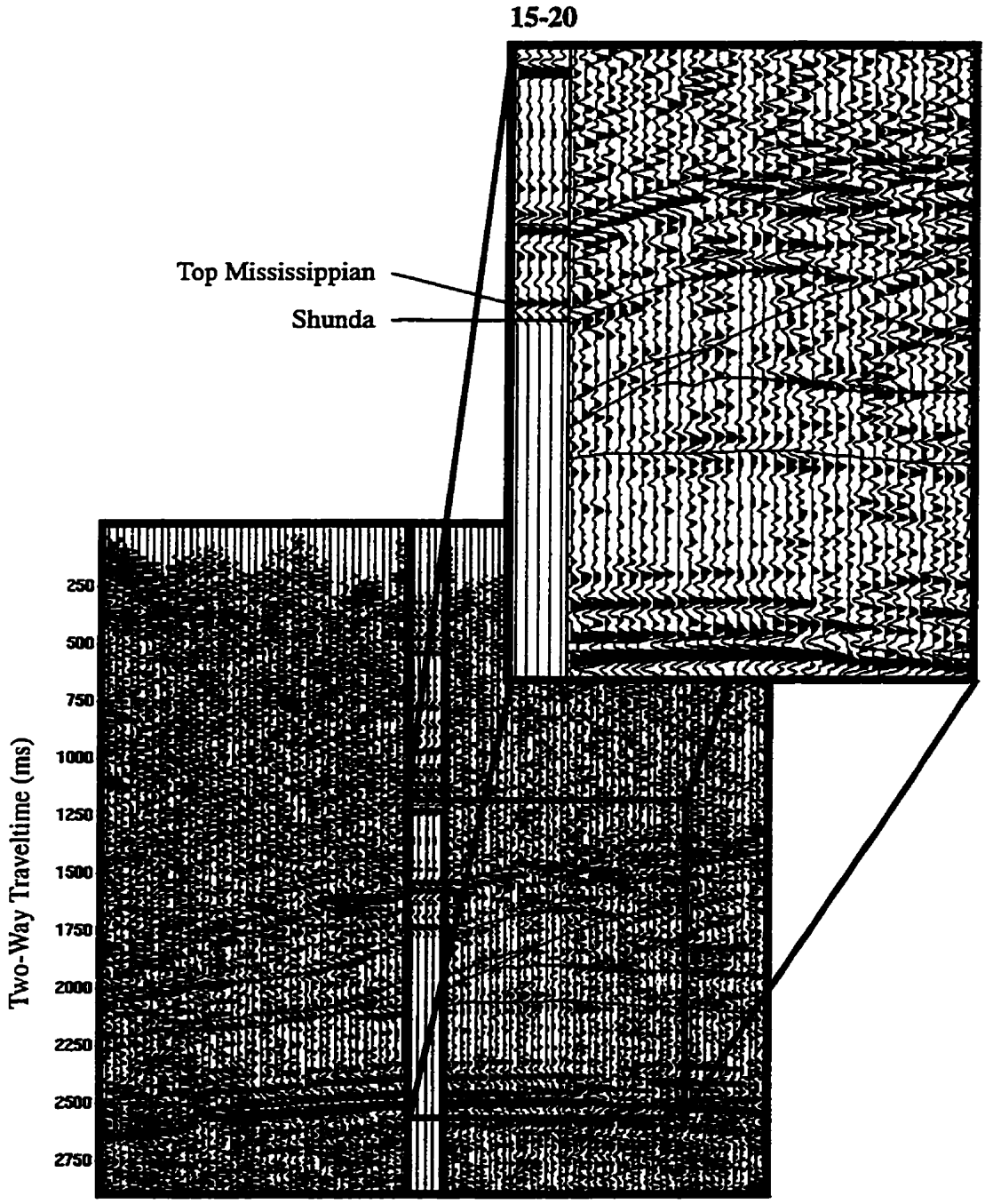

Figure 2.6. Synthetic seismogram created using sonic log data from well 15-20, tied to the dip line from the the 3-D seismic data volume crossing the well location (south of A-A', Figure 2.1). This figure illustrates the mismatch between the top Mississippian marker indicated in the well (indicated above - Top Mississippian) and the horizon picked to represent the top Mississippian (picks shown as light lines through the seismic data). The Top Mississippian horizon is likely in the Shunda Formation, based on these well data.

Final interpretation of a structure involving Mississippian strata in this area, using 3-D seismic data to constrain the geometry, illustrates a displacement transfer relationship between two thrust faults. The structure changes along the four-kilometer strike length of the 3-D survey from a single thrust sheet of Mississippian strata in the southeast, to a stack of two thrust sheets in the northwest (Figures 2.2 - 2.5). Figure 2.7 shows a time structure map of the Top Mississippian horizon in the hangingwall of the upper thrust sheet and in the autochthonous footwall. This map illustrates the areal extent of the structure within the survey area, indicated by the departure of the Top Mississippian marker from regional levels (at approximately 1600 ms, purple in Figure 2.7). The maximum amplitude of the time structure (approximately 350 ms) occurs at the northwest edge of the survey area. A general increase in structural level toward the northwest reflects the addition of the second, lower thrust sheet of Mississippian strata in this area (Figures 2.2 - 2.5, 2.7). A broad (1.5 km) negative time structure anomaly containing shorter-wavelength northeast-trending anomalies occurs along the southwestern edge of the survey area (Figure 2.7). Time structure anomalies on the Near Basement horizon correlate with those observed on the Top Mississippian time structure map (Figures 2.7, 2.8). The Near Basement time structure map shows a northwest-trending time structure anomaly in the central part of the survey area (up to 70 ms in amplitude) which corresponds to the area where the Top Mississippian horizon lies above regional levels (Figures 2.7, 2.8). The amplitude of this time structure anomaly increases toward the northwest, similar in trend to the increase in Top Mississippian time structure across this region (Figures 2.7, 2.8). This Near Basement time structure anomaly is interpreted as 'pull-up' related to the imbrication of higher-velocity Mississippian strata

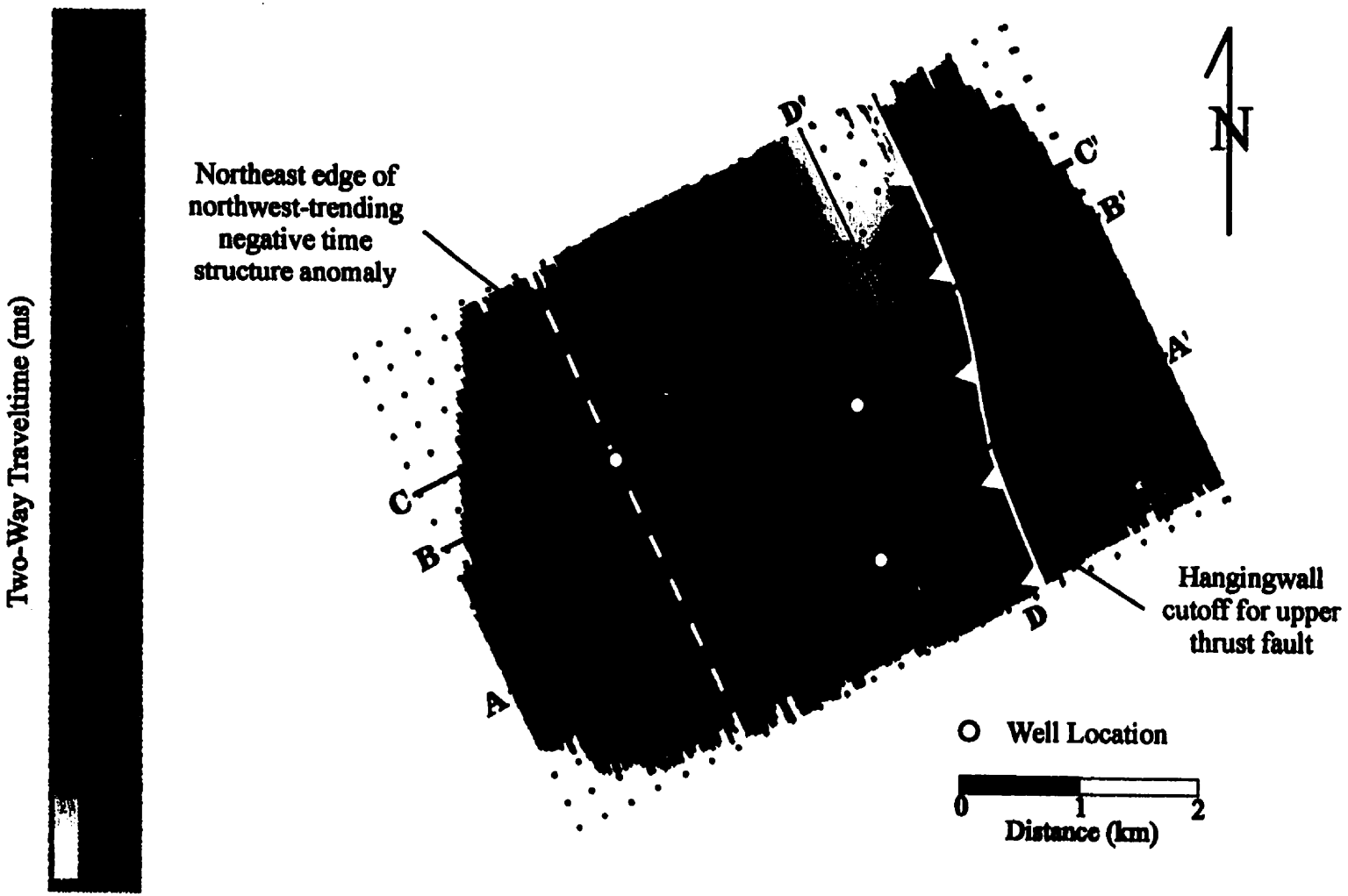

Figure 2.7. Time structure map of the Top Mississippian marker in the hangingwall of upper fault and the footwall of the structure from the interpretation of the Wildcat Hills 3-D seismic data (Figures 2.2-2.4). Note the increase in structural level (decrease in two-way traveltime) of the hangingwall Mississippian toward the northwest. Lines A-A', B-B', and C-C' indicate the location of seismic lines presented in Figures 2.2 - 2.4.

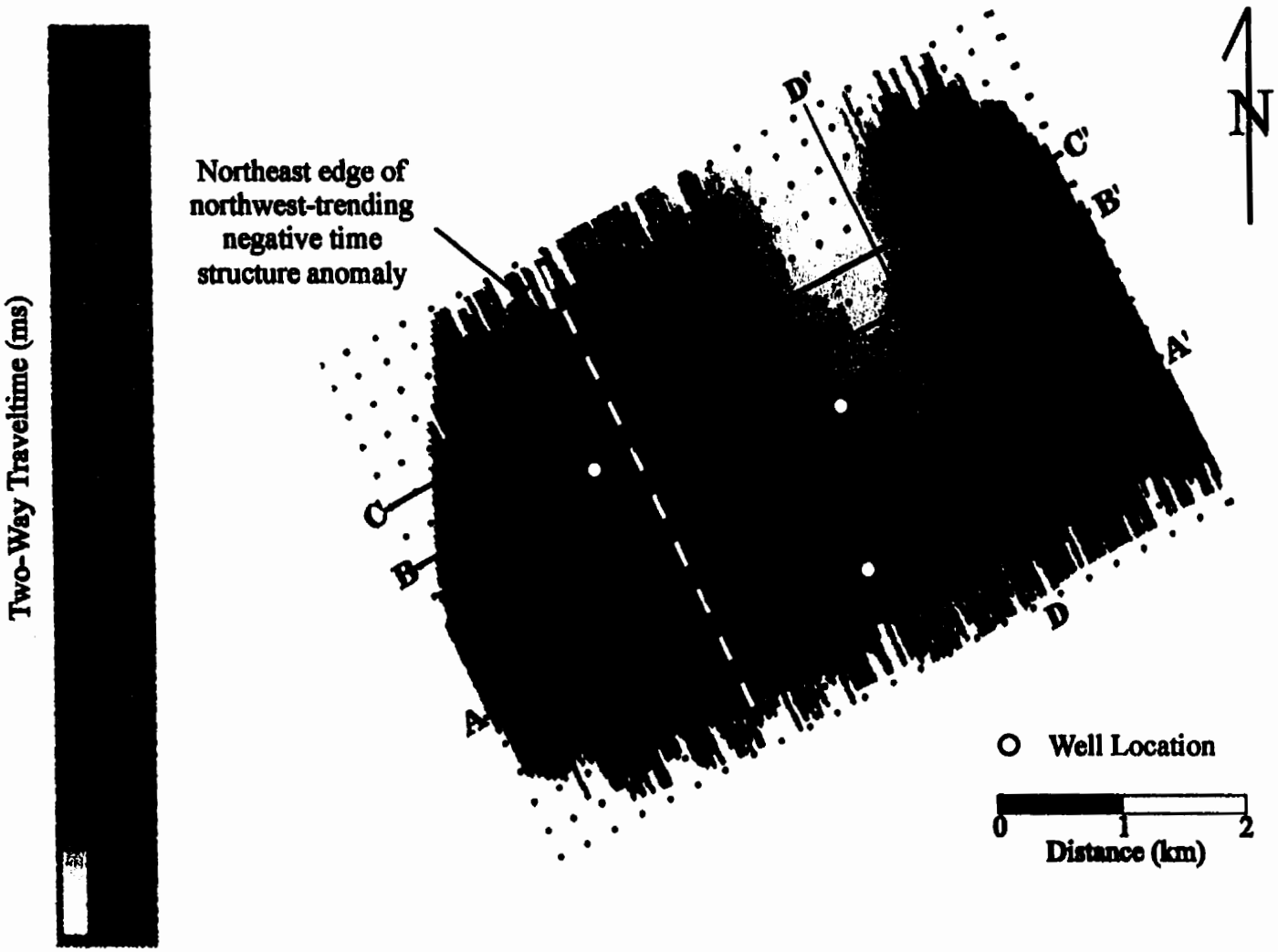

Figure 2.8. Time structure map of the Near-Basement marker in the Wildcat Hills 3-D seismic data (Figures 2.2-2.4). Note the increase in structural level (decrease in two-way traveltime) on this horizon toward the northwest below the Mississippian structure (Figure 2.6). This increase in time structural level is interpreted as indicating an increase in the effective thickness of high-velocity Mississippian strata above. Lines A-A', B-B', and C-C' indicate the location of seismic lines presented in Figures 2.2 - 2.4.

above (Figures 1.3, 2.2 to 2.5). The increasing amplitude of this pull-up anomaly toward the northwest corresponds to the addition of a second, lower thrust sheet of Mississippian strata in this area (Figures 2.2 - 2.5, 2.8). A broad (1.5 km) negative time structure anomaly, similar to that observed on the Top Mississippian time structure map, occurs along the southwest edge of the survey area (Figures 2.7, 2.8). This negative time structure anomaly may represent real basement-involved structure, or a 'push-down' anomaly related to the presence of low-velocity strata within the Mesozoic interval above this feature.

2.2 Structural Analysis

2.2.1 Structural geometry

Interpretation of the 3-D seismic data defined a structure formed by imbrication of Mississippian strata on two thrust faults with flat-ramp geometries and a common basal detachment. This common basal detachment facilitates displacement transfer between the two thrust faults (Dahlstrom, 1970). Displacement on the upper thrust fault decreases toward the northwest as displacement on the lower thrust fault increases (Figures 2.3, 2.5). Increased displacement on the lower thrust fault toward the northwest appears to lift and rotate the upper thrust sheet toward the southwest, causing the observed shallowing of the Top Mississippian marker in the hangingwall of the upper thrust (Figure 2.7). This interpretation implies that motion on the upper fault occurred prior to motion on the lower fault, although both faults were likely active contemporaneously during deformation (Dahlstrom, 1970; Liu and Dixon, 1991).

2.2.2 Structural balancing

The requirement of equal displacement of both the Top Mississippian and Base Mississippian horizons across a given fault was used to constrain the seismic data interpretation, and should ensure a reasonably balanced result for this structure. The horizon interpretations presented in Figures 2.2b - 2.4b were depth-converted and structurally balanced using Midland Valley Move-on-Fault software (Figures 2.9 - 2.11, respectively).

Vertical time-to-depth conversion of the horizons interpreted in the seismic data, using a simple interval velocity model, provides depth sections for structural balancing (Figures 2.9a - 2.11a). The velocity model consists of two intervals: (i) 4600 m/s between the surface and the Top Mississippian horizon (Mesozoic interval), and (ii) 6000 m/s between the Top Mississippian and Near Basement horizons (Paleozoic interval). The Mesozoic interval velocity reflects values typical of the lower part of this section where the thrust sheets of Mississippian strata (6000 m/s average velocity) occur. In all cases the depth conversion yields slightly irregular horizons in depth (Figures 2.9a - 2.11a), but the structural balancing results are relatively stable (Figures 2.9b - 2.11b).

The balanced sections were produced by joining the hangingwall and footwall cutoffs of the Base Mississippian horizon using a flexural-slip algorithm. The Base Mississippian cutoffs appear to be more precisely located in the seismic data than those of the Top Mississippian horizon and should provide the most accurate restoration result (Figures 2.2 - 2.4). The fault cutoffs are confidently located in the seismic data within one to two traces (+/- 25 - 50 m). Balancing results deteriorate slightly toward the north as the structure becomes more complex, reflecting: (i) increased difficulty in interpreting

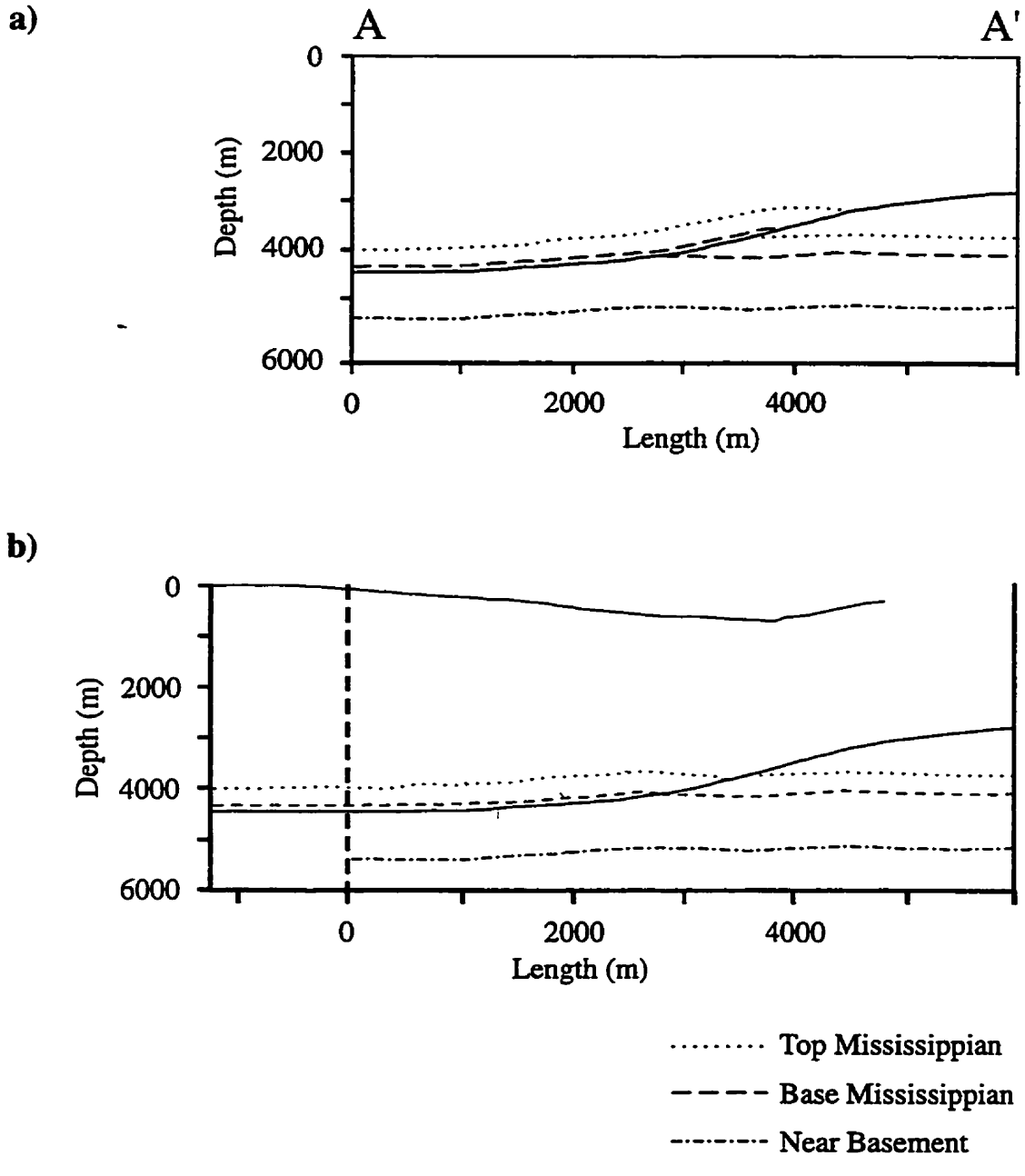

Figure 2.9. Structural balancing results for dipline A-A' (Figure 2.2). a) Depth section (vertical time-to-depth conversion). b) Restored depth section: Base Mississippian hangingwall and footwall cutoffs joined using a flexural slip algorithm. Shortening = 17%.

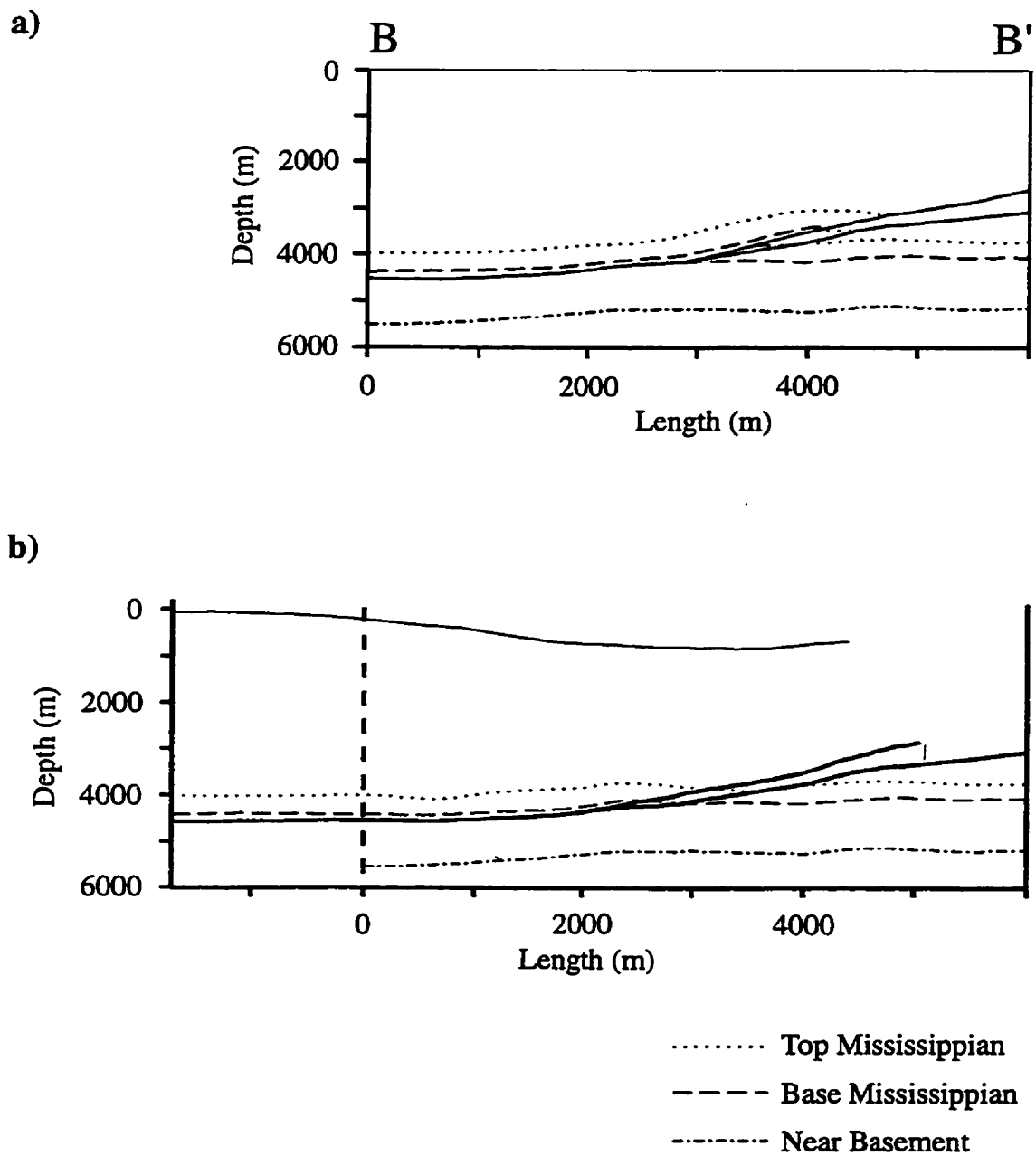

Figure 2.10. Structural balancing results for dipline B-B' (Figure 2.3). a) Depth section (vertical time-to-depth conversion). b) Restored depth section: Base Mississippian hangingwall and footwall cutoffs joined using a flexural slip algorithm. Shortening = 22%.

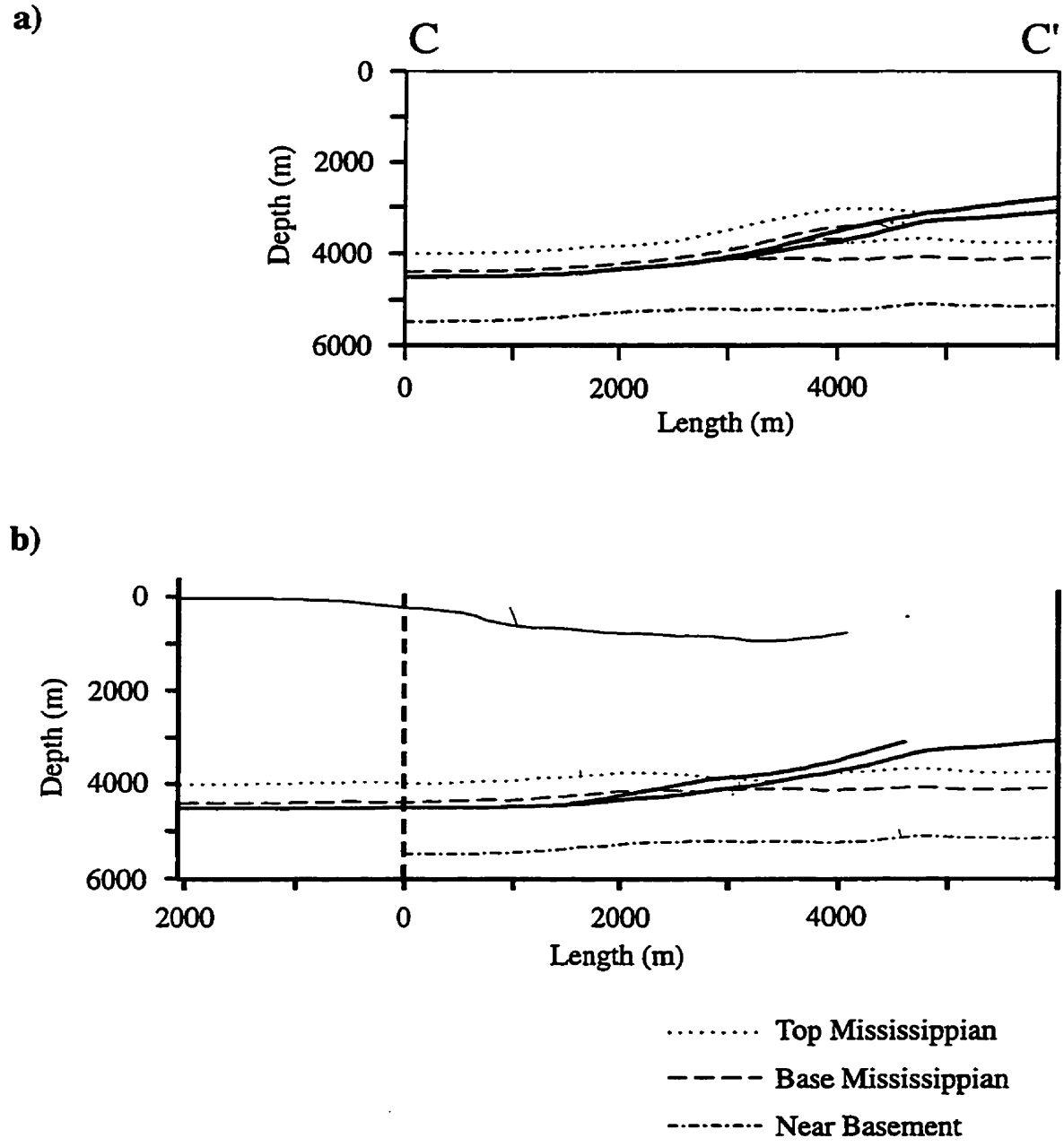

Figure 2.11. Structural balancing results for dipline C-C' (Figure 2.4). a) Depth section (vertical time-to-depth conversion). b) Restored depth section: Base Mississippian hangingwall and footwall cutoffs joined using a flexural slip algorithm. Shortening = 26%.

precise cutoff locations from the seismic data, (ii) increasing depth-conversion error resulting from velocity model and conversion method assumptions, and (iii) inaccuracy of the flexural-slip deformation assumption. Structural balancing error, apparent in the mismatch between the hangingwall and footwall cutoffs of the Top Mississippian horizon, ranges from 200 m in section A-A' to 550 m in section C-C' (Figures 2.9b - 2.11b). These structural balancing errors, if distributed between both horizons and (where applicable) both faults suggests an approximate error in the location of each fault cutoff on the order of 100 m. This suggests a maximum error in displacement analysis results (presented below) of approximately +/- 250 m.

The balancing results show an increase in structural shortening toward the northwest from 17% for section A, to 26% for section C (Figures 2.9 - 2.11). The calculation of structural shortening involves dividing the difference between the final, deformed state section length (the same for all three sections in this case) and the restored section length by final section length, and multiplying by 100.

2.2.3 Fault displacement

The relatively well-constrained 3-D geometry of this structure allows detailed analysis of changes in thrust fault displacement along-strike, without the ambiguity in interpretation of along-strike fault linkage relationships inherent in 2-D seismic data analysis. The distance between hangingwall and footwall cutoffs for a given horizon, measured along the fault plane defines displacement. Displacement of the Mississippian horizon, measured at 250 m intervals, allows detailed analysis of along-strike displacement variations on the thrust faults involved in this structure.

Figure 2.12 illustrates displacements measured on the two individual thrust faults, and the total displacement for the thrust system. Displacement on the upper thrust fault (Fault 1) increases toward the northwest (up to 1000 m), then decreases rapidly to 300 m near the northwest edge of the survey area (Figure 2.12a). The lower thrust fault (Fault 2) displays a steady increase in displacement toward the northwest beyond its initiation point, 1750 m from the southeast edge of the survey area (Figure 2.12a). Displacement on Fault 2 becomes relatively constant at 1100 m toward the northwest edge of the survey area (Figure 2.12a, beyond Point B). Figure 2.12b illustrates total displacement on the two thrust faults, with separate shaded regions representing the distribution of displacement between them. The total displacement curve indicates a relatively smooth, linear increase in displacement from approximately 800 m at the southeast edge of the survey area, to a maximum total displacement of approximately 1600 m at the northwest edge (Figure 2.12b). It is important to remember the possible error in fault cutoff locations highlighted in the balancing results presented above, however fault cutoffs are likely interpreted to within 1-2 traces (+/- 25-50 m) in the 3-D seismic data.

2.2.4 Fault cutoffs

Map traces of the hangingwall (HW) and footwall (FW) cutoffs help elucidate the geometry of the thrust system, and contribute to an understanding of the deformational history in this area. Figure 2.13a shows the present map traces of the HW and FW cutoffs for each of the two faults. The area between the HW and FW cutoffs for the Mississippian horizon on each fault represents the displacement (horizontal component)

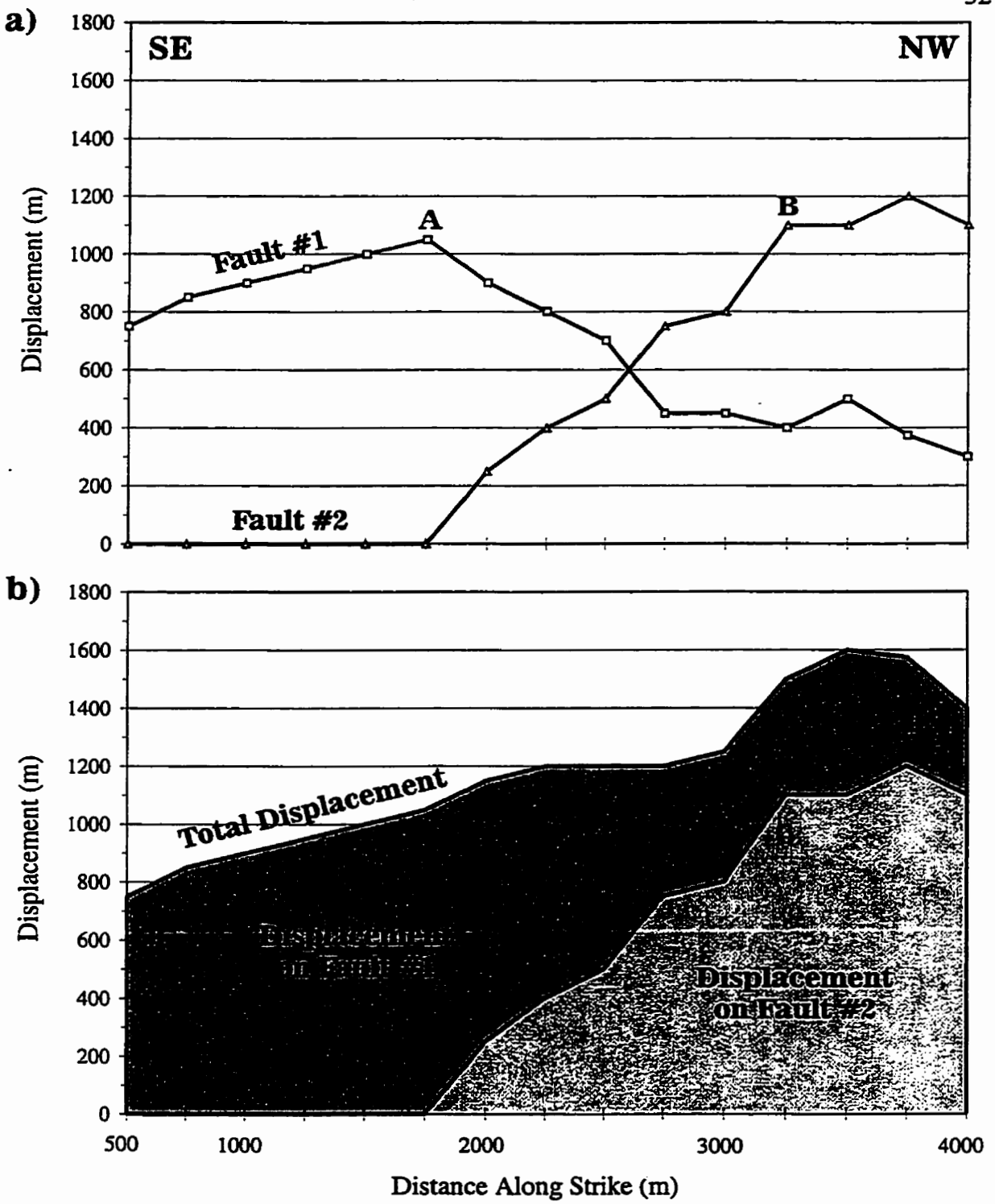

Figure 2.12. Displacement analysis for the thrust faults interpreted in the Wildcat Hills 3-D survey area (displacement measured on diplines every 250 m). a) Graph illustrating the changes in displacement along-strike southeast to northwest (left to right, respectively) on the individual faults: Fault #1 = upper thrust fault, Fault #2 = lower thrust fault (e.g. Figure 2.4). b) Graph illustrating displacement on individual faults (shaded), and the total displacement for the thrust system.

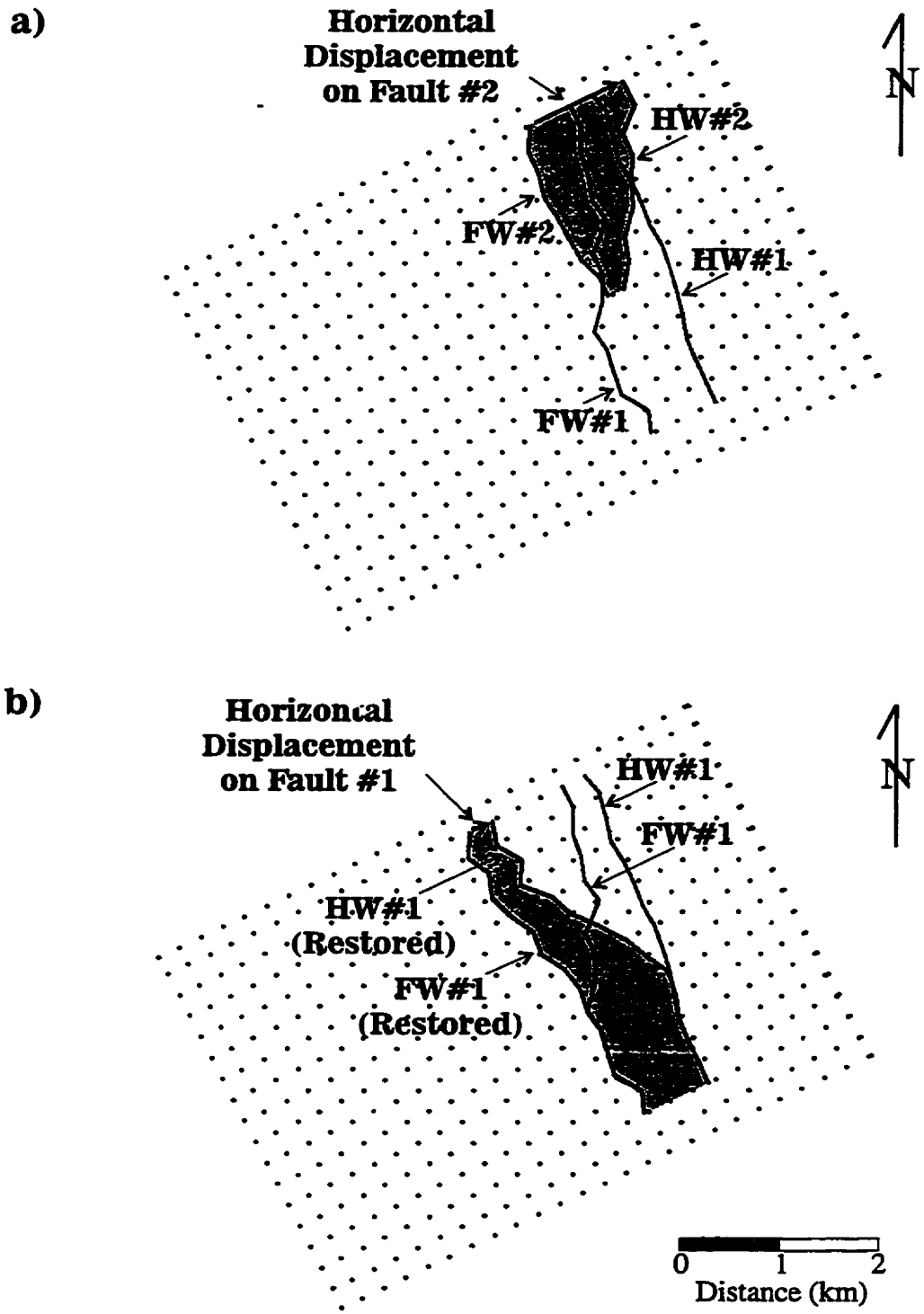

Figure 2.13. Hangingwall (HW) and footwall (FW) cutoff maps for the Top Mississippian horizon. a) Present map locations of cutoffs, with displacement on Fault #2 (lower thrust fault) shaded. b) Map location of cutoffs for Fault #1 (upper thrust fault) before and after restoration of displacement (horizontal component) on Fault #2. Note the consistent northwest orientation of the footwall cutoff for Fault #2 (a), and the restored location of the footwall cutoff for Fault #1 (b). Grid node separation = 250 m.

on that fault. The horizontal displacement for Fault 2 (HW minus FW, shaded on Figure 2.13a), subtracted from the HW and FW cutoffs for Fault 1 produces a map of their approximate restored position prior to displacement on Fault 2 (Figure 2.13b). The restored FW cutoff for Fault 1 has a trend of 326°, close to that of the present FW cutoff trend for Fault 2 (335°) (Figures 2.13a,b). This assumption of discrete deformation episodes for each fault is an over-simplification, as the thrust faults likely developed contemporaneously. Again, these data are subject to the possible fault cutoff location errors described above.

The consistent orientation of FW cutoffs may provide an important clue as to why thrust faults developed in this location. For example, the similarity in orientation between the observed FW cutoffs and the trend of a 1.5 km wide time structure anomaly on the Top Mississippian and Near Basement horizons along the southwest edge of the survey area may indicate structural control on the location of these thrust fault ramps (Figures 2.7, 2.8). The FW cutoffs lie east of this time structure anomaly, 4 km from the southwest edge of the survey, but the similarity in trend is striking (Figures 2.7, 2.8, 2.13). If the faults formed independently of some pre-existing discontinuity (stratigraphic or structural), strictly in response to compressional stress, then the local principal stress direction during deformation was likely perpendicular to the FW cutoff trend (approximately 060°). The later hypothesis is consistent with physical model results, which suggest coplanar faults may nucleate along a buckle fold that develops perpendicular to the principal stress direction prior to thrusting (Liu and Dixon, 1991).

CHAPTER 3: WILDCAT HILLS 3-D NUMERICAL DEPTH MODEL

3.1 Model Building Procedure

The procedure used in converting the structural interpretation of the Wildcat Hills 3-D seismic survey (Chapter 2) into a numerical depth model consists of several steps, summarized graphically in Figure 3.1. 3D-AIMS numerical modeling software, provided to the University of Calgary by GX Technologies, is the platform used for model building and ray-tracing experiments in this thesis.

The first step in the model building procedure was to create a link between the seismic interpretation software (SEISX) and the model building software (3D-AIMS) (Figure 3.1). Interpreted horizons were smoothed (250 x 250 m moving average) and exported from SEISX in ASCII format. The file contained X, Y, and time coordinates for a grid over the survey area (100 m grid node spacing). This file was edited to match 3D-AIMS ASCII grid file format by removing UTM coordinates and converting line number references to X and Y distance coordinates. Edited grid data, imported into 3D-AIMS, constrain numerical time model horizons (Figure 3.1). This time model, depth-converted using 3D-AIMS, provides geometric constraints for a final numerical depth model (Figure 3.1). The following sections describe the model building procedure in more detail.

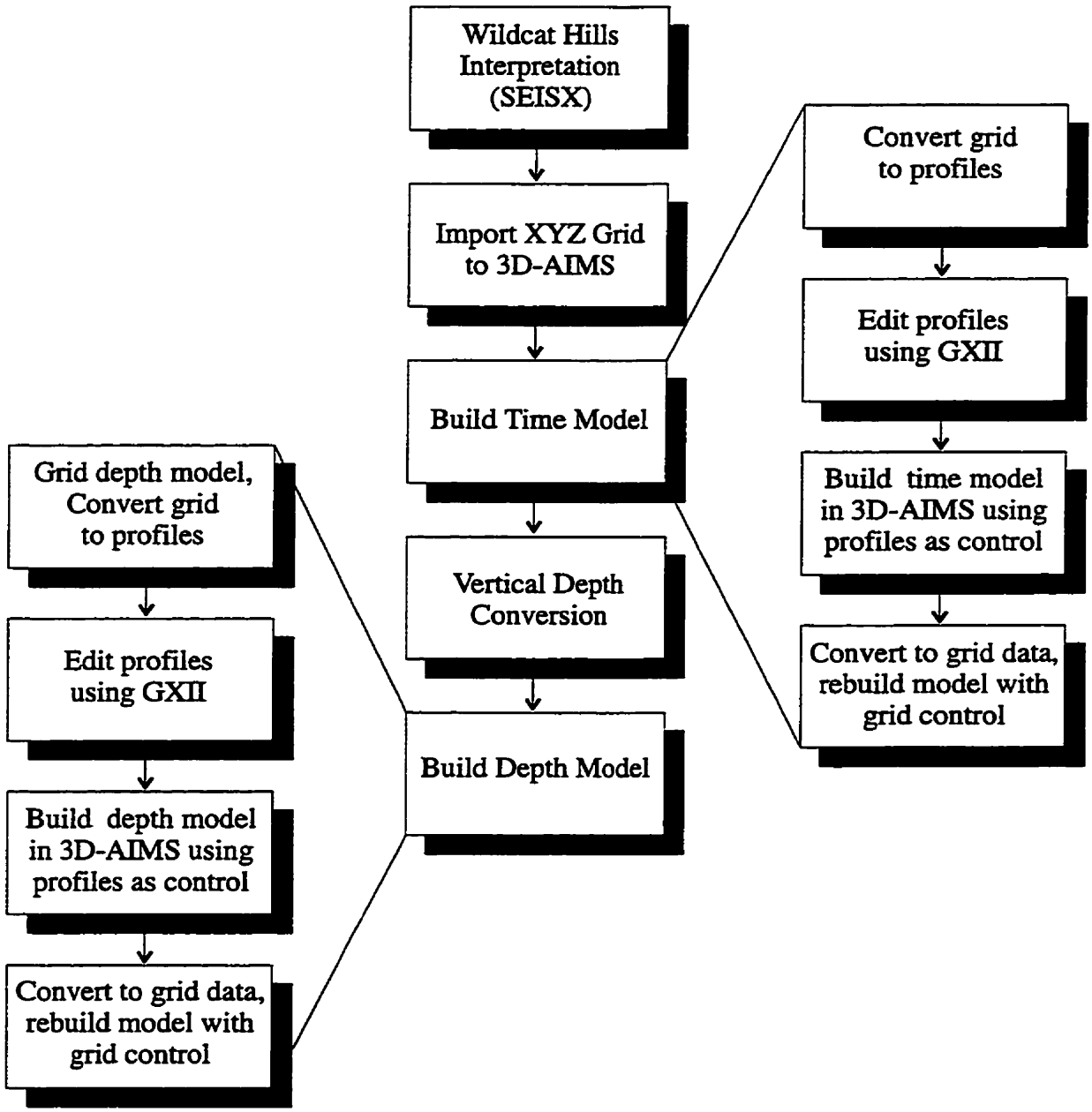

Figure 3.1. Flow chart illustrating the model building procedure. Main work flow outlined in the central column, with more detailed work flows for time and depth model construction also shown. Refer to text for more detailed discussion of model building procedure.

3.2 Time Model Construction

The grid data generated from the seismic data interpretation (imported into 3D-AIMS) were converted into profiles every 100 m in the dip direction, producing 42 profiles (Figure 3.1). The grid data were incomplete near the edges of the survey area where seismic data are missing or the interpretation is incomplete because of low signal to noise ratios (Figure 3.2). Profiles with sufficient control points on all interpreted horizons and faults were selected for editing (Figures 3.1, 3.2). Profile #6 was the complete profile closest to the southern boundary of the model area, 500 m from the edge. Profile #40 was the profile nearest the northern boundary of the model area with complete horizons and faults, 200 m from this edge. Profiles #6 and #40 were copied to profile locations #1 and #46 to constrain the geometry of the model at its northwest and southeast boundaries (Figure 3.2). Profiles missing faults were removed, creating an average final profile spacing of approximately 200 m in the central part of the model, increasing up to 500 m near the edges of the model. Figure 3.2 shows the locations of profiles selected to constrain the geometry of the numerical model.

The selected profiles (Figure 3.2) were edited, as described below, using GX2 (GX Technologies); a 2-D numerical modeling package with a more powerful profile-editing module than 3D-AIMS (Figure 3.1). The models presented here do not include the Base Mississippian horizon (Chapter 2) because this horizon caused problems in early model-building attempts. Using GX2, the Top Mississippian and Near Basement horizons were: (i) joined across zones where grid data were incomplete, and (ii) tied to

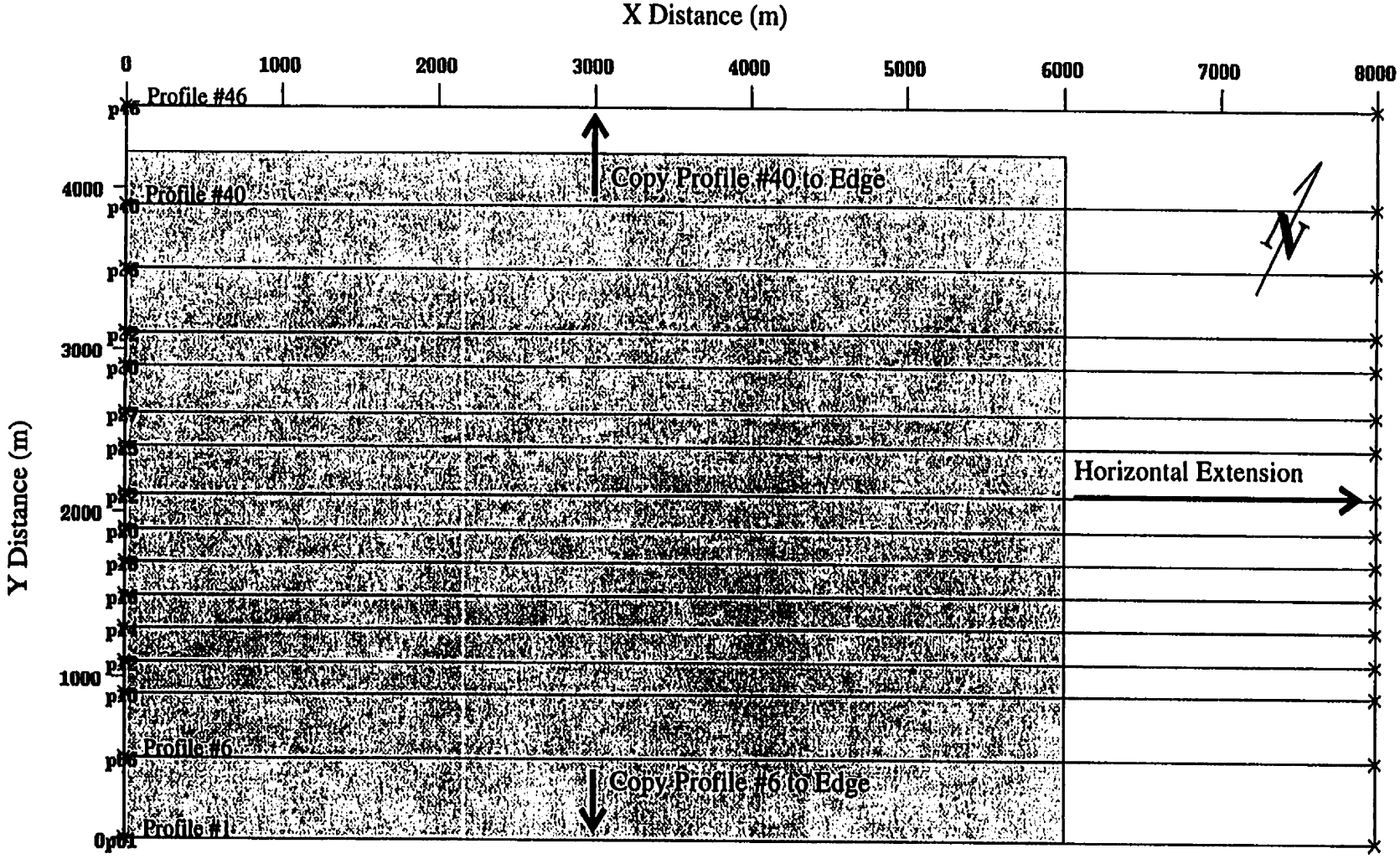

Figure 3.2. Profiles from interpretation grid data (Survey dimensions shaded) selected for editing and use in constraining time model construction (Final time model dimensions shown) (north arrow indicates model north). Profile #1 = copy of Profile #6. Profile #46 = copy of profile #40. Refer to text for discussion of profile selection and editing criteria.

model boundaries and faults. The profiles were also continued east of the survey area to allow collection of larger source-receiver offsets in ray-tracing experiments (Figure 3.2).

3-D surfaces, constrained using the edited profiles, define the structural geometry of the model (Figure 3.1). Spline patches were used to create horizon surfaces between control profiles (Figure 3.1, 3.2). This procedure produced discontinuities at patch boundaries (along control profiles) that caused problems in ray tracing. The large number of patches produced in this procedure also reduced the computational efficiency of ray-tracing algorithms in 3D-AIMS. Converting this model to grid data (100 m grid node separation) and re-building horizons using a minimum number of spline patches resolves these problems (Figure 3.1).

The time model preserved the broad structural detail of the seismic data interpretation for all horizons included in the model. Figure 3.3 shows a comparison between time structure contour maps of the Top Mississippian horizon in the hangingwall of the upper thrust sheet for: a) the smoothed seismic data interpretation (contoured where seismic data exists), and b) the final time model. This horizon is accurately reproduced in the model, except for areas near the edges of the model and the slightly sinuous nature of contours between 1640 and 1700 m. The sinuous nature of these contours is likely an artifact of the spline surface-fitting procedure. Figure 3.4 is similar to Figure 3.3, but compares time structure maps of the Near Basement horizon before and after model building. The time model horizon is a reasonable facsimile of the interpreted horizon from the seismic data except near the model edges and, obviously, beyond the area of seismic data coverage (Figure 3.4).

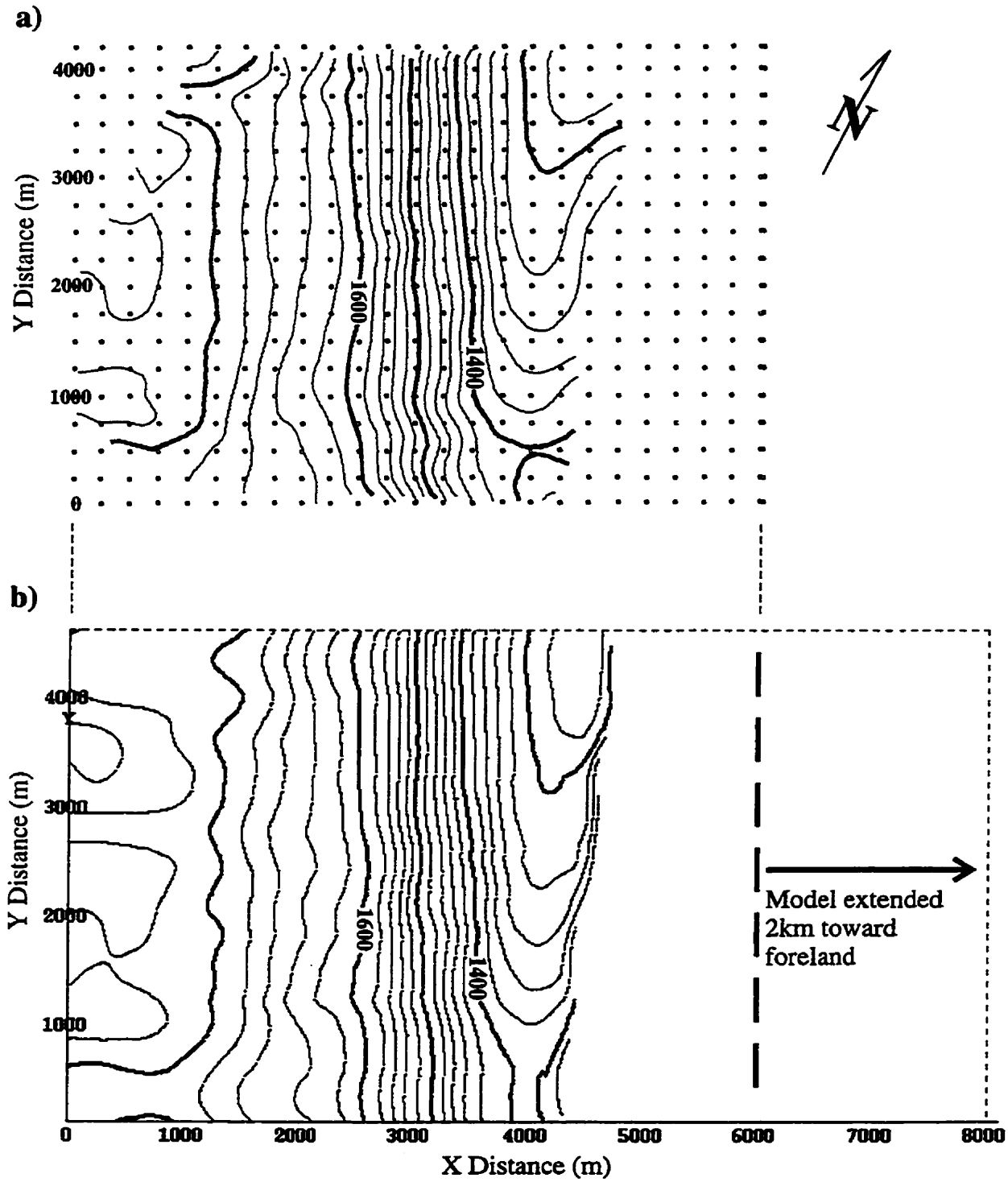

Figure 3.3. Time structure map comparison for the hangingwall Mississippian in the upper thrust sheet between: (a) 3-D seismic interpretation, and (b) the final time model. The model preserves the time structure observed in the interpretation, except near the edges of the 3-D survey area where grid data were incomplete and assumptions (described in text) were made. Contour interval = 20 ms. North arrow indicates model north.

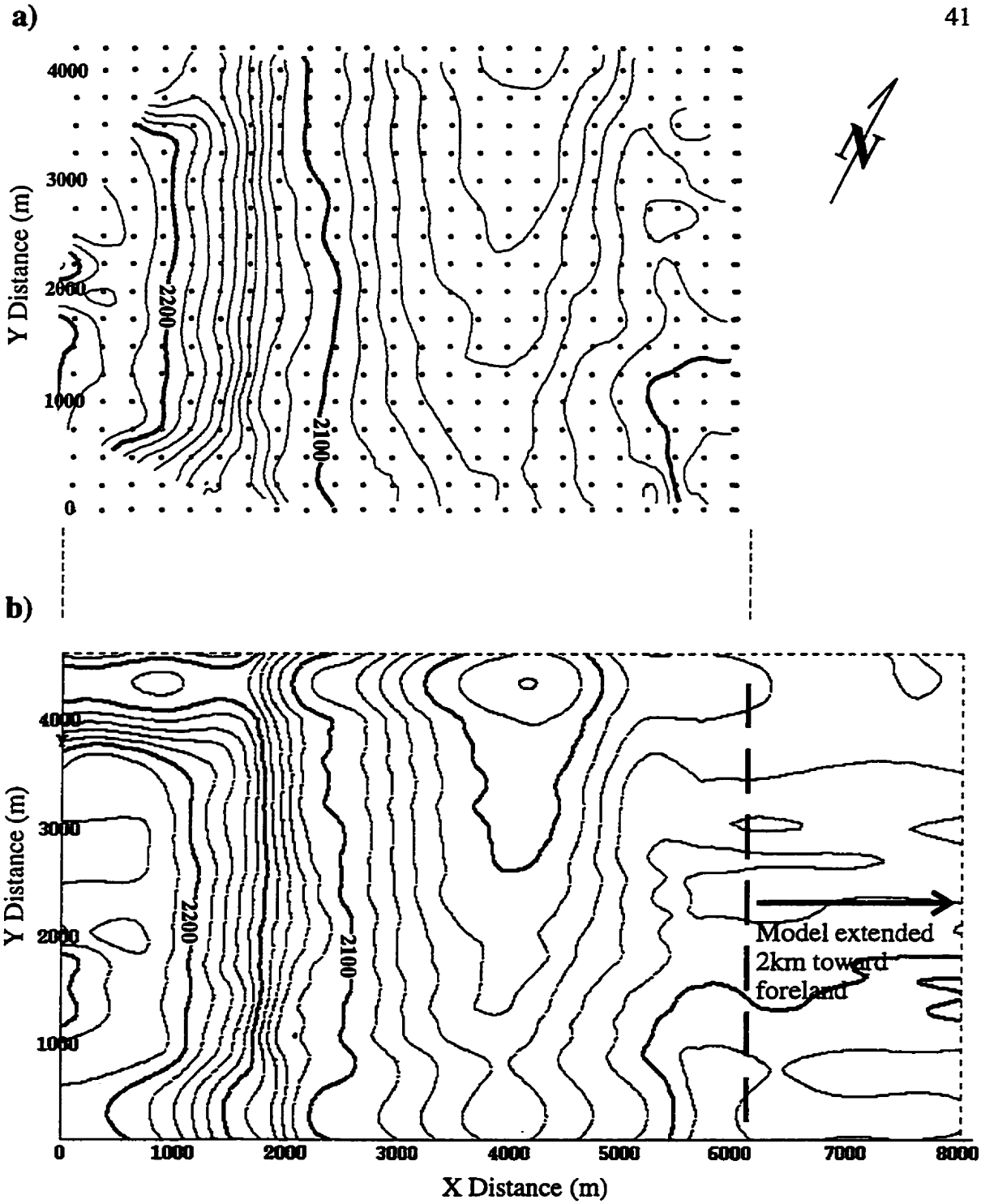

Figure 3.4. Near Basement time structure map comparison between: (a) the interpretation, and (b) the final time model. The model preserves time structure observed in the interpretation except near the edges of the 3-D survey where grid data were incomplete and assumptions (described in text) were made. Contour interval = 10 ms.

3.3 Depth Model Construction

3.3.1 Time-to-depth conversion

Time-to-depth conversion provides the link between the time model and the depth model (Figure 3.1). The two variables that control the depth conversion results are: (i) the velocity model, and (ii) the depth-conversion method.

3.3.1.1 *Velocity model*

The structurally complex nature of the Mesozoic section in the Wildcat Hills area (Figure 1.2) requires simplification of the velocity model for this interval. The three wells within the Wildcat Hills 3-D survey area with available digital sonic log data (Figure 2.1) were used to construct the velocity model in this interval. Figure 3.5 shows the sonic log data through the Mesozoic interval, and the results of linear regression on these data for each well. The intercept (surface) velocities vary within 5% (average = 3547 m/s) and the velocity gradient varies within 15% (average = 0.323 s^{-1}). The linear regression results constrain the vertical velocity gradient (0.32 s^{-1}) and intercept (surface) velocity (3500 m/s) used for the Mesozoic interval in the model (Figure 3.6a). This vertically-varying interval velocity model, created using available sonic log data, is based on the assumption that velocity increases with depth of burial. The Mesozoic interval velocity used in the depth conversion of profiles for structural balancing (4600 m/s, Chapter 2) could not include a vertical gradient so an average interval velocity for the lower part of the section was used (below 2800 m in well 6-30, Figure 3.5).

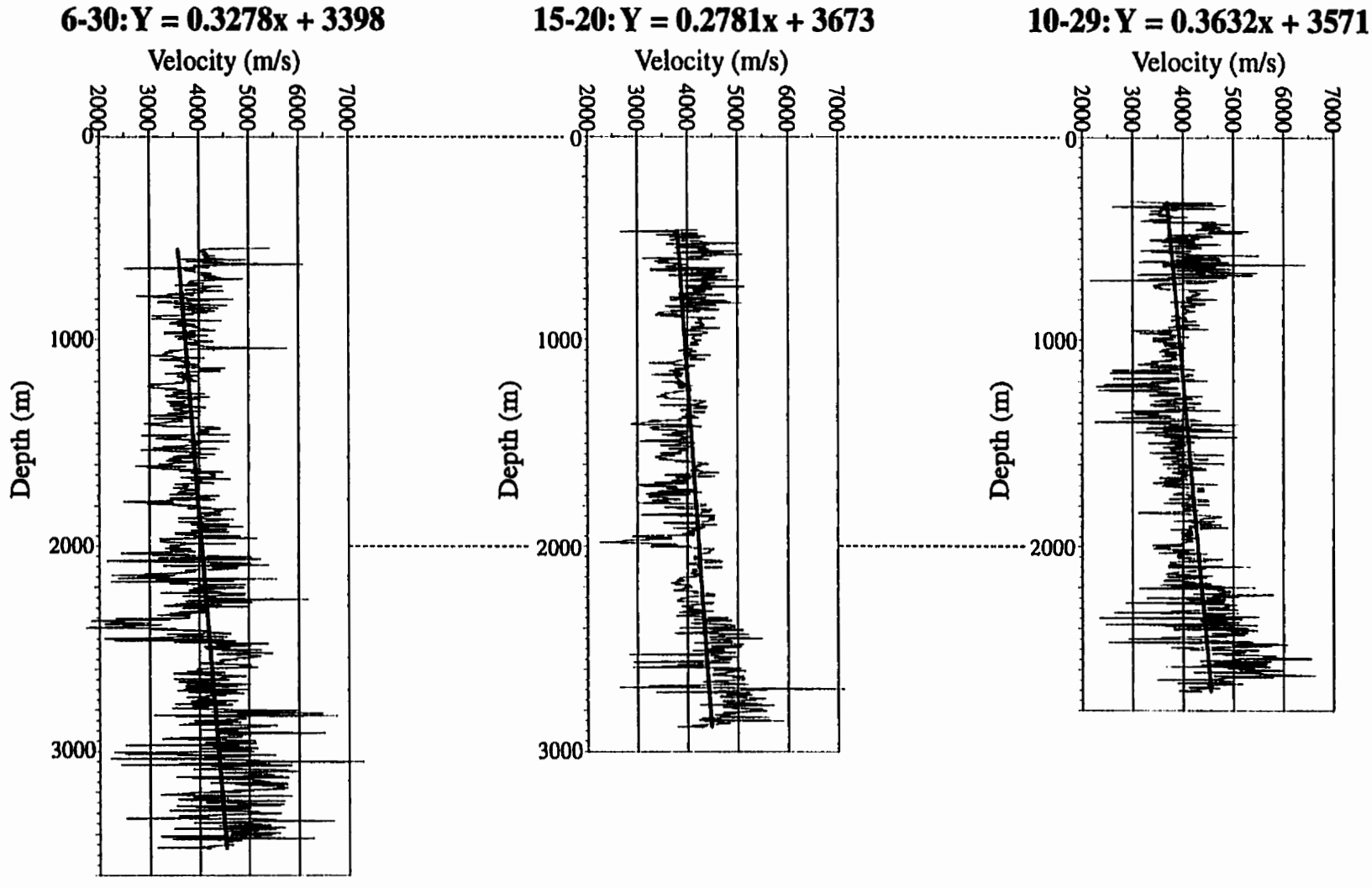

Figure 3.5. Sonic logs for the three wells within the Wildcat Hills 3-D survey area (Figure 2.1) with linear regression curves and equations shown. Intercept velocity (V_0) and gradient values are relatively stable with averages of 3547 m/s and 0.3230 s^{-1} respectively. Intercept velocity = velocity at kelly bushing (approximately = surface velocity). Average kelly bushing elevation for these wells = 1246 m, with a deviation of +/- 5 m.

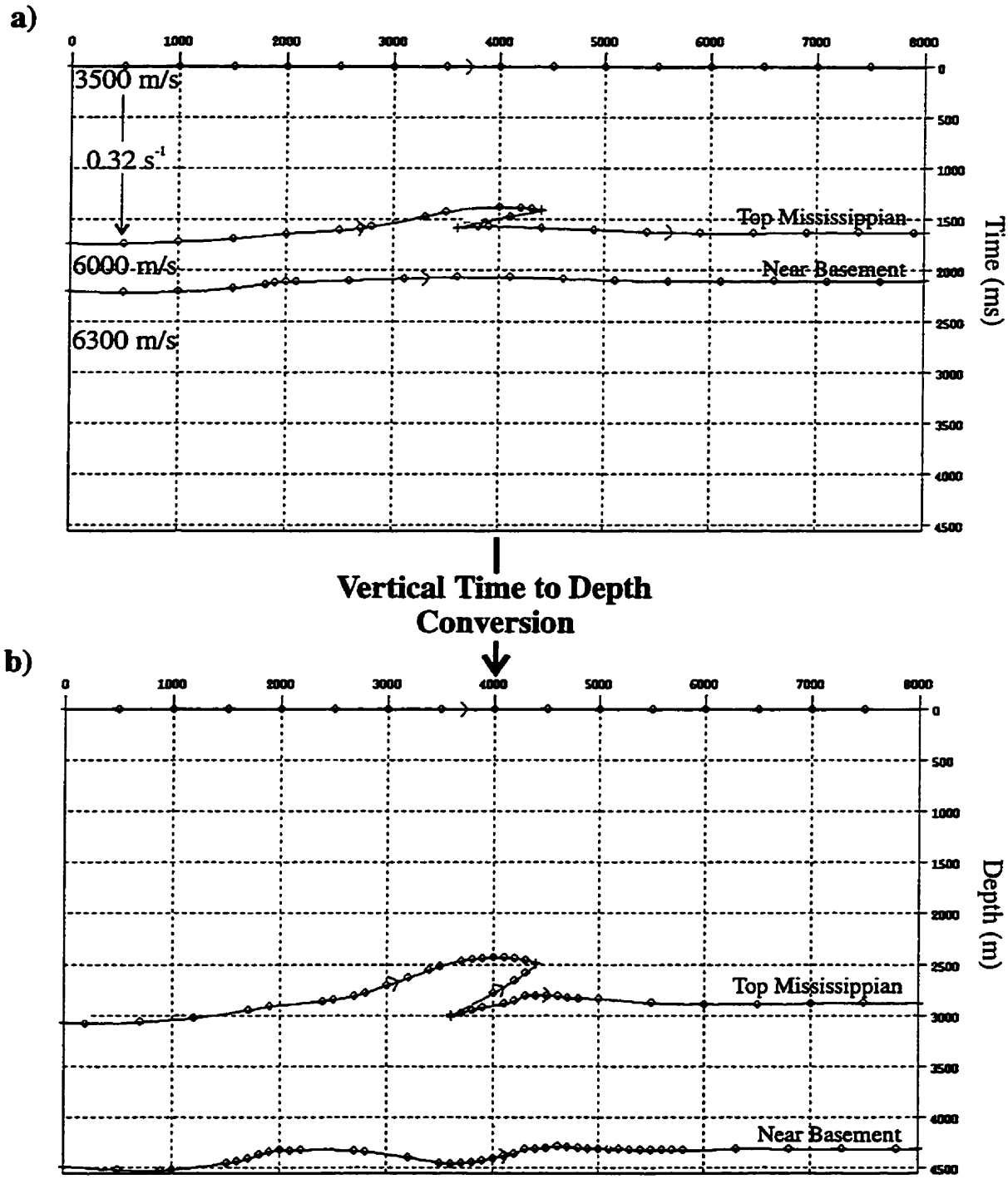

Figure 3.6. Figure illustrating the effect of vertical time-to-depth conversion (interval velocities annotated) on a dip profile through the numerical model located 1000 m north of the southern edge of the model (refer to Figure 3.4 for location): a) section through final time model, and b) section through depth-converted model. Refer to text for discussion of results.

The paucity of sonic log data below the Mesozoic section in this area requires the assumption of a constant interval velocity for the Paleozoic section. A constant 6000 m/s velocity describes the entire Paleozoic interval, representing a regional average (Figures 1.3, 3.6a). The half-space (below the Near Basement horizon) is assigned a velocity of 6300 m/s (Figure 3.6a) in order to produce an impedance contrast which will generate reflections from the Near Basement horizon in ray-tracing experiments.

3.3.1.2 *Depth conversion method*

The vertical time-to-depth conversion method was used for this model. This procedure uses interval velocities to convert two-way-traveltimes to depth, and assumes that reflection energy travels vertically through the section. Depth conversion using image rays is more appropriate for time-migrated data (such as the Wildcat Hills 3-D data), however 3D-AIMS was unable to depth convert using this method at the time of model building. The vertical time-to-depth conversion procedure provides an acceptable depth conversion result for the purposes of this study (Figure 3.6). The time structure anomaly below the thrust repeats of Mississippian strata on the Near Basement and footwall Top Mississippian horizons was slightly overcompensated (Figure 3.6b), which suggests that the interval velocity model, depth conversion method, or seismic data interpretation were incorrect.

3.3.2 Final depth model

The procedure for depth-model construction followed that described above for time-model construction (Figure 3.1), using grid data generated from the depth-

conversion results rather than directly from the seismic data interpretation. The depth-converted model was converted to grid data (100 m grid node spacing), and then to dip profiles with a 200 m line spacing (Figure 3.1). Figure 3.7 illustrates the procedure for removal of the depth anomaly on the footwall Top Mississippian and Near Basement horizons below the thrust repeats of Mississippian strata. This anomaly, described above as the result of improper depth conversion, does not likely represent real depth structure. The correction involved moving points on the footwall Top Mississippian horizon up to a flat datum and shifting corresponding points on the Near Basement horizon an equal distance (Figure 3.7). This correction is based on the assumption that the Top Mississippian horizon in the footwall of the structure is flat.

Horizons in the depth model were first built using spline patches between the edited profiles, and then grid data generated from these horizons were used to define a minimum number of spline patches in the final depth model. Figure 3.8 shows perspective views of the final depth model viewed in the strike direction: a) looking northwest, and b) looking southeast. Figure 3.9 shows perspective views looking in the dip direction: a) from the northeast, and b) from the southwest. These perspective views of the model help visualize the structural variability along strike in the area, including changes in: (i) elevation of the structure, (ii) the number of faults, and (iii) displacement on these faults (Figures 3.8, 3.9). East- and northeast-trending low-amplitude, short-wavelength structural variations are apparent on the Mississippian horizon in the hangingwall of the upper thrust sheet (Figures 3.8, 3.9). These features are more apparent on a structure contour map of this horizon (Figure 3.10a). The east-trending features near

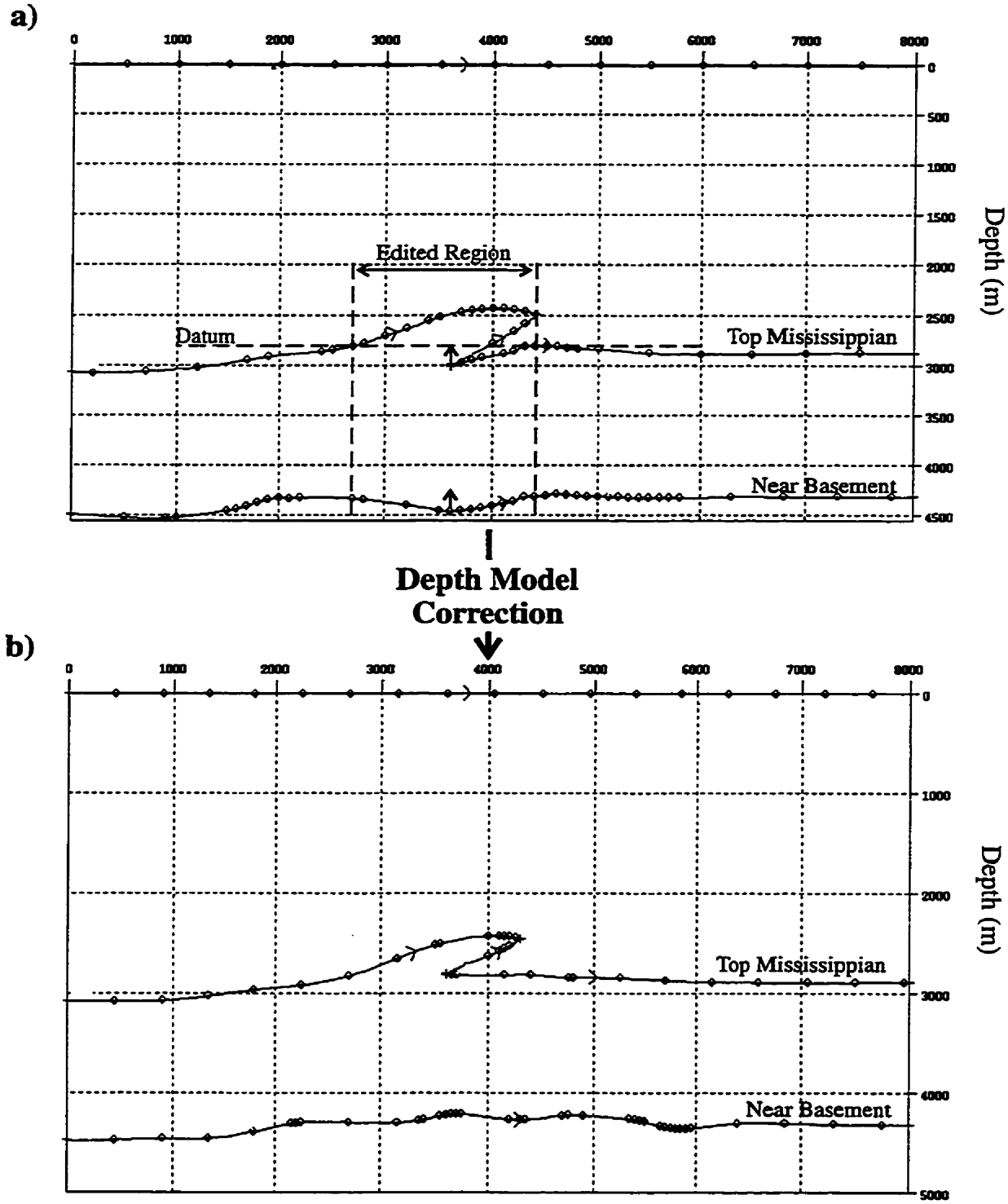

Figure 3.7. Figure illustrating the effect of editing the depth-converted model, using the same profile shown in Figure 3.6. Section (a) shows the depth-converted result (as in Figure 3.6b), section (b) illustrates the final depth model after removal of depth conversion errors below the structure and re-gridding (procedure described in text).

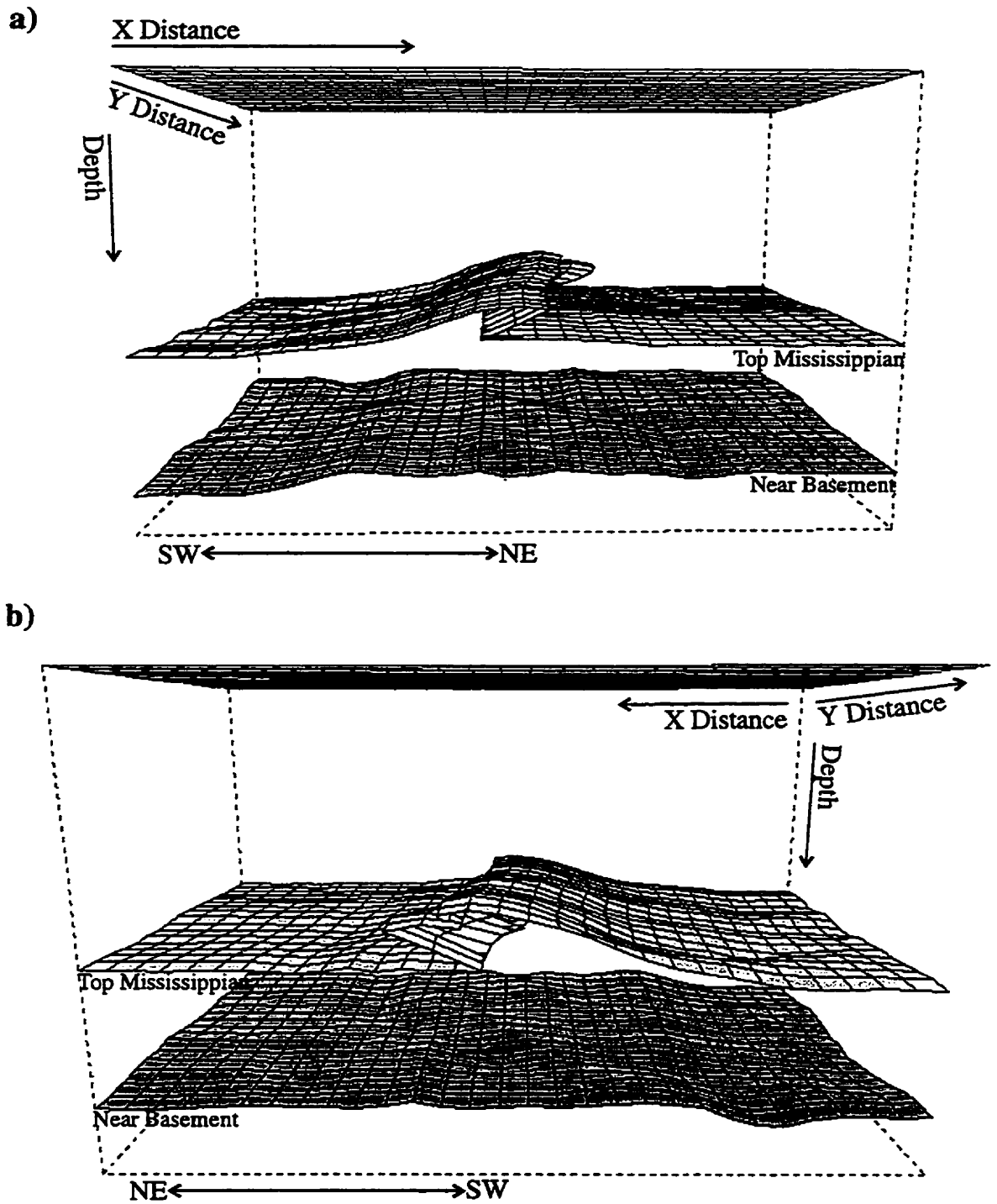

Figure 3.8. Perspective views of the final depth model looking in the strike direction: a) looking northwest, b) looking southeast. Note the increase in structural level of the Top Mississippian marker and the addition of the lower thrust slice toward the north. Note also the irregular nature of the Near-Basement and hangingwall Mississippian horizons. Refer to contour maps for horizon depth information (Figure 3.10).

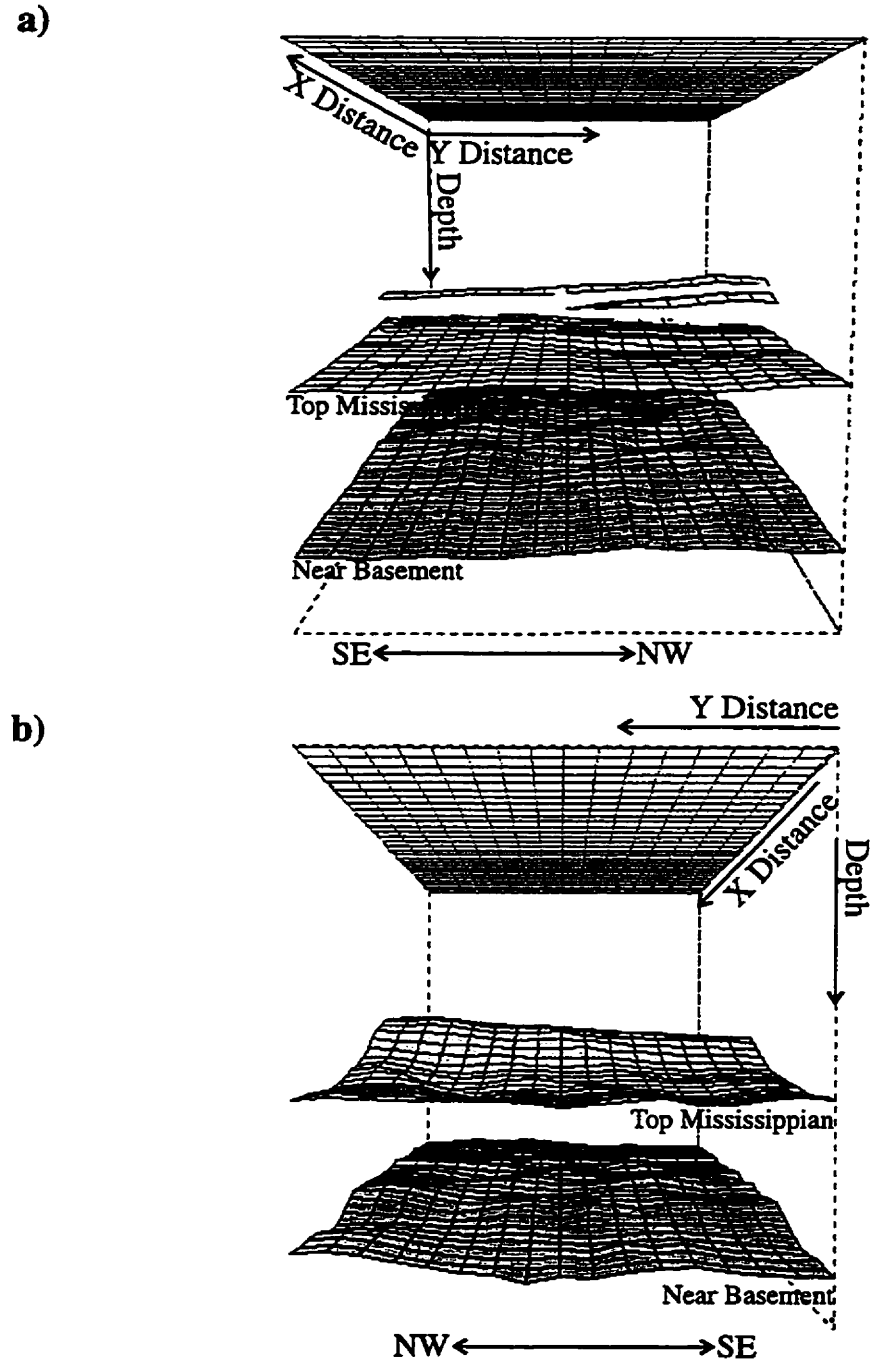

Figure 3.9. Perspective views of the final depth model looking in the dip direction: a) looking southwest, b) looking northeast. Note the increase in structural level of the Top Mississippian marker and the addition of the lower thrust slice toward the north. Note also the irregular nature of the Near-Basement and hangingwall Mississippian horizons. Refer to contour maps for horizon depth information (Figure 3.10).

a)

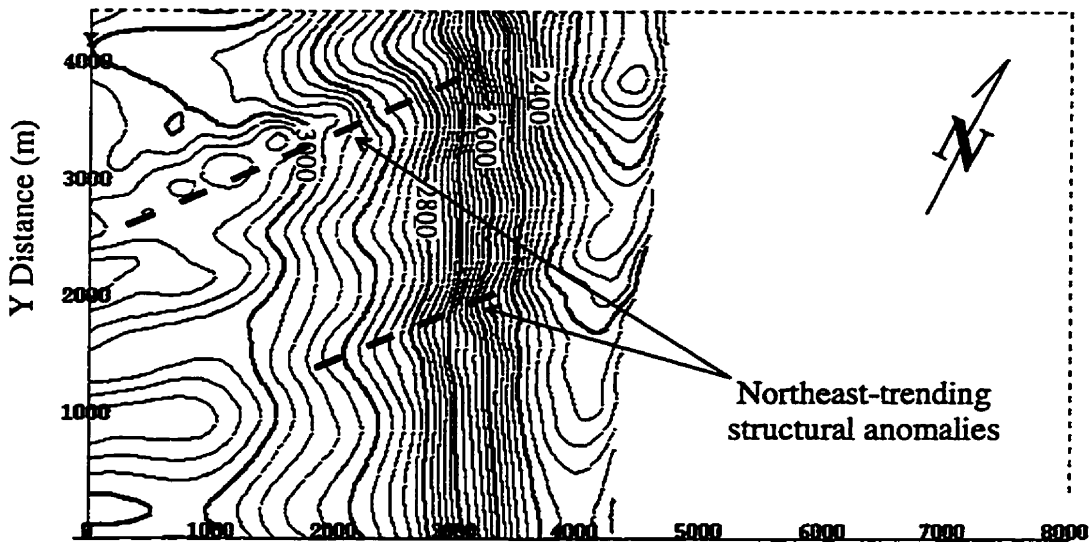

b)

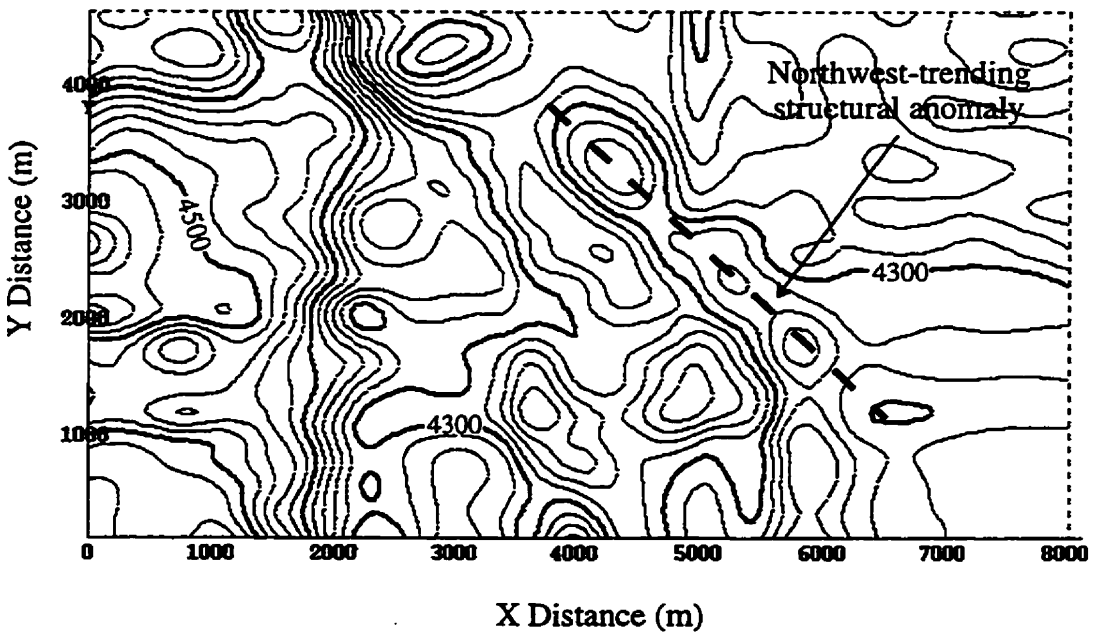

Figure 3.10. Structure contour maps of the final depth model: a) Top Mississippian in the hangingwall of the upper thrust, b) Near Basement. Note the increase in structural level of the Top Mississippian horizon toward the north. Note also the irregular nature of the Near Basement horizon and the presence of east- and northeast-trending structural variations on the hangingwall Mississippian horizon. Contour interval = 20 m for both maps.

the western edge of the model correspond to anomalies on the time structure map for this horizon, discussed in Chapter 2 (Figure 2.6). The northeast-trending structures, not obvious on the time structure map, appear to be an artifact (of unknown origin) generated during depth-conversion. The Near Basement horizon (Figure 3.10b) is somewhat irregular in the final depth model, but it is relatively flat with no anomaly below the location of thrust repeats of Mississippian strata. The Near Basement structure contour map shows a curious northwest-trending structural low in the west-central part of the model (Figure 3.10b). A relatively sharp break in structural level (60 m) 2 km from the southwestern edge of the model corresponds roughly to the northeast boundary of a broad negative time-structure anomaly observed on both the Top Mississippian and Near Basement horizons in the Wildcat Hills 3-D survey area (Figure 2.7).

CHAPTER 4: 2-D Ray-Tracing Over the 3-D Numerical Model

4.1 Introduction

The ray-tracing experiment described in this chapter aims to evaluate the effects of 3-D subsurface structure on 2-D seismic data (the out-of-plane problem) in the Wildcat Hills area, using the numerical depth model described in Chapter 3. Out-of-plane imaging is an important problem in the interpretation of 2-D seismic data from areas with complex subsurface structure, such as the southern Alberta Foothills. The results of this work will help quantify potential errors in the delineation of subsurface structure using 2-D seismic data in similar areas.

The approach used in this evaluation of out-of-plane imaging involves collecting synthetic 2-D seismic data along five lines over the model (Figure 4.1). Results from ray tracing over the 3-D depth model (the 3-D result) are compared to those from ray-tracing using 2-D vertical sections extracted from the model (the 2-D result), for each line. Differences between the 2-D and 3-D results, which share the same acquisition and processing parameters, will illustrate out-of-plane effects on 2-D seismic data collected over the 3-D model. This study focuses on the impact of out-of-plane imaging on structural definition, with no detailed discussion regarding possible effects on reflection wavelet character. The five lines chosen for this study include four lines perpendicular to the regional structural trend (dip lines), and a single line 45° to the structural trend (oblique line). Dip line DL-1 crosses the southeastern part of the model, where a single

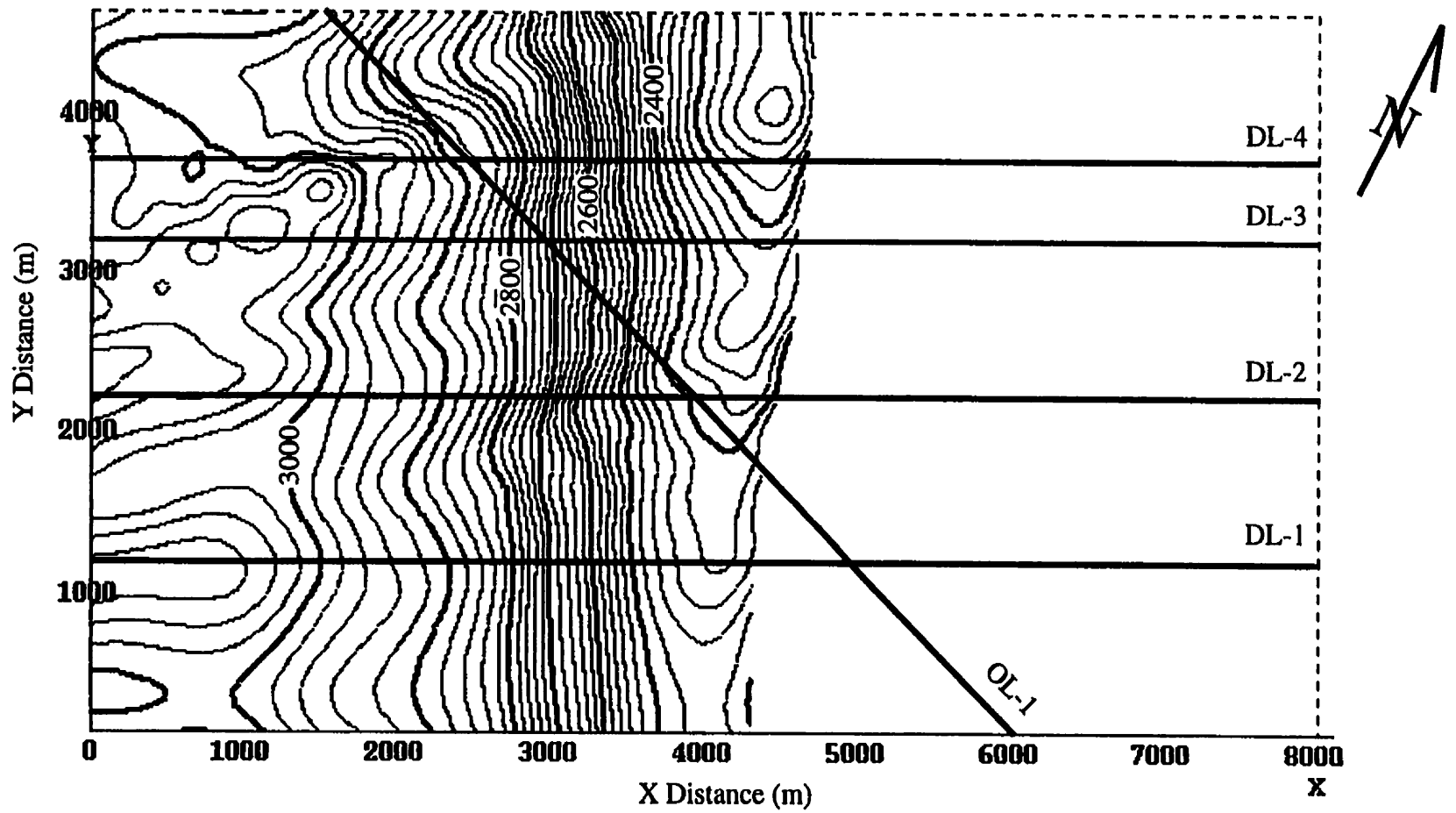

Figure 4.1. Location map for 2-D seismic lines over the 3-D numerical depth model. Structure contour map of the Top Mississippian horizon in the hangingwall of the upper thrust fault shown for reference (contour interval = 20 m).

thrust sheet of Mississippian strata creates a gently plunging structure (Figure 4.2a). Dip line DL-2 crosses the structure where it changes from a single thrust sheet of Mississippian strata to a stack of two sheets (Figure 4.2b). The other two dip lines (DL-3 and DL-4) cross the more complex part of the structure where two thrust faults, with laterally varying displacements, cause imbrication of Mississippian strata (Figure 4.3). Together, the four dip lines allow the evaluation of changes in out-of-plane effects as the structure becomes increasingly complex toward the northwest. Collection of seismic data perpendicular to the regional structural trend is the preferred, and most common, geometry used in hydrocarbon exploration. Line OL-1, which crosses the crest of the structure near the transition between one and two thrust sheets, illustrates out-of-plane effects on 2-D seismic data collected oblique to the structural trend (Figure 4.4). Acquisition of seismic data oblique to the structural trend is occasionally used in exploration programs, often to make use of existing cut-lines or roads.

4.2 Experimental Procedure

This section presents a generic discussion of the procedures used in the acquisition, processing, and analysis of multi-offset synthetic seismic data collected in this experiment. Multi-offset synthetic seismic data were collected in this study in order to simulate acquisition and processing procedures commonly used in natural experiments.

3D-AIMS numerical modeling software is used in the collection of synthetic seismic data through ray tracing, and these data represent the full 3-D acoustic seismic response for the numerical depth model, including out-of-plane effects. The ray-tracing

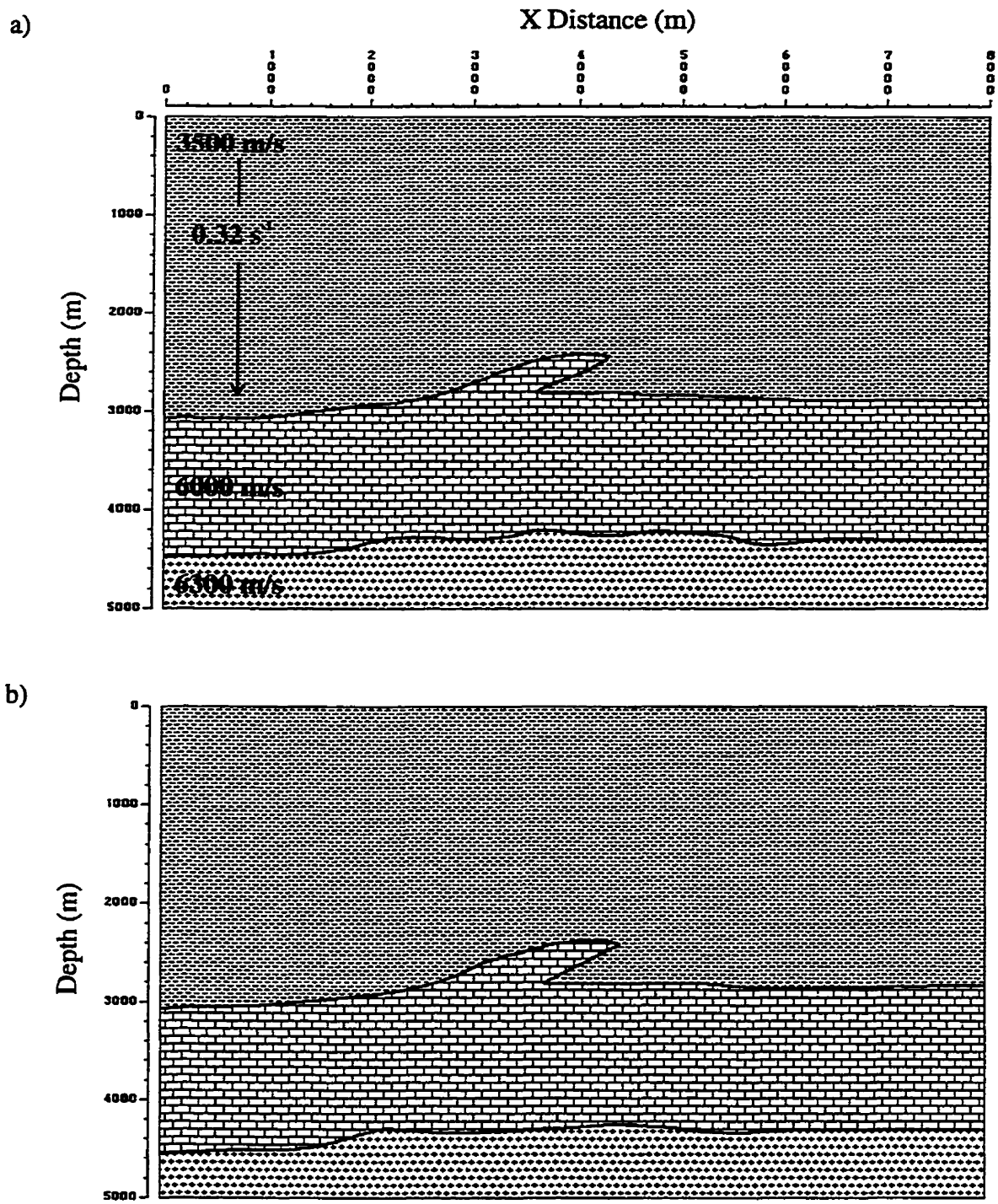

Figure 4.2. Cross-sections through the 3-D numerical depth model below lines: (a) DL-1, and (b) DL-2 (Figure 4.1). The target structure in this, the southern part of the model consists of a single thrust sheet of Mississippian strata (brick pattern) but immediately north of line DL-2 significant along-strike structural variation occurs as a second, lower thrust sheet begins to develop. The basement (cross pattern) has a highly irregular upper boundary over the entire model. Interval velocity model annotated.

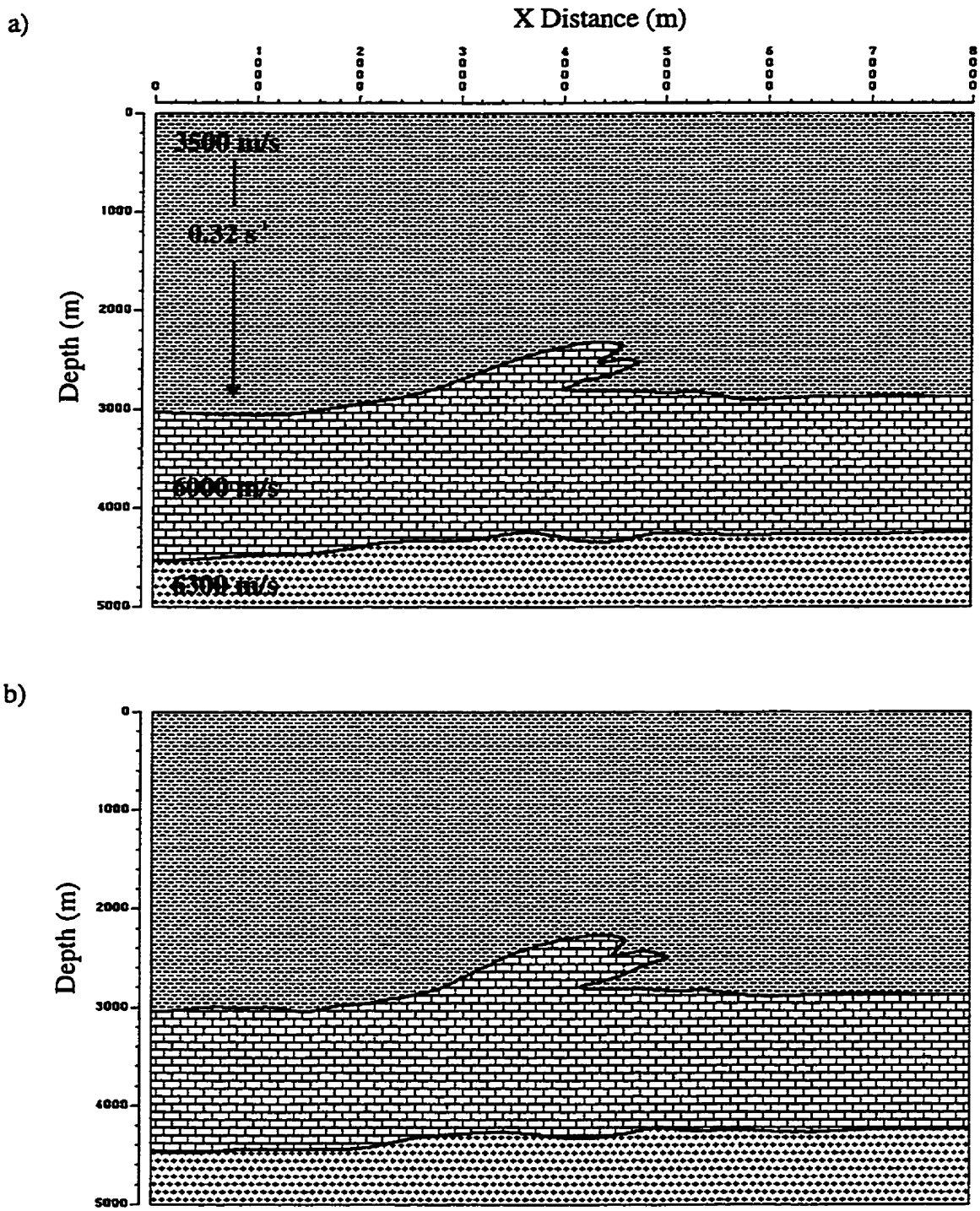

Figure 4.3. Cross-sections through the 3-D numerical depth model below lines: (a) DL-3, and (b) DL-4 (Figure 4.1). The target structure in this, the northern part of the model consists of two thrust sheets of Mississippian strata (brick pattern) with displacement on each thrust fault varying along strike (compare sections a and b). Interval velocity model annotated.

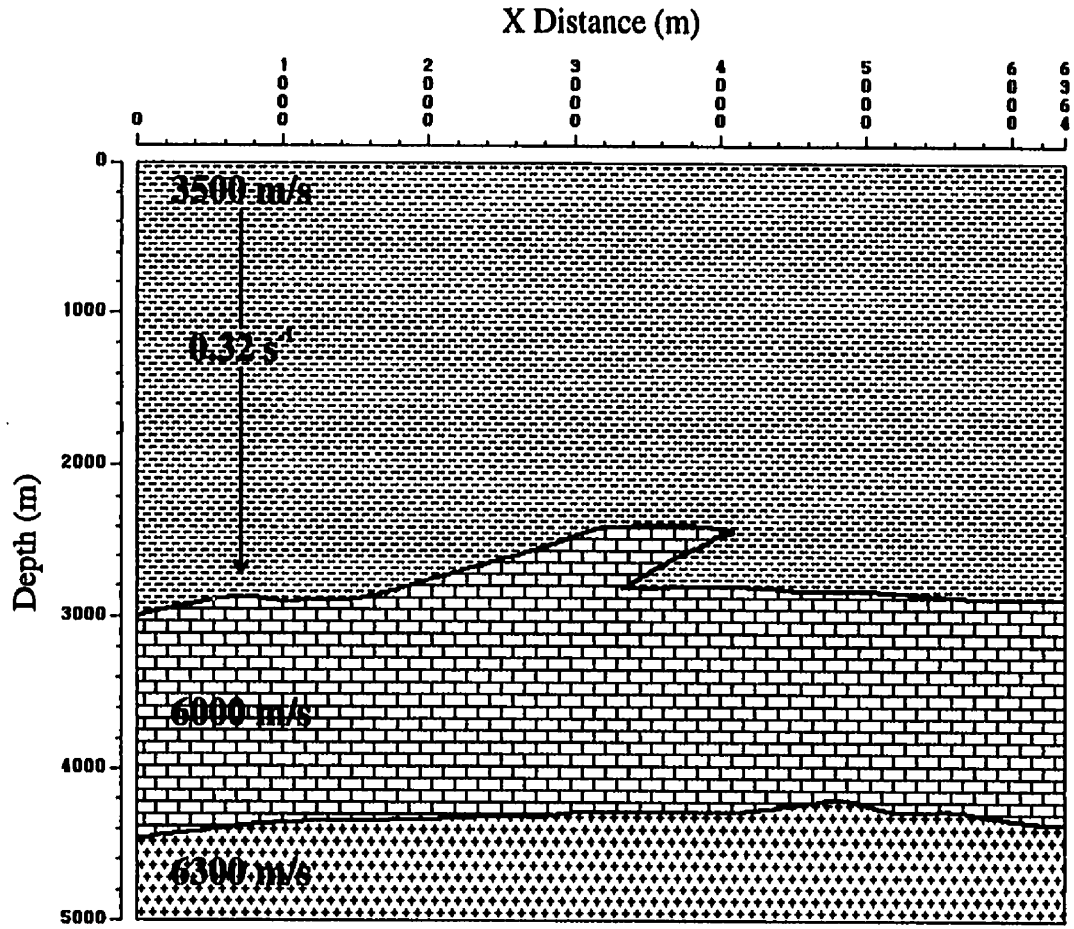

Figure 4.4. Cross-section through the 3-D numerical depth model below line OL-1 (Figure 4.1). The target structure below the profile is a single thrust sheet of Mississippian strata (brick pattern). This profile runs at 45° to the structural trend and therefore the cross-line dip for the west-dipping hangingwall of the structure should be similar in magnitude to the apparent dip in this section, and much more severe than in the dip lines. This section crosses the crest of the structure near the transition from one thrust sheet to two. Interval velocity model annotated.

procedure used by 3D-AIMS is a two-step process involving the generation of 'shooting rays' and 'two-point rays' for a given source point, reflecting from a target horizon. Shooting rays emanate in all directions from the source point, reflect from the target horizon at a user-defined density of reflection points, and return to the recording surface. When a shooting ray returns to the recording surface close to a receiver location two-point ray tracing is initiated to find the exact ray path between that source and receiver. This two-point ray is then used to initialize two-point rays for neighboring receivers. Two-way traveltimes and amplitudes calculated for successful two-point rays are used to generate synthetic seismic data. This ray-tracing procedure is repeated for all sources, and all horizons selected for analysis. 3D-AIMS will not generate diffracted rays, which should emanate from discontinuities in the subsurface.

2-D ray tracing was performed using GX2 numerical modeling software using vertical depth sections extracted from the 3-D model below each seismic line (Figure 4.1). The synthetic seismic data acquired through ray tracing using these cross-sections (Figures 4.2 – 4.4) represents the true 2-D seismic response for the structure below each line, with no out-of-plane effects. GX2 uses only two-point rays to generate synthetic seismic data. The two-point rays emanate from the source, reflect from a target horizon, and return to the recording surface. Two-way traveltimes and amplitudes are calculated for two-point rays that return to the recording surface near a receiver (within a user-defined capture radius), and used to generate synthetic seismic data. Amplitudes calculated in GX2 are based on reflection coefficients at model boundaries, and modified by the effects of energy transmission, spreading, and attenuation. Diffracted rays,

generated by GX2, emanate from discontinuities at a user-defined angular increment and travel to the recording surface.

The synthetic seismic data from both the 2-D and 3-D ray-tracing experiments share the acquisition and processing parameters outlined in Tables 4.1 and 4.2, respectively. Synthetic shot records (band-pass filtered) were exported from GX2 and 3D-AIMS, and processed using PROMAX software (Advance Geophysical Corporation). The processing flow is identical for all synthetic data presented in this study, with the exception of the velocity models used for each line (Table 4.2). Figure 4.5 shows the interval and RMS velocity models used to process line DL-1. NMO correction using RMS velocities may not provide an optimal solution, however using the RMS velocity model (converted from the interval velocity model) avoids introducing differences in the resulting sections based on different velocity analysis results.

Differences between the seismic sections generated by 2-D and 3-D ray tracing will indicate areas where out-of-plane reflections occur. The analysis presented here uses time structure differences on post-stack time-migrated synthetic seismic sections to evaluate out-of-plane imaging. The procedure used to determine time structure error was to overlay horizons and faults interpreted from the 2-D ray-tracing result onto the interpreted 3-D ray-tracing result. This approach allows the analysis of subtle time-structure differences between 2-D and 3-D ray-tracing results. Time structure differences were quantified for the Top Mississippian horizon in the hangingwall of the

Table 4.1: Acquisition Parameters for Model Seismic Data

Source Interval:	200 m
Group Interval:	50 m
Split-Spread Length:	2000 m
Time Sample Rate:	2 ms
Record Length:	3 s
Acquisition Filter:	5/10 - 50/70 Hz

Table 4.2: Processing Flow for Model Seismic Data

Import SEG-Y Data from 3D-AIMS/GX2
↓
Automatic Gain Control (500 ms window)
↓
Build Interval Velocity Model
↓
Convert Interval Velocities to RMS Velocities
↓
Common Midpoint Gathers
↓
Normal Moveout using RMS Velocity Model
↓
CMP Stack
↓
Kirchhoff Time Migration

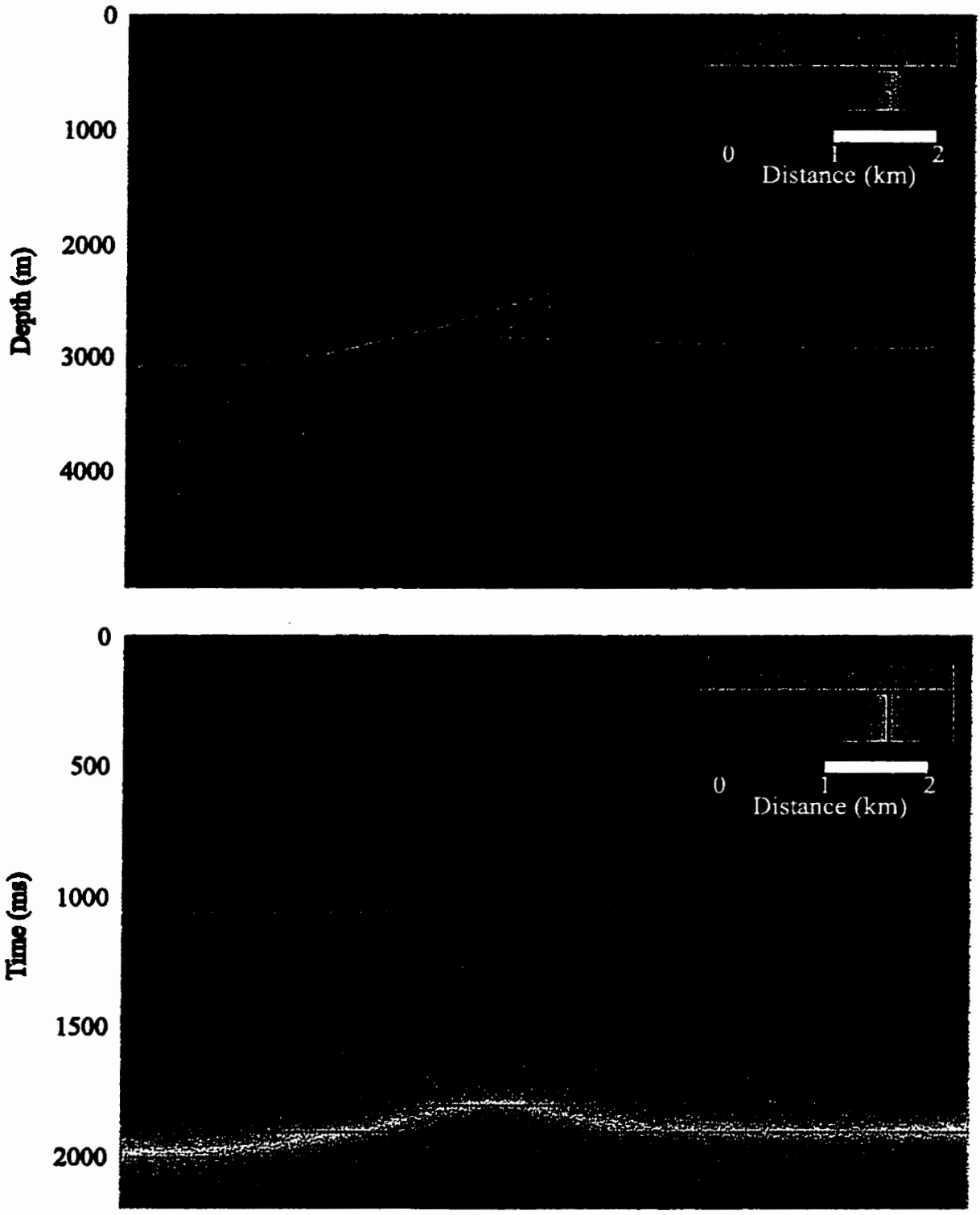

Figure 4.5. Velocity model used in processing line DL-1: (a) interval velocity model in depth created using control points from the numerical depth model (Figure 4.2a); (b) interval velocity model from (a) converted to an RMS velocity model used in NMO correction and time migration.

upper thrust sheet by calculating the separation between the two interpretations for each line. Calculation of this time structure error involves subtracting two-way traveltimes for 3-D result from the 2-D result.

Reflection points for successful two-point rays in the 3-D experiment illustrate the source of out-of-plane reflections on synthetic seismic data. Analysis of reflection points on the Top Mississippian horizon in the hangingwall of the upper thrust sheet illustrates the source of time structure differences observed between the 2-D and 3-D ray-tracing results. Reflection point displays also indicate areas where significant out-of-plane reflections do not cause significant traveltime error.

4.3 Results

4.3.1 Line DL-1

Line DL-1 crosses the southeastern part of the model where the structure consists of a single thrust sheet of Mississippian strata (Figures 4.1, 4.2a). The structure in this area shows little variation along strike, with only a slight plunge toward the southeast. The 2-D and 3-D ray-tracing results are expected to be similar in this region.

The synthetic seismic data for the 2-D ray-tracing experiment using the cross-section illustrated in Figure 4.2a are presented in Figure 4.6: (a) the stacked section, and (b) the post-stack time-migrated section. Time migration of the stacked section has the effect of: (i) collapsing diffractions, (ii) moving dipping reflectors to their proper spatial location (in a time section), and (iii) restoring dipping reflectors to their correct time-dip. The 'smiles' on the migrated section (Figure 4.6b) are likely an artifact of the migration

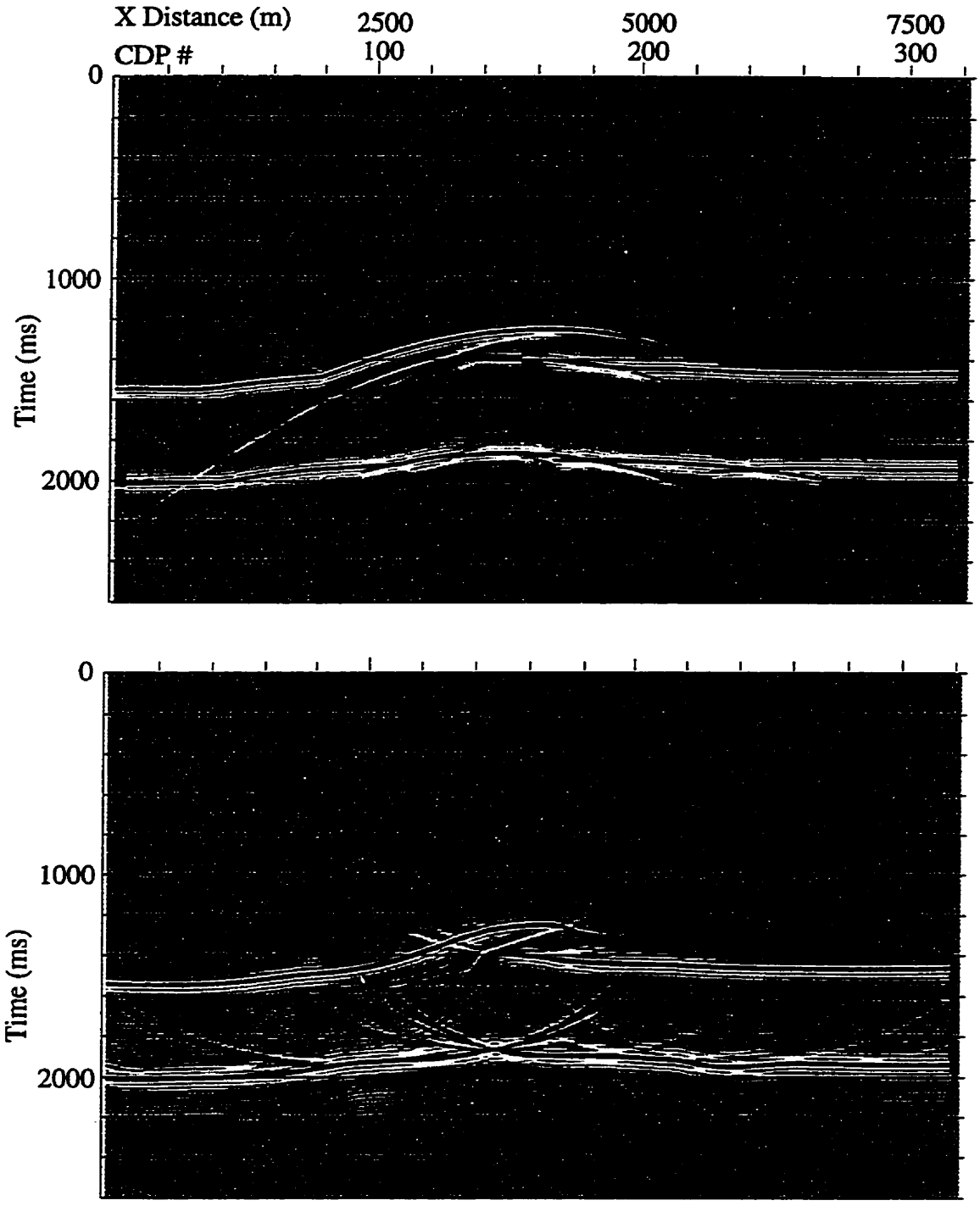

Figure 4.6. Synthetic seismic data from the 2-D ray-tracing experiment for line DL-1 (Figure 4.1): (a) stacked section, and (b) post-stack time-migrated section. Acquisition parameters and processing flow described in Tables 4.1 and 4.2, respectively. Compare to the 3-D ray-tracing result for line DL-1, presented in Figure 4.7. Refer to text for discussion of results. Sections 1:1 at 4000 m/s.

process, produced because these model data do not contain complete diffraction information or noise to interfere with these events. The migrated section accurately reflects the geometry of the depth model horizons, except in the region below the structural repetition of Mississippian strata where horizons appear at a higher structural level (Figures 4.2a, 4.6b). This 'pull-up' observed in time sections is the result of an increased thickness of higher-velocity Mississippian strata, which decreases two-way traveltimes to horizons lower in the section.

Figure 4.7 shows the stacked and migrated synthetic seismic sections from the 3-D ray-tracing experiment for line DL-1 (Figure 4.1). The stacked section is similar to that of the 2-D ray-tracing experiment (Figure 4.6a) except for the lack of diffractions, which are not generated in 3D-AIMS. The migrated 3-D ray-tracing result (Figure 4.7b) is similar to the 2-D ray-tracing result (Figure 4.6b), except for a decrease in the continuity of the Near Basement horizon. This decrease in continuity on the Near Basement horizon (e.g. between CDP #60 and #80) is the result of out-of-plane reflections from this irregular surface. The hangingwall and footwall cutoffs of the Mississippian horizon, and the ends of the thrust fault are not as well defined in the 3-D result as on the 2-D result (Figures 4.6b, 4.7b). This is, in part, an artifact of the migration procedure related to the lack of diffractions in the 3-D ray-tracing result. The 'hole' in the stacked and migrated sections, located at approximately X = 4000 m and time = 1900 ms, is a modeling artifact of unknown origin.

Figure 4.8a shows the interpretation of the migrated 3-D ray-tracing result (dark colors), and the interpretation of the migrated 2-D result (light colors), providing a

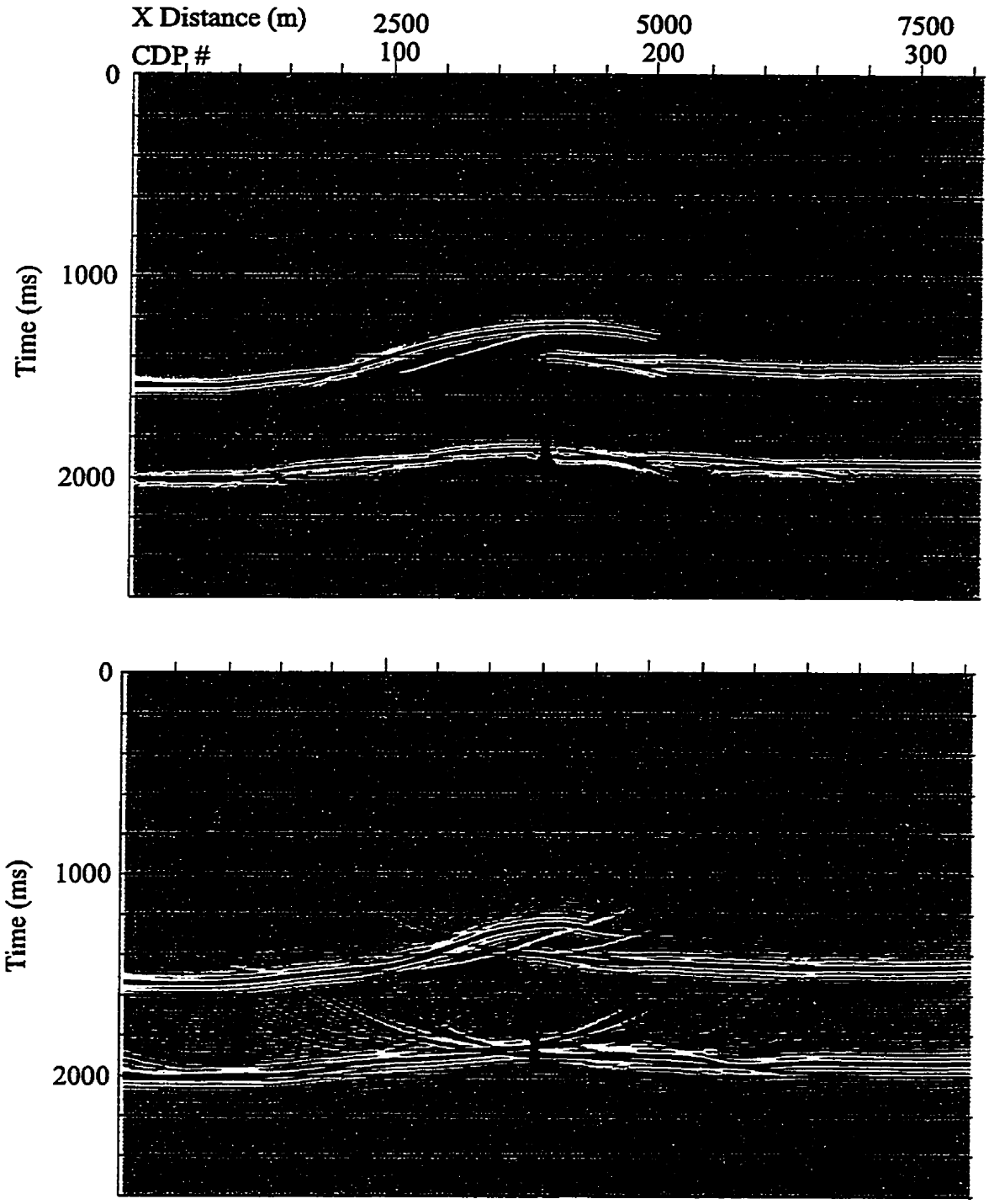

Figure 4.7. Synthetic seismic data from the 3-D ray-tracing experiment for line DL-1 (Figure 4.1): (a) stacked section, and (b) post-stack time-migrated section. Acquisition parameters and processing flow described in Tables 4.1 and 4.2, respectively. Compare to the 2-D ray-tracing result for line DL-1, presented in Figure 4.6. Refer to text for discussion of results. Sections 1:1 at 4000 m/s.

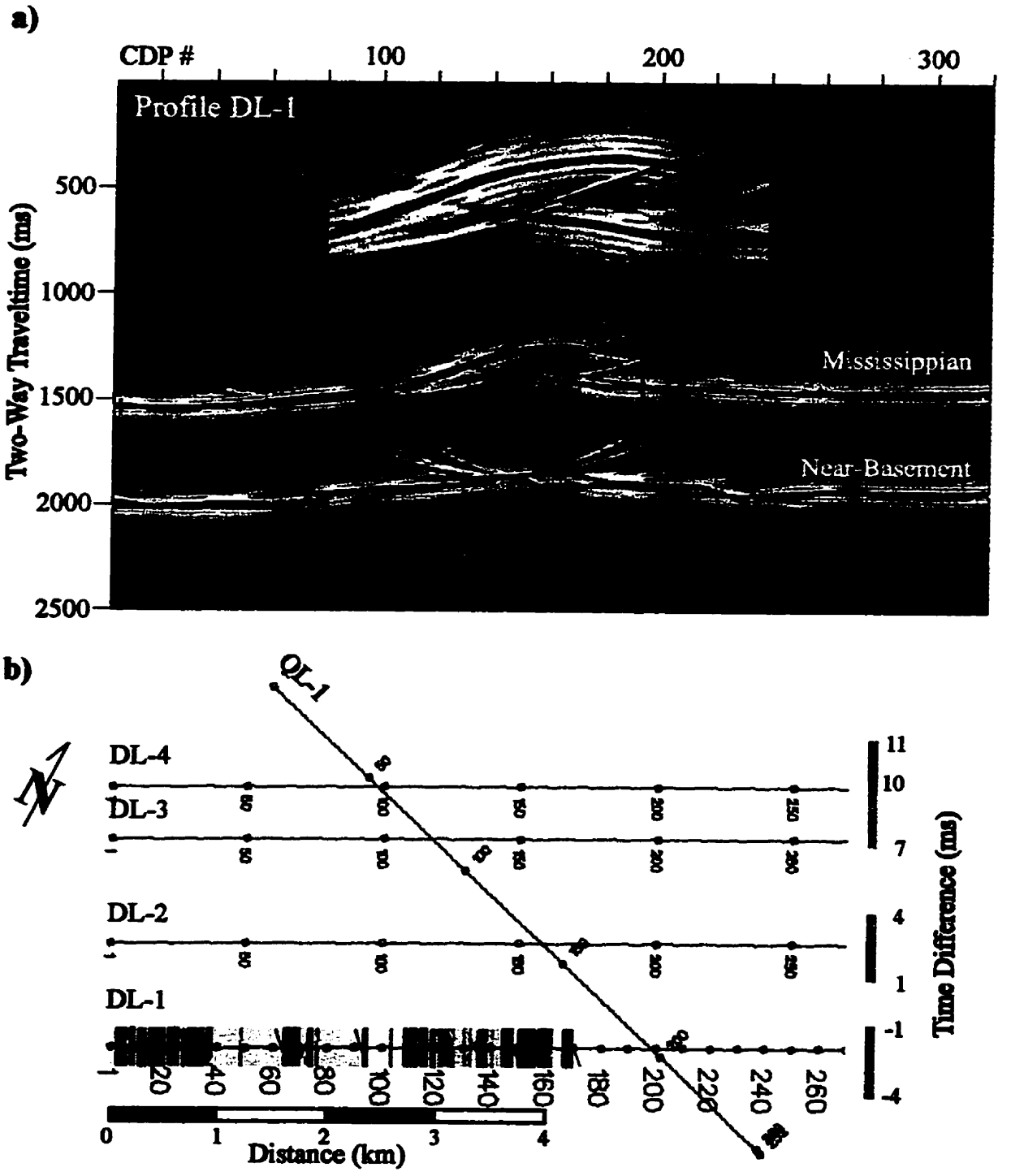

Figure 4.8. Analysis of time structure differences between post-stack time-migrated results of the 2-D and 3-D ray-tracing experiments for line DL-1 (Figure 4.1): a) comparison of horizon interpretations for the 3-D result (blue, purple, red) over the transposed 2-D result interpretation (green, magenta, yellow), b) time structure error map for the hangingwall Mississippian event. CDP #'s plotted along the line for reference. Seismic section approximately 1:1 at 4000 m/s

direct comparison of horizon geometry in both sections. Time structure differences are small in this section, as expected. Figure 4.8b shows the time structure error calculated for the Mississippian horizon in the hangingwall of the thrust structure. The time structure error for this horizon ranges from -4 to 11 ms (-8 to 22 m depth error at 4000 m/s), and does not represent a serious interpretation problem.

Figure 4.9 shows source and receiver locations along line DL-1 and reflection points from the 3-D ray-tracing experiment for the Mississippian horizon in the hangingwall of the structure. The distribution of reflection points away from line DL-1 indicates significant out-of-plane contributions to the seismic section at the southwest end of the line, where it crosses a local structural depression (Figure 4.9). These out-of-plane reflections, which do not cause significant time structure differences between the 2-D and 3-D ray-tracing results, originate up to 400 m from the line. The distance of reflection points from the line does not appear to vary systematically with calculated time structure differences (Figures 4.8b, 4.9).

4.3.2 Line DL-2

Line DL-2 crosses the model in the dip direction over the central part of the model, 1000 m northwest of line DL-1 (Figure 4.1). The structure below this line consists of a single thrust sheet of Mississippian strata, but changes just north of this line to a stack of two thrust sheets (Figure 4.2b). The structure below this line is similar to that below line DL-1 but more severe out-of-plane effects, related to the addition of a second thrust sheet north of this line, are anticipated.

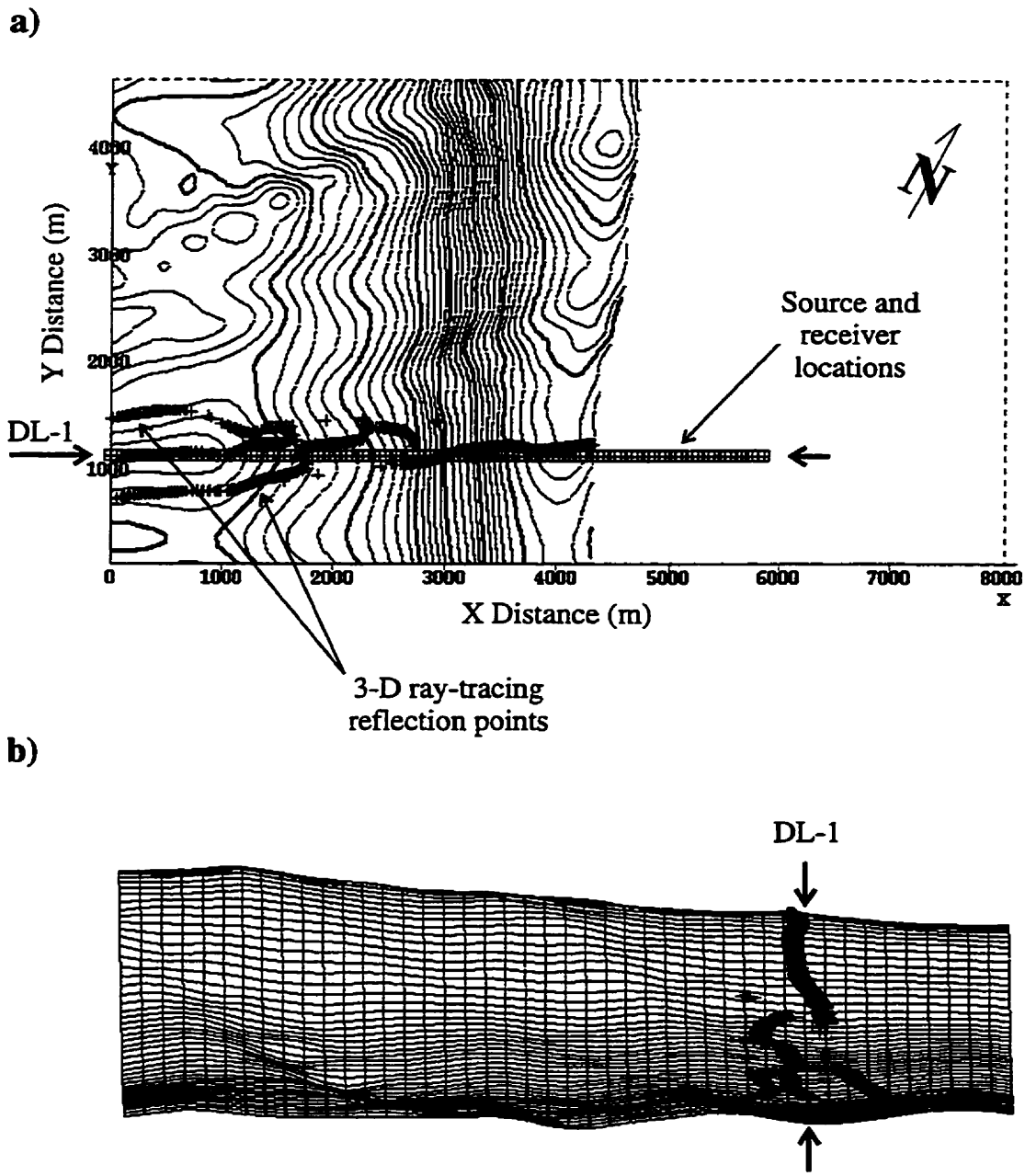

Figure 4.9. Reflection points and source/receiver points from the 3-D offset ray-tracing experiment for line DL-1, illustrating the origin of out-of-plane reflections from the Top Mississippian horizon in the hangingwall of the structure: a) structure contour map (20 m contour interval), and b) a perspective view looking northeast, in the dip direction (100 m grid). Arrows indicate the location and trend of line DL-1.

Figure 4.10 shows the migrated sections for the 2-D and 3-D ray-tracing results for line DL-2 (Figure 4.1). Differences between these sections include (for the 3-D result): (i) reduced continuity on the Near-Basement horizon, (ii) poor definition of the Top Mississippian hangingwall cutoff, and (iii) an additional reflection event in the core of the structure. The first two features are similar to those described and discussed for line DL-1. The additional event in the 3-D result (centered at CDP #170 and 1300 ms) is an out-of-plane reflection from the Top Mississippian horizon in the hangingwall of the lower thrust sheet north of this line.

Figure 4.11a shows both the interpretation of the migrated 3-D result (dark colors) and the interpretation from the migrated 2-D result (light colors). Time structure differences on the Mississippian horizon in the hangingwall of the upper thrust sheet range from 0 to 23 ms (up to 46 m depth error at 4000 m/s), consistently higher than the differences observed for line DL-1 (Figures 4.8b, 4.11b). Analysis of reflection points from the 3-D ray-tracing experiment indicates that the source of time structure error on this horizon is local structural variations on the Top Mississippian horizon in the hangingwall of the structure, oblique to the structural trend (Figure 4.12). These local structural variations have a much greater effect on reflection point locations for this line than on line DL-1. The distance of reflection points from the line correlates broadly with time structure differences between 1000 m (CDP #40) and 3800 m (CDP #150) on line DL-2 (Figures 4.11b, 4.12). Over this interval an increase in distance between the oblique structure and the line corresponds to an increase in time structure error.

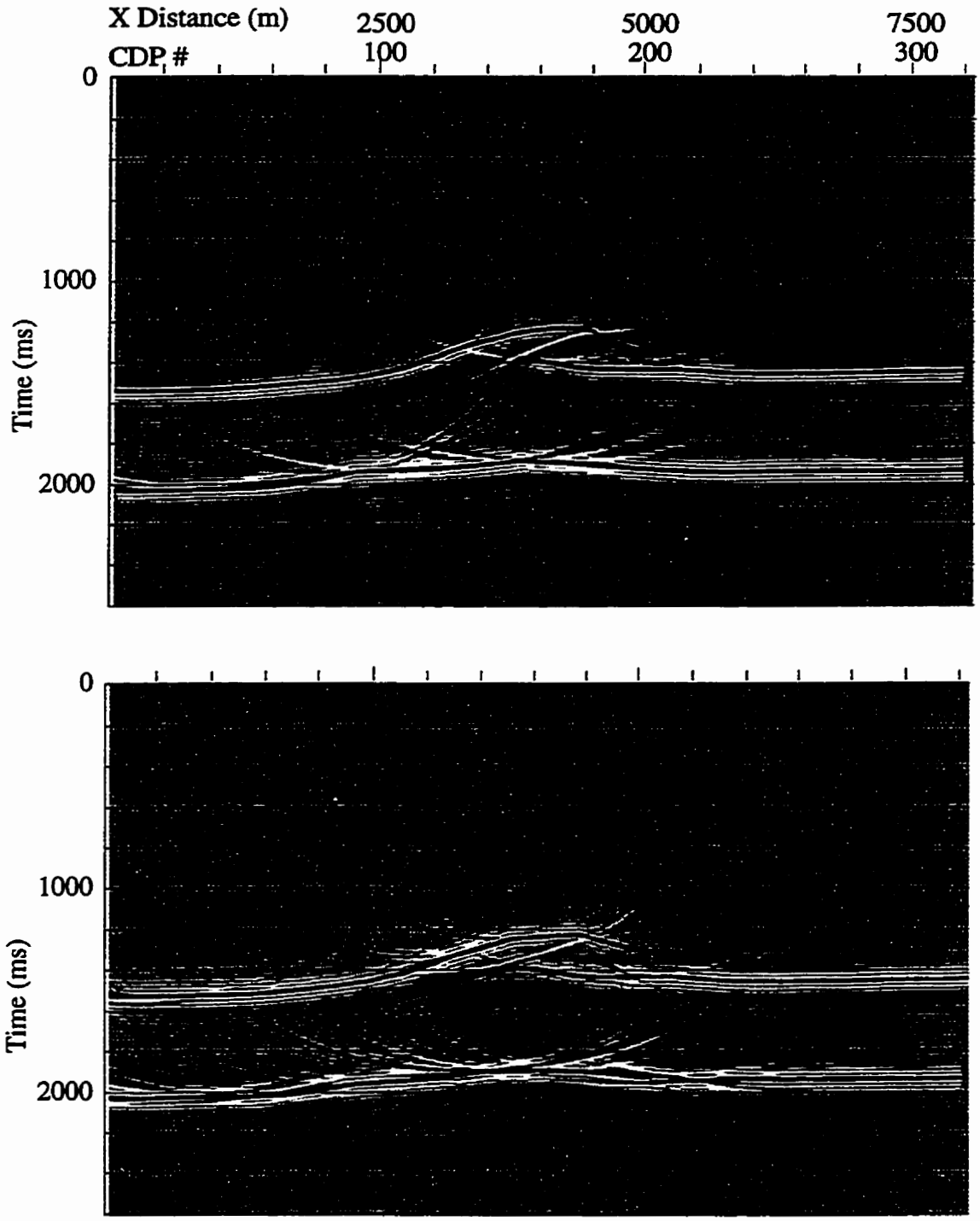

Figure 4.10. Synthetic post-stack time-migrated seismic sections from the ray-tracing experiments for line DL-2 (Figure 4.1): (a) 2-D result, and (b) 3-D result. Acquisition parameters and processing flow described in Tables 4.1 and 4.2, respectively. Refer to text for discussion of results. Sections 1:1 at 4000 m/s.

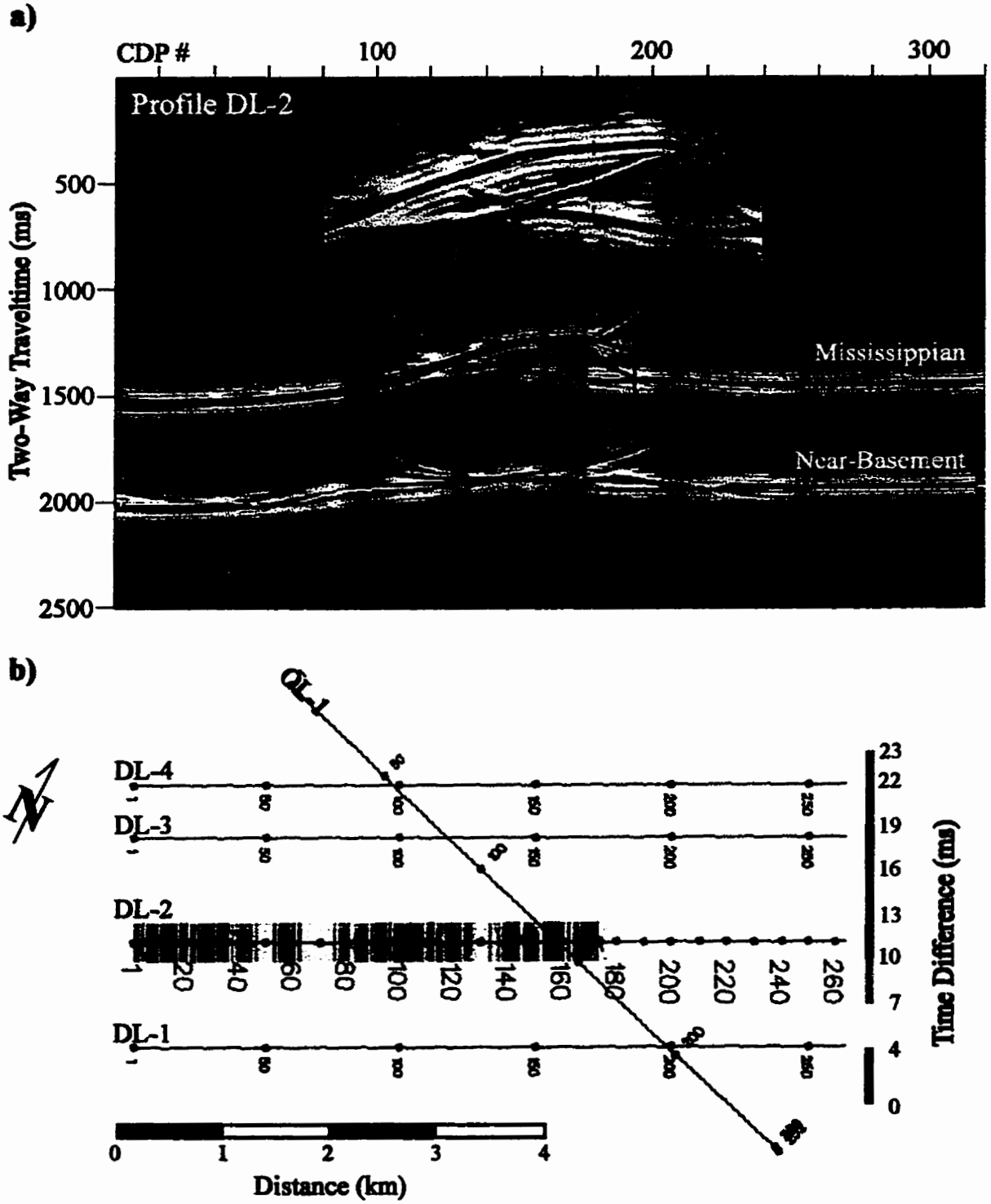

Figure 4.11. Analysis of time structure differences between post-stack time-migrated results of the 2-D and 3-D ray-tracing experiments for line DL-2 (Figure 4.1): a) comparison of horizon interpretations for the 3-D result (blue, purple, red) over the transposed 2-D result (green, magenta, yellow), b) time structure error map for the hangingwall Mississippian event. CDP #'s plotted along the line for reference. Seismic section approximately 1:1 at 4000 m/s.

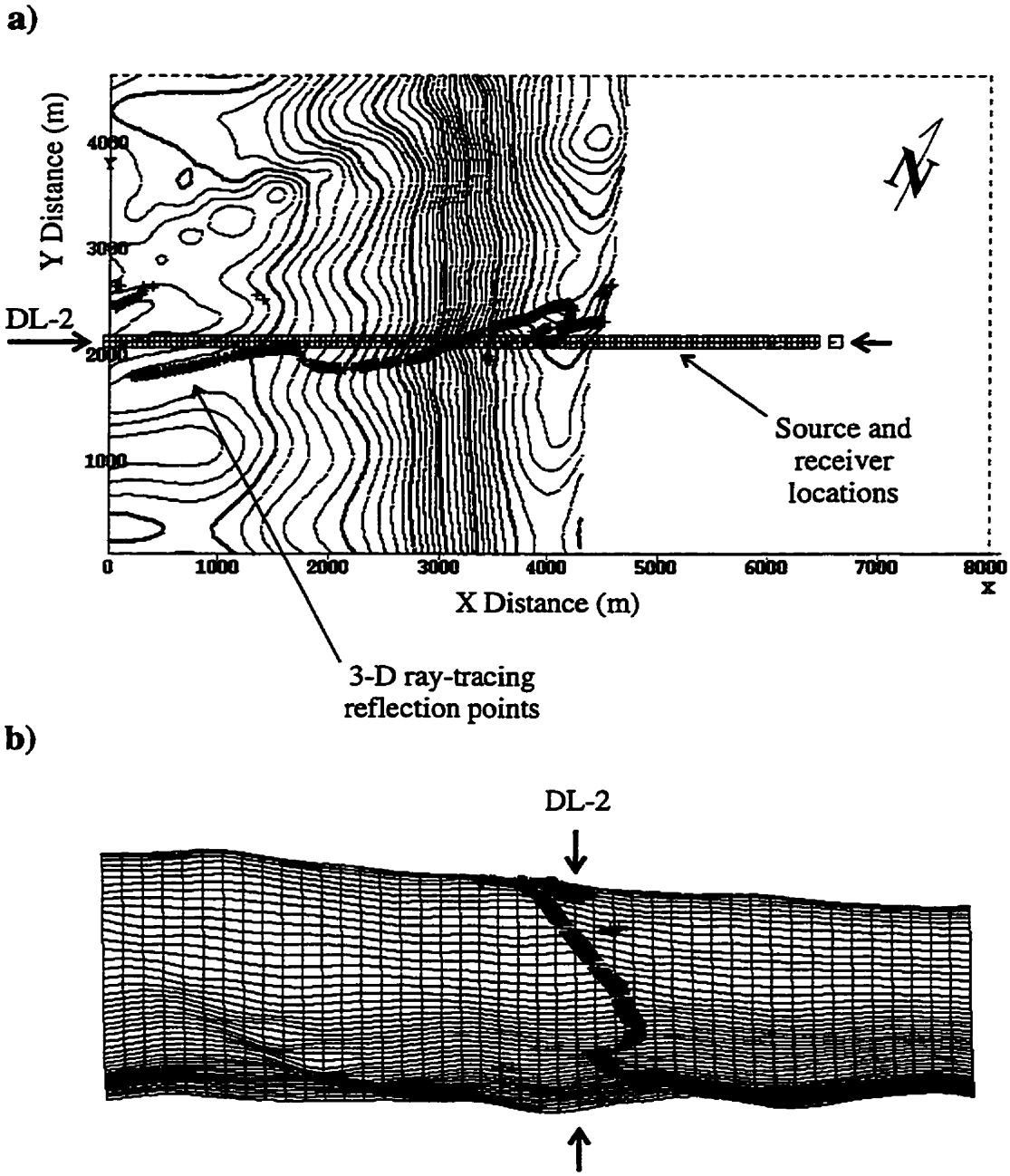

Figure 4.12. Reflection points and source/receiver locations from the 3-D offset ray-tracing experiment for line DL-2, illustrating the origin of out-of-plane reflections from the Top Mississippian horizon in the hangingwall of the structure: a) structure contour map (20 m contour interval), and b) a perspective view looking northeast, in the dip direction (100 m grid). Arrows indicate the location and trend of line DL-2.

4.3.3 Line DL-3

Line DL-3 crosses the northwestern part of the model (Figure 4.1) where the structure consists of two stacked thrust sheets of Mississippian strata (Figure 4.3a). Line DL-3 is located 1000 m northwest of the structural transition from one to two thrust sheets and illustrates the transfer of displacement from the upper to the lower thrust fault (Figure 4.3a). The structure below this line is more complex than that below lines DL-1 and DL-2, and represents a more difficult seismic imaging problem. The plunge of the structure is enhanced where the lower thrust sheet is present, and this change in the broad geometry of the structure is anticipated to increase out-of-plane effects on this line.

Figure 4.13 shows the migrated seismic sections from the 2-D and 3-D ray-tracing experiments for line DL-3. The migrated 2-D result is an accurate representation of reflector geometry in the depth model except for pull-up below the thrust structure, similar to that observed for line DL-1. Differences between the 2-D and 3-D ray-tracing results include (for the 3-D result): (i) reduced reflection continuity on all horizons, (ii) changes in reflection geometry in the core of the structure, (iii) poor definition of hangingwall cutoffs for both thrust sheets, and (iv) incorrect imaging of the footwall Mississippian reflection below the structure (southwest of X = 4750 m). Changes in reflection geometry in the core of the structure reflect an increase in the overall plunge of the structure caused by the addition of the lower thrust sheet, which plunges sharply toward the southeast. In the migrated 3-D result the footwall Mississippian event below the structure is a migration artifact (energy swept into this position during migration) and does not reflect the true geometry of this horizon (Figure 4.13b).

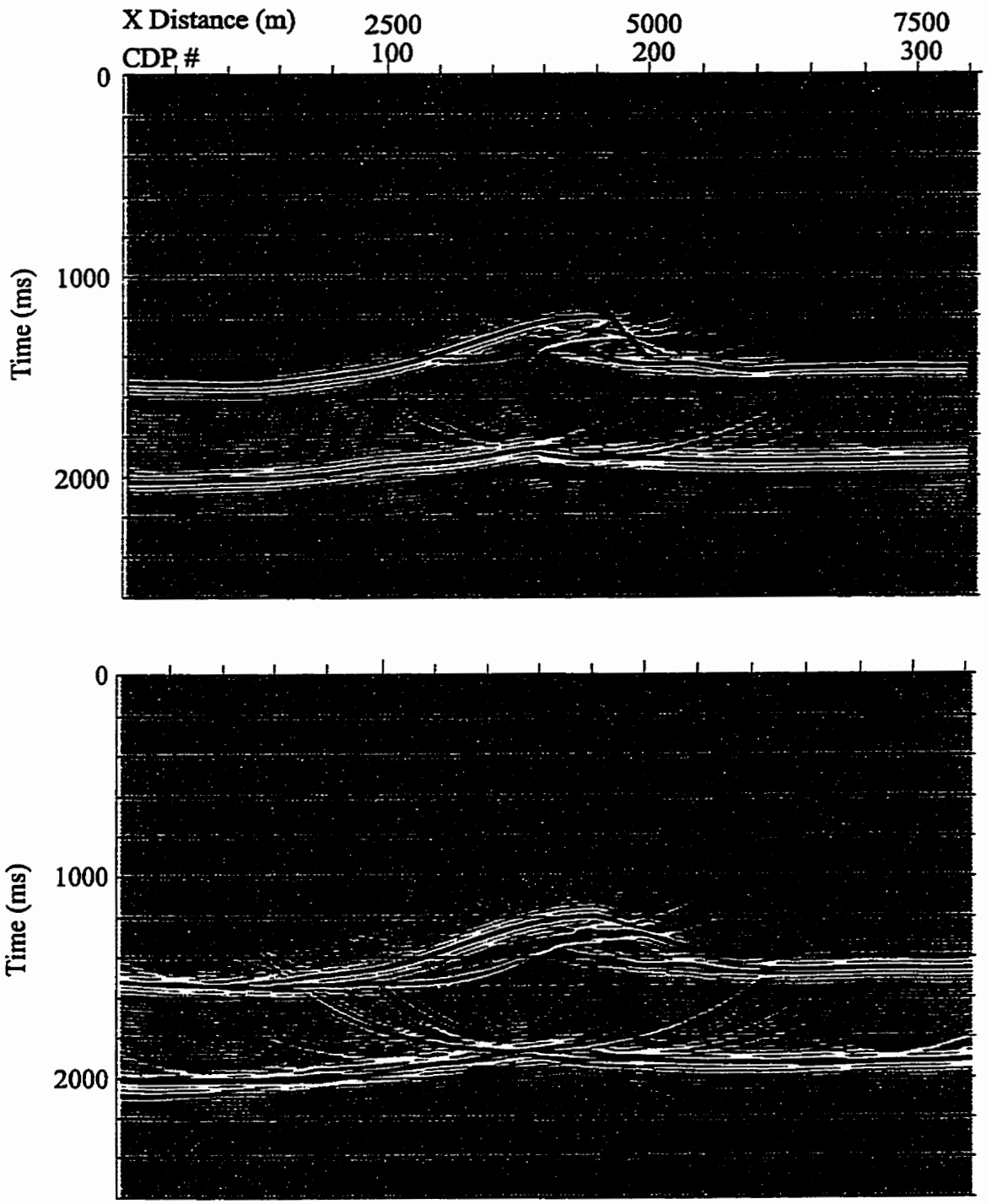

Figure 4.13. Synthetic post-stack time-migrated seismic sections from the ray-tracing experiments for line DL-3 (Figure 4.1): (a) 2-D result, and (b) 3-D result. Acquisition parameters and processing flow described in Tables 4.1 and 4.2, respectively. Refer to text for discussion of results. Sections 1:1 at 4000 m/s.

Figure 4.14a shows the interpretation on the migrated 3-D ray-tracing result (dark colors), over the interpretation from the migrated 2-D ray-tracing result (light colors). Time structure differences between the two results are obvious on all horizons, especially in the core of the structure (note the change in orientation of the upper thrust fault, Figure 4.14a). Figure 4.14b illustrates time structure error calculated for the Mississippian horizon in the hangingwall of the upper thrust sheet. Time structure error ranges between -12 and 15 ms (-24 to 30 m depth error at 4000 m/s), with a slightly higher average than that observed for line DL-2.

The source of out-of-plane reflections from the hangingwall Mississippian horizon for the 3-D ray-tracing experiment is apparent on a reflection point map for this horizon (Figure 4.15). This reflection point map indicates that almost all of reflections from this horizon originate out-of-plane, as far as 900 m from the line. The reflection points follow local east- and northeast-trending structural variations on the hangingwall Mississippian horizon; similar to the behavior observed for line DL-2 but for different local structures (Figure 4.15). Greater time structure errors for this line correlate broadly with increasing distance of reflection points away from the line-of-section between 1500 (CDP #60) and 4500 m (CDP #180), similar to behavior noted for line DL-2 (Figures 4.14b, 4.15).

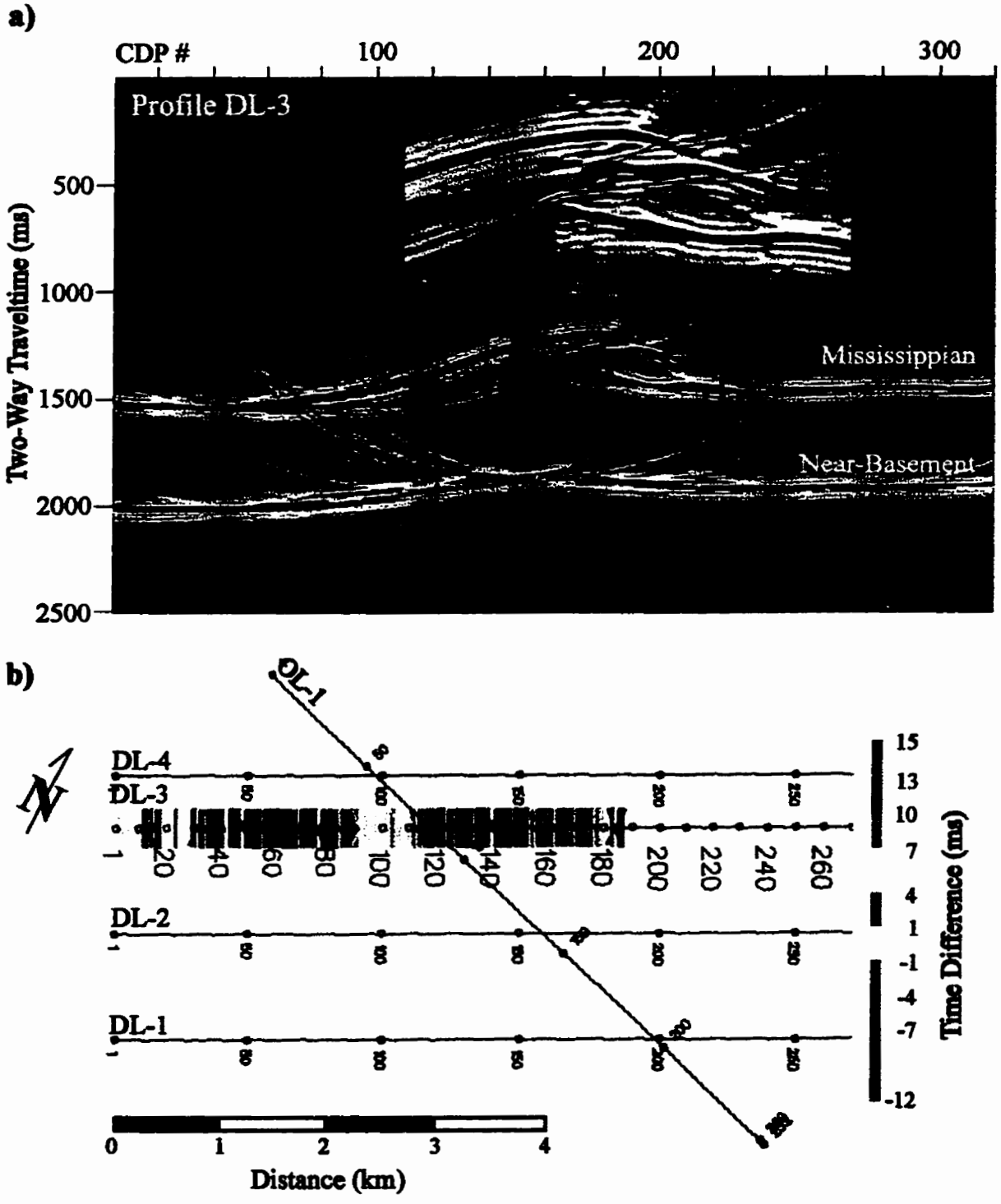

Figure 4.14. Analysis of time structure differences between post-stack time-migrated results of the 2-D and 3-D ray-tracing experiments for line DL-3 (Figure 4.1): a) comparison of horizon interpretations for the 3-D result (blue, purple, red) over the transposed 2-D result (green, magenta, yellow), b) time structure error map for the hangingwall Mississippian event. CDP #'s plotted along the line for reference. Seismic section approximately 1:1 at 4000 m/s.

a)

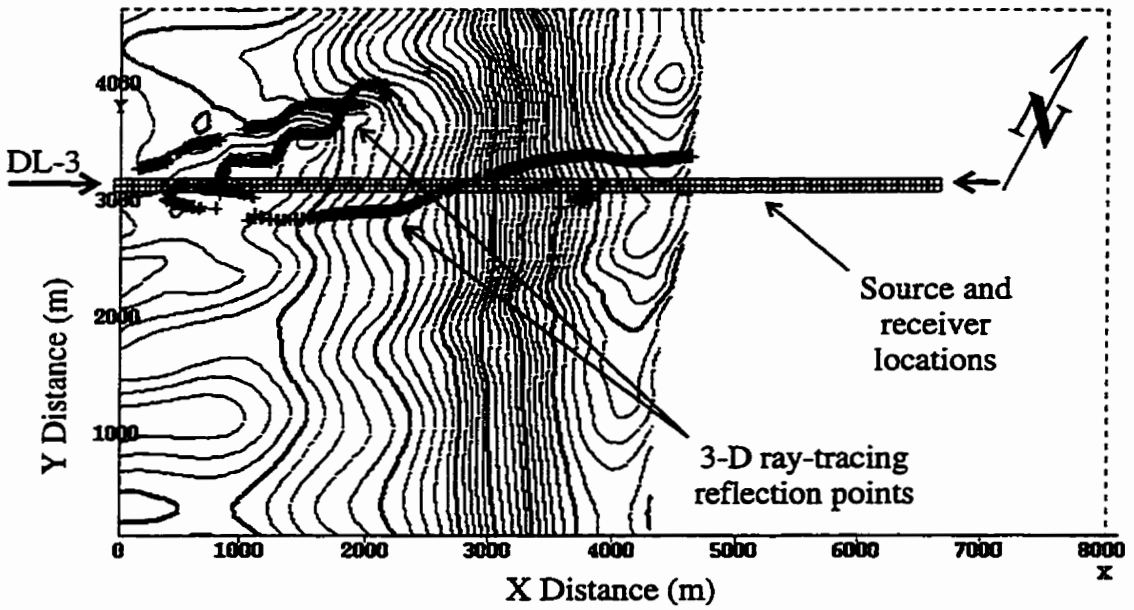

b)

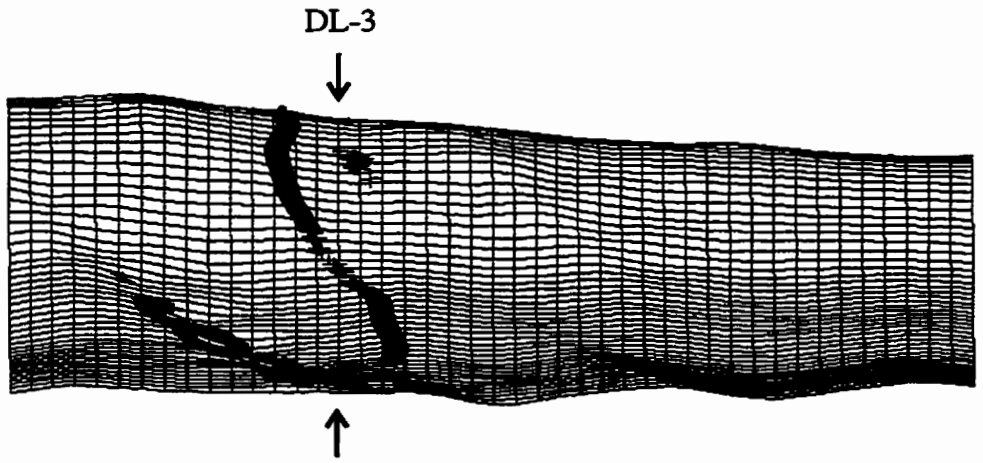

Figure 4.15. Reflection points and source/receiver locations from the 3-D offset ray-tracing experiment for line DL-3, illustrating the origin of out-of-plane reflections from the Top Mississippian horizon in the hangingwall of the structure: a) structure contour map (20 m contour interval), and b) a perspective view looking northeast, in the dip direction (100 m grid). Arrows indicate the location and trend of line DL-3.

4.3.4 Line DL-4

Profile DL-4 crosses the northern part of the model (Figure 4.1), and the structure below this line is very similar to line DL-3. This line is located 500 m northwest of profile DL-3, and illustrates continued transfer of displacement from the upper to the lower thrust fault (Figure 4.3). Differences between the migrated sections for the 2-D and 3-D ray-tracing experiments are similar to those noted for line DL-3 (Figures 4.13, 4.16).

Direct comparison of interpretations from the migrated 2-D and 3-D ray-tracing results highlights time-structure errors related to out-of-plane imaging in the 3-D ray-tracing experiment (Figure 4.17a). These time structure differences are locally severe, especially where different reflection events with similar amplitudes occur at the same location. For example, on the Near-Basement horizon between CDP #80 and #140 the interpreter would likely pick the earlier reflection event with the appropriate amplitude in the absence of evidence to support picking the later event. Time structure error, calculated for the Mississippian marker in the hangingwall of the upper thrust sheet, ranges from –12 to 33 ms (-24 to 66 m depth error at 4000 m/s) for this line (Figure 4.17b). Average time structure error is similar to that observed for line DL-3 east of CDP #120 (Figures 4.14b, 4.17b; note scale change).

Local structural variations control the distribution of reflection points on the Top Mississippian horizon (up to 700 m from the line, Figure 4.18). As noted for lines DL-2 and DL-3, an increase in the distance of reflection points from the line corresponds to an increase in time structure error east of 3000 m (CDP #120) on line DL-4.

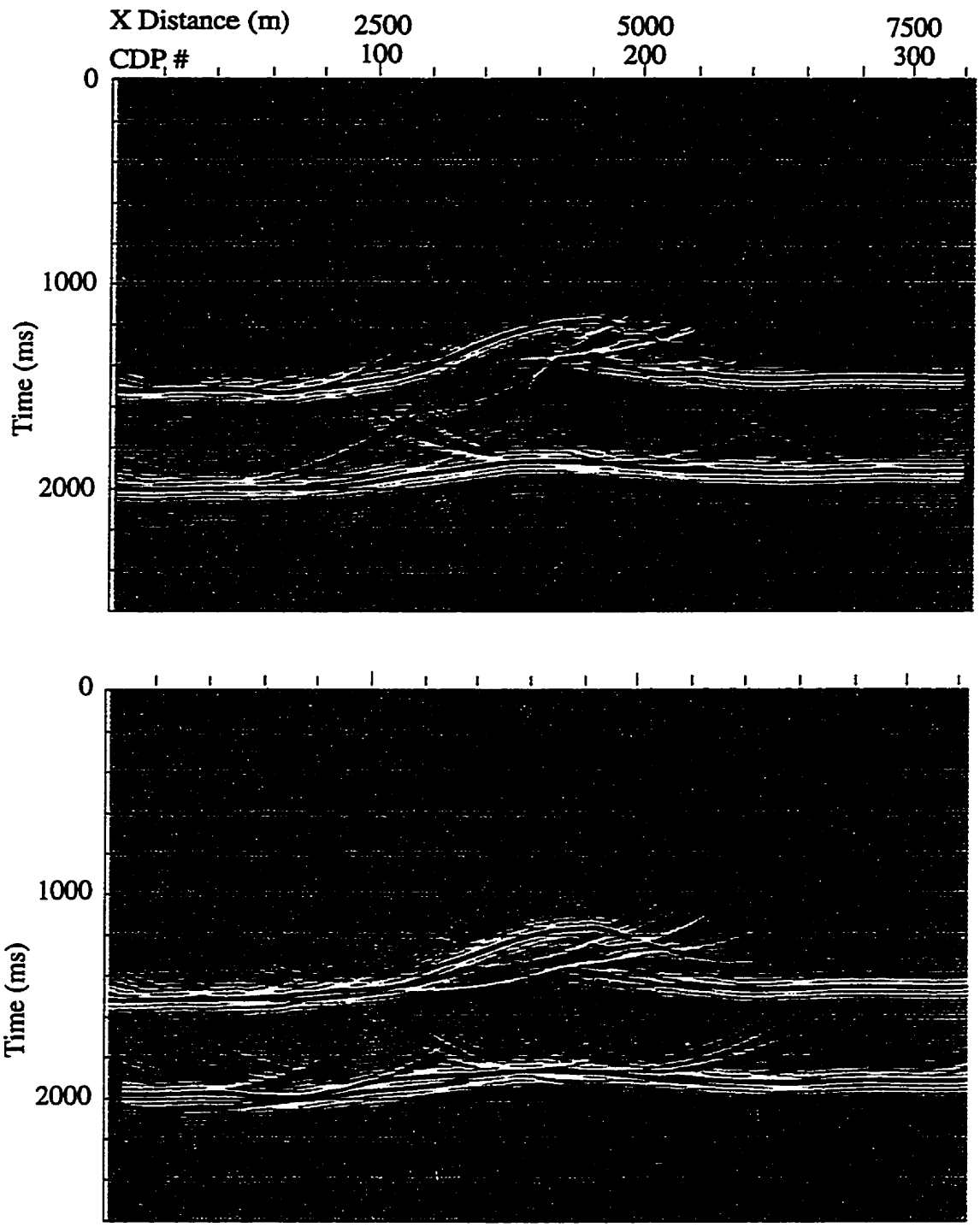

Figure 4.16. Synthetic post-stack time-migrated seismic sections from the ray-tracing experiments for line DL-4 (Figure 4.1): (a) 2-D result, and (b) 3-D result. Acquisition parameters and processing flow described in Tables 4.1 and 4.2, respectively. Refer to text for discussion of results. Sections 1:1 at 4000 m/s.

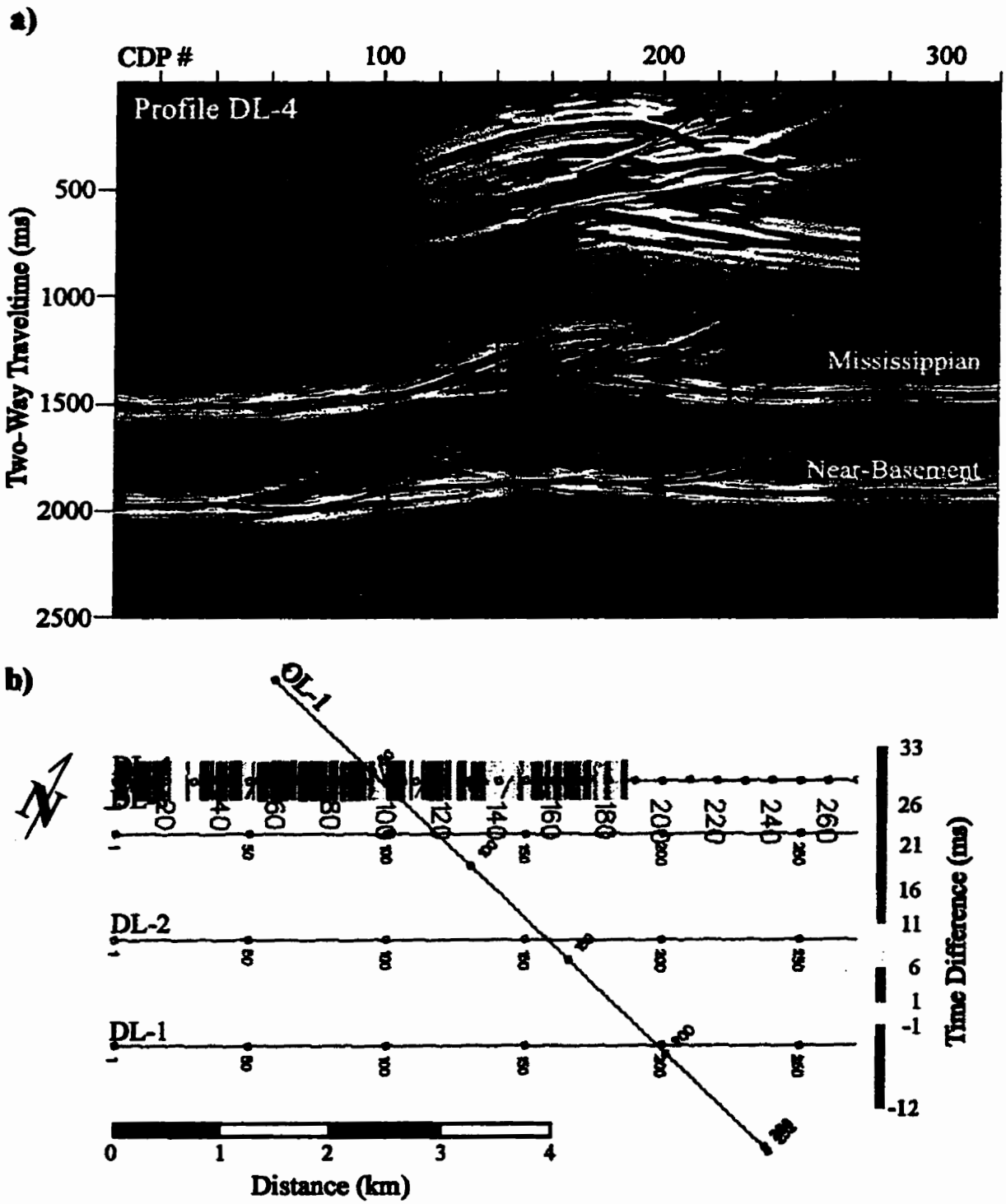

Figure 4.17. Analysis of time structure differences between post-stack time-migrated results of the 2-D and 3-D ray-tracing experiments for line DL-4 (Figure 4.1): a) comparison of horizon interpretations for the 3-D result (blue, purple, red) over the transposed 2-D result (green, magenta, yellow), b) time structure error map for the hangingwall Mississippian event. CDP #'s plotted along the line for reference. Seismic section approximately 1:1 at 4000 m/s.

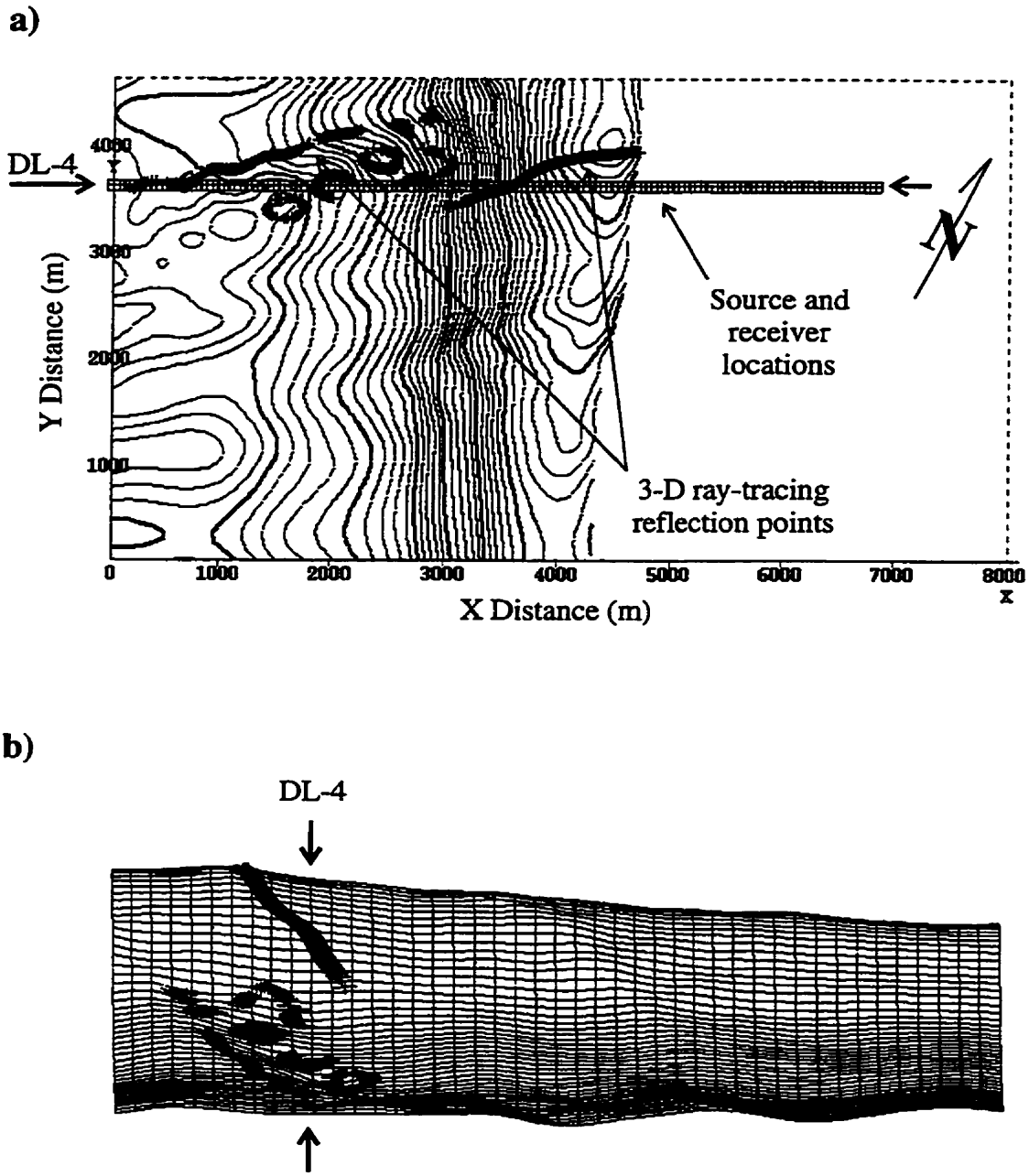

Figure 4.18. Reflection points and source/receiver locations from the 3-D offset ray-tracing experiment for line DL-4, illustrating the origin of out-of-plane reflections from the Top Mississippian horizon in the hangingwall of the structure: a) structure contour map (20 m contour interval), and b) a perspective view looking northeast, in the dip direction (100 m grid). Arrows indicate the location and trend of line DL-4.

4.3.5 Line OL-1

Line OL-1 crosses the model oblique to the regional trend of the structure (Figure 4.1). The structure below this line consists of a single Mississippian thrust sheet, but the line crosses the crest of the structure just south of the transition from one to two thrust sheets (Figure 4.4). This line crosses the structure at 45° to the structural trend, and therefore the cross-line dip for the overall southwest-dipping Mississippian structure should be similar to the dip observed in the model cross-section (approximately 15°, Figure 4.4).

Differences in the migrated sections for the 2-D and 3-D ray-tracing results include (for the 3-D result): (i) reduced continuity on the Near-Basement event, especially at the northwest end of the line, (ii) obvious time-structure differences on the northwest-dipping portion of the hangingwall Mississippian event, (iii) poor definition of the Mississippian hangingwall cutoff, (iv) shallower dip for the thrust fault reflection, and (v) a coherent out-of-plane reflection (centered at CDP #140 and 1300 ms) from the Mississippian horizon in the lower thrust sheet (Figure 4.19). These time structure differences are apparent in Figure 4.20a, which shows the interpretations from the migrated sections for both the 2-D and 3-D ray-tracing results. Obvious time structure differences between the two interpretations occur on the Mississippian horizon in the hangingwall of the structure between CDP #60 and #110 (Figure 4.20a). Changes in reflection geometry in the core of the structure are also obvious in this analysis, especially the addition of an out-of-plane reflection from the Top Mississippian horizon in the hangingwall the lower thrust slice (Figure 4.20a).

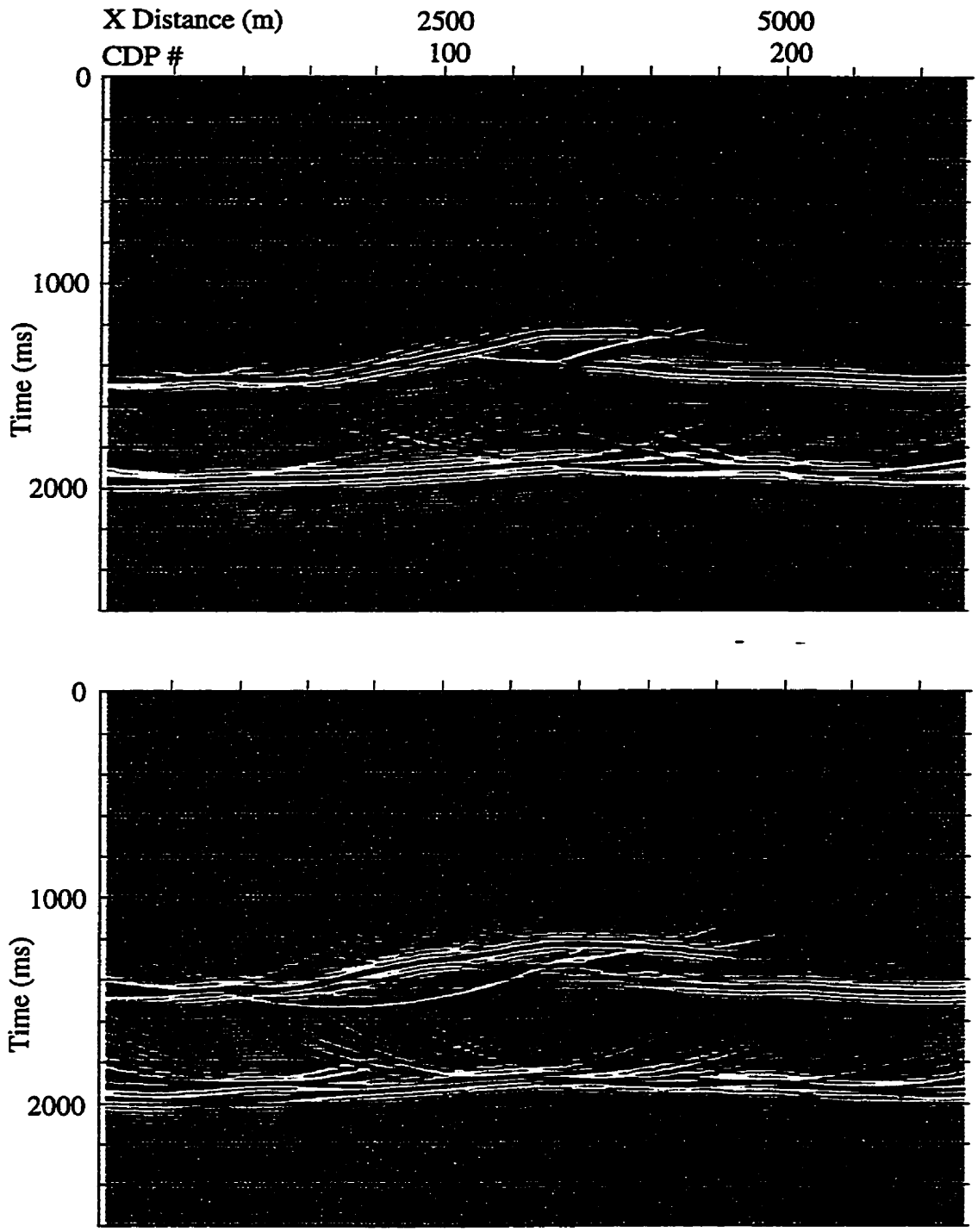

Figure 4.19. Synthetic post-stack time-migrated seismic sections from the ray-tracing experiments for line OL-1 (Figure 4.1): (a) 2-D result, and (b) 3-D result. Acquisition parameters and processing flow described in Tables 4.1 and 4.2, respectively. Refer to text for discussion of results. Sections 1:1 at 4000 m/s.

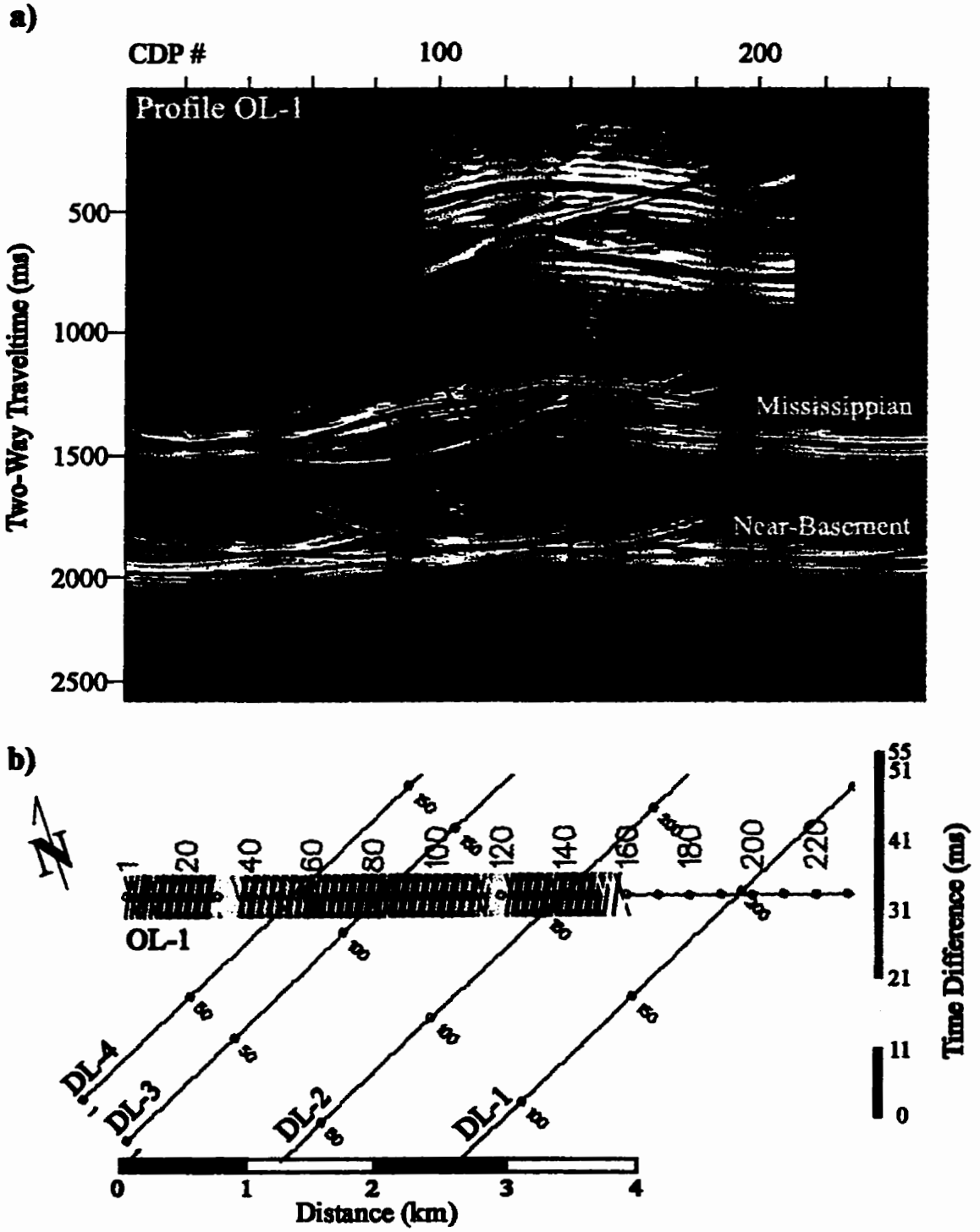

Figure 4.20. Analysis of time structure differences between post-stack time-migrated results of the 2-D and 3-D ray-tracing experiments for line OL-1 (Figure 4.1): a) comparison of horizon interpretations for the 3-D result (blue, purple, red) over the transposed 2-D result (green, magenta, yellow), b) time structure error map for the hangingwall Mississippian event. CDP #'s plotted along the line for reference. Seismic section approximately 1:1 at 4000 m/s.

Time structure differences between the 2-D and 3-D results, calculated for the Mississippian horizon in the hangingwall of the upper thrust sheet reflect out-of-plane imaging effects on this line (Figure 4.20b). The time structure error is generally greater than that observed for lines oriented in the dip direction. Time structure errors range from 0 to 55 ms (up to 110m depth error at 4000 m/s), and appear to vary systematically with respect to location along the line.

A map of reflection points (from the 3-D ray-tracing experiment) on the Mississippian horizon in the hangingwall of the upper thrust sheet illustrates the source of out-of-plane reflections on line OL-1 (Figure 4.21). The distribution of reflection points away from the line appears to be controlled principally by the broad geometry of the structure, modified by the location of the local structural variations (Figure 4.21). Time structure error increases toward the southeast along line OL-1 as reflection points approach the southwest-dipping portion of the structure, then decreases as the depth to, and local dip of the structure decreases (Figures 4.20b, 4.21).

An alternative method for dealing with 2-D seismic profiles oblique to the structural trend is to project these lines into the dip direction prior to migration. This procedure essentially involves compressing the stacked section (reducing the trace spacing) by multiplying the trace spacing by the cosine of the angle between the line and the true dip direction. The projected time-migrated sections for the 2-D and 3-D results for OL-1 are presented in Figure 4.22. Projection of these data into the dip direction did not reduce the imaging error on the Top Mississippian horizon in the hangingwall of the structure, and time structure errors up to 60 ms (120 m depth error at 4000 m/s) persist.

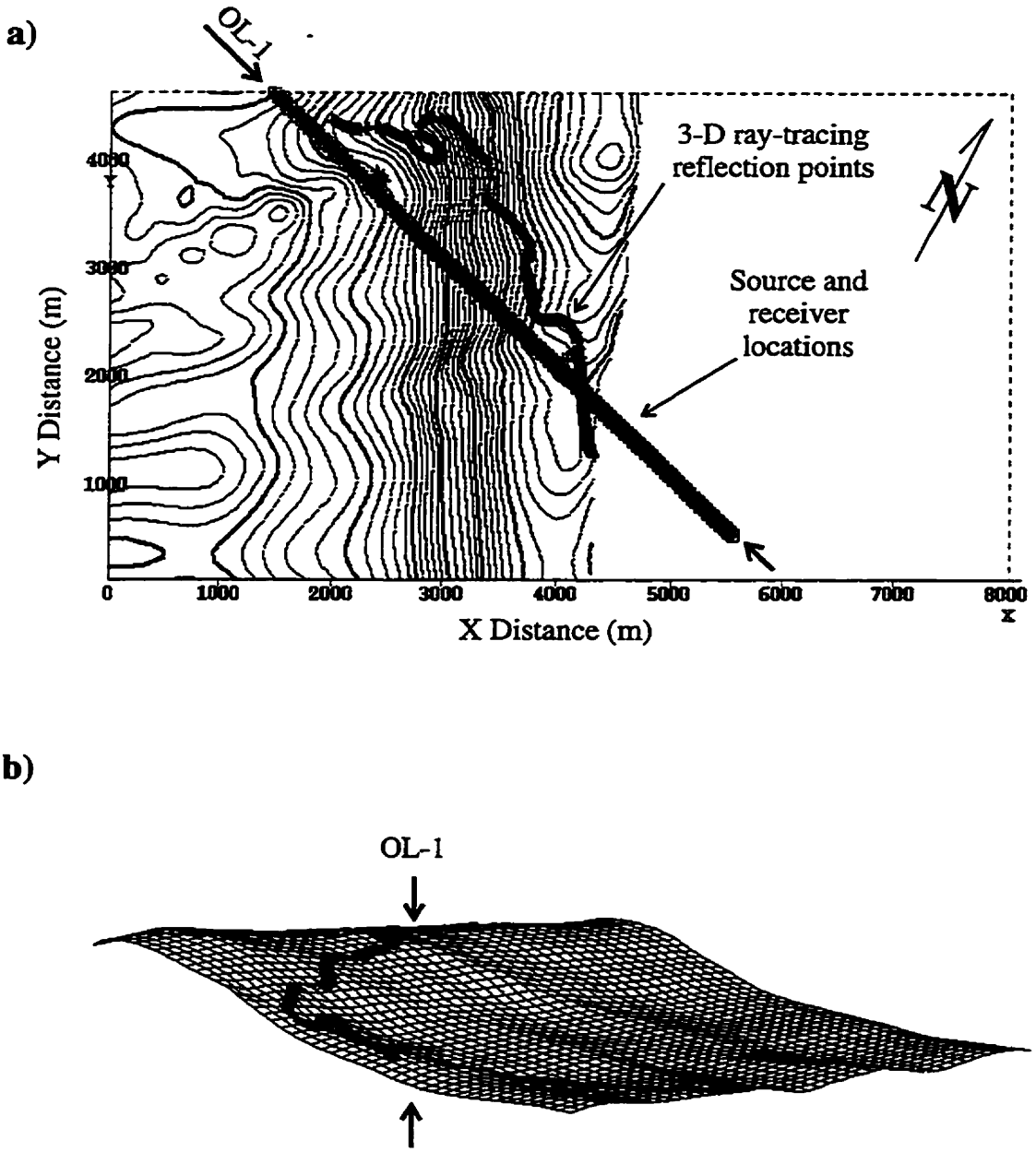

Figure 4.21. Reflection points and source/receiver locations from the 3-D offset ray-tracing experiment for line OL-1, illustrating the origin of out-of-plane reflections from the Top Mississippian horizon in the hangingwall of the structure: a) structure contour map (20 m contour interval), and b) a perspective view looking southeast (100 m grid). Arrows indicate the location and trend of line OL-1.

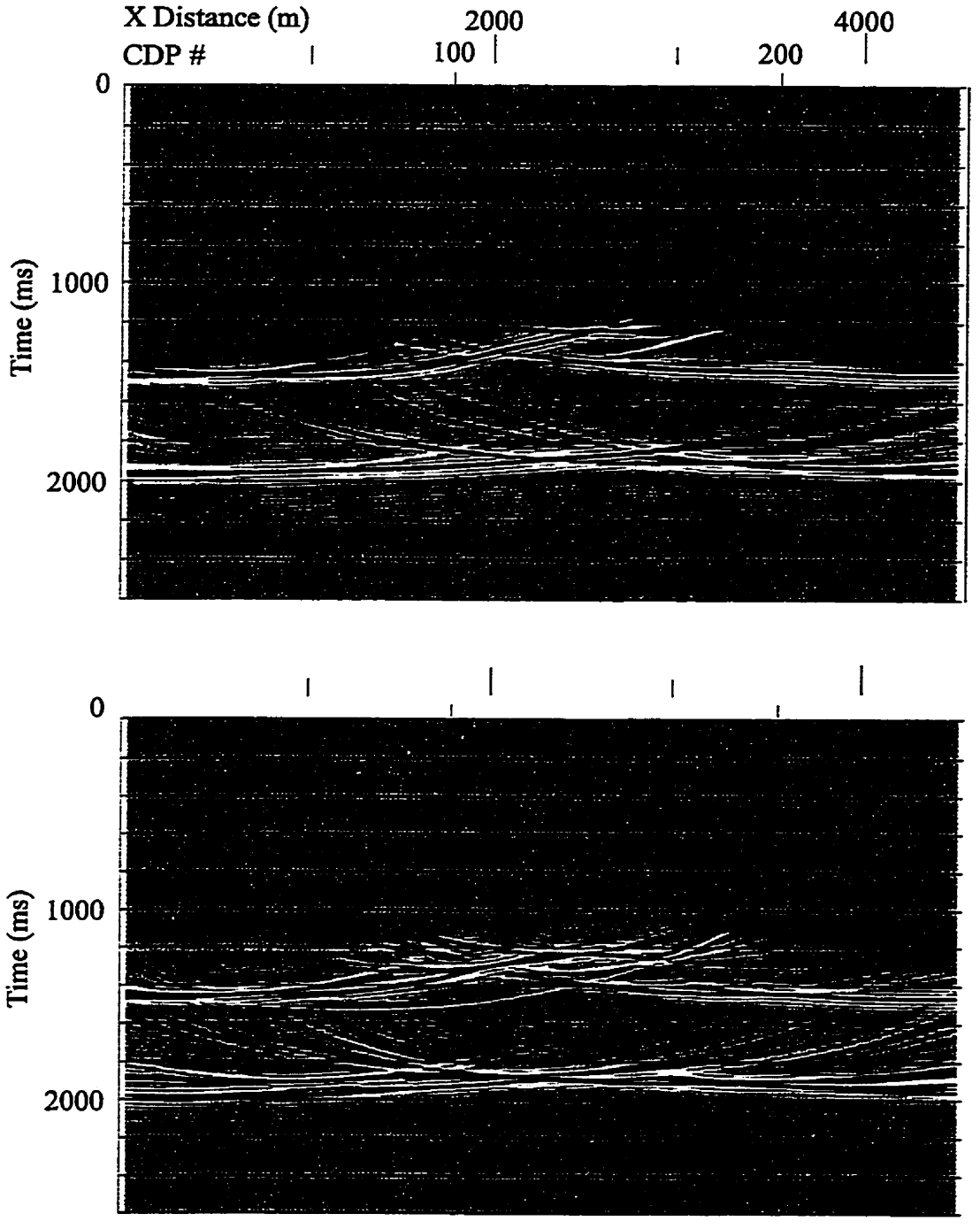

Figure 4.22. Post-stack time-migrated seismic sections using data projected from line OL-1 into the dip-direction (Figure 4.1): (a) 2-D result, and (b) 3-D result.

4.4 Summary of Results

The results of this experiment demonstrate wide variations in out-of-plane imaging error on 2-D seismic lines across various parts of the structure, and in different orientations. Figure 4.23 shows the time structure errors related to out-of-plane effects for all lines in this experiment, calculated for the Top Mississippian horizon in the hangingwall of the upper thrust sheet and presented at the same scale. These time structure errors range between –12 and 33 ms (-24 to 66 m depth error at 4000 m/s) for the four dip lines, and generally are below 15 ms (30 m). Time structure error on the dip lines, controlled by local short-wavelength (1 – 2 km) structural variations, generally increases toward the northwest but does not appear to correlate with the broad geometry of the structure (Figure 4.22). These short-wavelength local structural variations on the Top Mississippian horizon in the hangingwall of the structure have low amplitudes (up to 50 m) and trend oblique to the structural trend.

The oblique line results provide the most striking example of out-of-plane imaging error in this experiment, with errors of up to 55 ms (up to 110 m depth error at 4000 m/s) on the hangingwall Mississippian horizon. The time structure errors on this line are controlled principally by the broad geometry of the structure and modified by the short-wavelength structural variations described above. The oblique line displays a systematic increase in time structure error with proximity to the southwest-dipping backlimb of the structure, and decrease in error as the depth to, and local dip of the structure decreases.

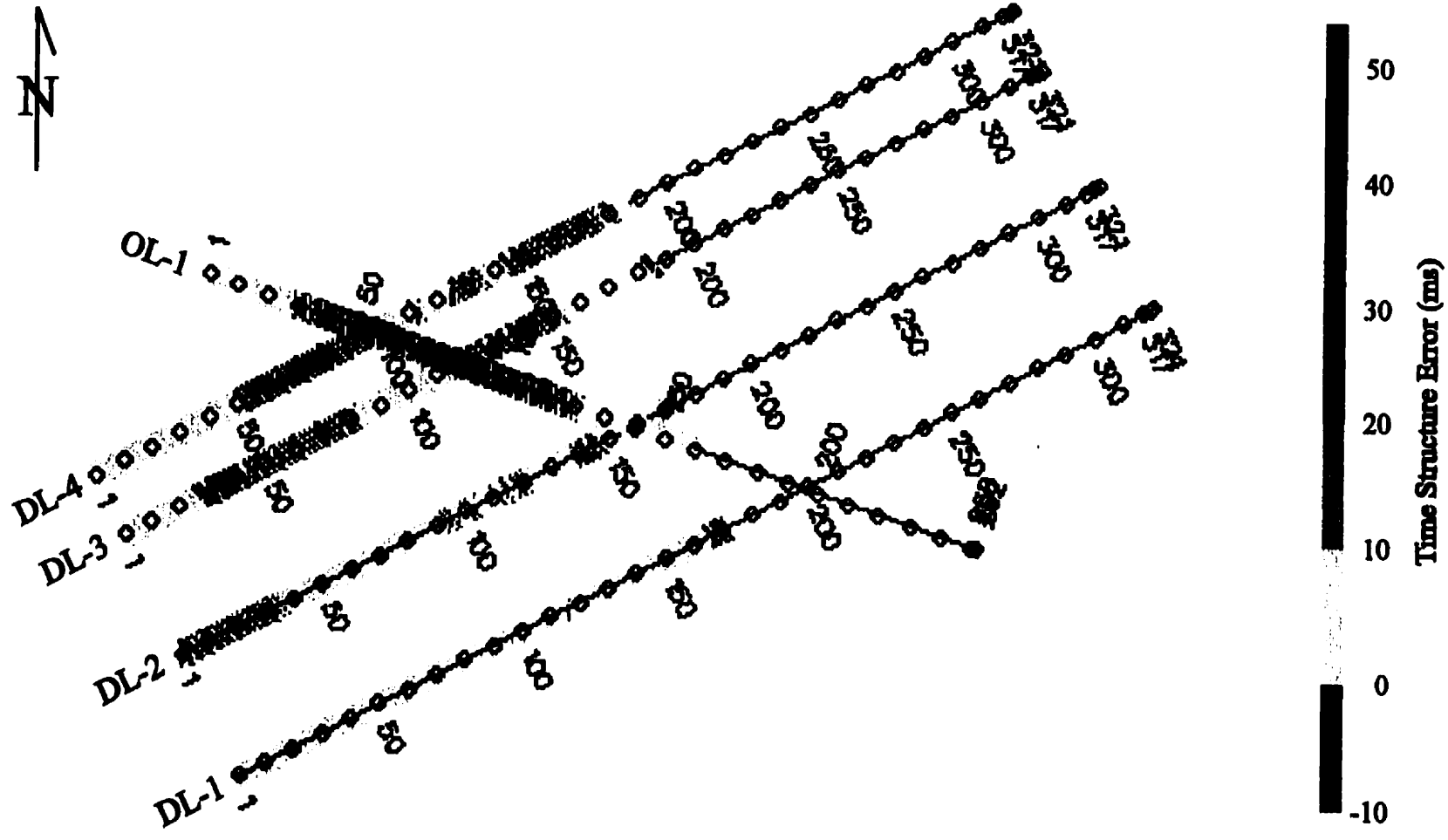

Figure 4.23. Map showing time structure error between the 2-D and 3-D ray-tracing results on all lines for the Top Mississippian horizon in the hangingwall of the structure. Errors for all lines shown at the same scale. CDP numbers plotted along each line for reference.

Reflection point maps for all 2-D seismic lines in this experiment illustrate the source of out-of-plane reflections. These reflections originate from up to 1000 m from the line-of-section for line DL-3. It is informative to consider the significance of this out-of-plane contribution to the seismic section with respect to the Fresnel zone for these data. The Fresnel zone is the area from which reflected energy will return to the receivers with phases differing by no more than half a cycle, and will therefore interfere constructively. The Fresnel zone is normally reported as a radius (R_F), and calculated as follows:

$$R_F = (V/2)(t/\nu)^{1/2},$$

where V is the average velocity, t the arrival time, and ν the frequency. If the average velocity in the Mesozoic section is 4000 m/s, the central frequency of the recorded data is 40 Hz, and the maximum traveltime to the Top Mississippian horizon is 1.5 s, then the Fresnel zone has a maximum radius of approximately 400 m for this horizon. The departure of a reflection point from the line of section can be described in terms of the Fresnel zone. For the Top Mississippian horizon in the hangingwall of the structure in this experiment reflection points originate up to approximately 3 Fresnel zones from the line-of-section. The out-of-plane contributions to line DL-1 (Figure 4.9) lie within the Fresnel zone, originating up to 400 m from the line-of-section. Proper migration should collapse the Fresnel zone to zero, however this is only strictly valid for 3-D migration. The 2-D time migration of the data in this study will only collapses the Fresnel zone in the plane of the section, so it remains an important consideration for out-of-plane reflections.

CHAPTER 5: DISCUSSION AND CONCLUSIONS

5.1 Discussion of results

Thrust sheets of Mississippian strata in Wildcat Hills, interpreted using 3-D seismic data, create a structure that varies along strike in response to changes in thrust fault displacement. Displacement is transferred, via a common basal detachment, between the two thrust faults interpreted in this area. One fault extends over the entire survey area and displaces the Top Mississippian marker up to 1000 m. The second, lower thrust fault initiates in the middle of the survey area and gains displacement (up to 1100 m) toward the northwest, as displacement on the upper fault decreases rapidly to 300 m at the northwest edge of the survey area. Together, the two faults define a thrust system that displays a near-linear increase in total displacement across the survey area. The hangingwall of the thrust structure created by these two thrust faults dips 20 - 25° toward the southwest, and has an overall structural plunge of approximately 5° toward the southeast.

A 3-D numerical depth model, created using horizons interpreted from the 3-D seismic volume facilitated analysis of out-of-plane imaging on 2-D seismic data. The numerical depth model used two horizons (Top Mississippian and Near Basement) to describe the subsurface structural geometry, and employed a simple interval velocity model for depth conversion and ray tracing. Five 2-D seismic lines over this model (four dip lines and one oblique line) illustrate the effects of out-of-plane imaging on synthetic seismic data. The analysis of out-of-plane imaging presented in this thesis focuses on

time structure errors on the Mississippian horizon in the hangingwall of the structure. Time structure errors are quantified by calculating the difference between horizons interpreted on migrated sections from the 2-D and 3-D ray-tracing results for the same line. These errors, calculated for the Top Mississippian horizon in the hangingwall of the structure, range from 0 - 50 ms (up to 100 m depth error at 4000 m/s). The dip lines provide a relatively accurate representation of time structure below the line of section, with errors only locally exceeding 10 ms (20 m depth error at 4000 m/s). Time structure errors on the dip lines are caused by local short-wavelength (1-2 km), low amplitude (up to 50 m) structural variations on the Top Mississippian reflector. Although the time structure error on these dip lines generally increases toward the northwest, a relationship to broad changes in structural geometry toward the northwest is not clear. An oblique line (45° from dip direction) displays time structure errors greater than 10 ms over most of the line, ranging up to 50 ms (up to 100 m depth error at 4000 m/s). Out-of-plane reflections for this line are controlled principally by the broad geometry of the structure, which has a cross-line dip of approximately 15°. Time structure error on the oblique line increases toward the southwest-dipping hangingwall of the structure, then decreases as the structure becomes shallower. The short-wavelength, low-amplitude structural variations that controlled the error in the dip lines are a secondary control on out-of-plane reflections in the oblique line.

Time structure errors observed on the dip lines in this study would not severely affect structural interpretation of the Top Mississippian horizon in the hangingwall of this structure. An increase in time structure error on the oblique line suggests that seismic data acquired oblique to the structural trend must be interpreted with caution. Out-of-

plane reflections are common in all seismic sections presented in this thesis. Reflections from the Mississippian horizon in the hangingwall of the structure originate up to 1000 m (approximately 3 Fresnel radii) from the line, and only occasionally originate from directly below the line.

5.2 Conclusions

- Structural interpretation of 3-D seismic data from the Wildcat Hills area of the southern Alberta foothills delineated a thrust structure that varies along strike because of displacement transfer between two thrust faults repeating Mississippian strata.
- 3-D ray-tracing results suggest that 2-D dip lines are adequate for delineation of the hangingwall for this gently southeast-plunging structure. short-wavelength structural variations in the hangingwall are largely responsible for the observed average time-structure errors of 5-10 ms (10 to 20 m depth error at 4000 m/s).
- Synthetic 2-D seismic data acquired oblique (45°) to the regional structural trend illustrates the sensitivity of 2-D seismic data to cross-line dip (the apparent dip of the structure perpendicular to the line-of-section). Time-structure errors for the hangingwall of the structure (up to 50 ms, or 100 m depth error at 4000 m/s) relate principally to the broad geometry of the structure, with secondary effects related to short-wavelength structural variations on the Top Mississippian horizon.
- 3-D ray-tracing results illustrate that out-of-plane reflections are common on 2-D seismic sections over this structure, but that the impact of this out-of-plane imaging (up to 1000 m from the line of section) does not severely affect the delineation of the target structure using dip lines.

5.3 Recommendations for Future Work

Improvement of the numerical depth model (geometry and interval velocities), especially in the Mesozoic interval, would allow the creation of more realistic synthetic seismic data. Improved structural definition would likely result from reprocessing the Wildcat Hills 3-D seismic data volume using 3-D depth migration and focusing on improving the structural image in the Mesozoic section. Delineation of structures in the Mesozoic interval would improve velocity model control, and allow an extension of displacement analysis work to include these structures. The depth migration would also allow construction of the numerical depth model directly from interpreted horizons and avoid errors related to depth conversion. Detailed displacement analysis using available 3-D seismic data control will provide insight into the development of the fold and thrust structures not possible using 2-D seismic data control.

REFERENCES

Bally, A.W., Gordy, P.L., and Stewart, G.A., 1966, Structure, seismic data and orogenic evolution of southern Canadian Rockies: Bulletin of Canadian Petroleum Geology, 14, 337-381.

Dahlstrom, C.A., 1970, Structural geology in the eastern margin of the Canadian Rocky Mountains: Bulletin of Canadian Petroleum Geology, 18, 332-406.

Ellis, M.A., and Dunlap, W.J., 1988, Displacement variation along thrust faults: implications for the development of large faults: Journal of Structural Geology, 10, 183-192.

Fagin, S.W., 1991a, Defining a salt sill using three-dimensional ray-trace modeling and inversion: in S.W. Fagin ed., Seismic modeling of geologic structures - applications to exploration problems: Geophysical Development Series, 2, Hoover, G.M., ed., Society of Exploration Geophysicists, Tulsa, 209-248.

Fagin, S.W., 1991b, Seismic modeling of geologic structures - applications to exploration problems: Geophysical Development Series, 2, Hoover, G.M., ed., Society of Exploration Geophysicists, Tulsa, 348p.

French, W.S., 1974, Two-dimensional and three-dimensional migration of model-experiment reflection profiles: Geophysics, 39, 265-277.

Houck, R.T., House-Finch, N.J., Carpenter, D.G., and Johnson, M.L., 1996, Mapping 3-D structure using 2-D seismic: The Leading Edge, August 1996, 894-903.

Johansen, S.E., Kibsgaard, S., Andresen, A., Henningsen, T., and Granli, J.R., 1994, Seismic modeling of a strongly emergent thrust front, West Spitsbergen Fold Belt, Svalbard: American Association of Petroleum Geologists Bulletin, 78, 1018-1027.

Lawton, D.C., Sukaramongkol, C., and Spratt, D.A., 1996, Seismic characterization of a "compound tectonic wedge" beneath the Rocky Mountain foreland basin, Alberta: Bulletin of Canadian Petroleum Geology, 44, 258-268.

Lawton, D.C., Spratt, D.A., and Hopkins, J.C., 1994, Tectonic wedging beneath the Rocky Mountain foreland basin, Alberta Canada: Geology, 22, 519-522.

Lingrey, S., 1991, Seismic modeling of an imbricate thrust structure from the foothills of the Canadian Rocky Mountains: in S.W. Fagin ed., Seismic modeling of geologic structures - applications to exploration problems: Geophysical Development Series, 2, Hoover, G.M., ed., Society of Exploration Geophysicists, Tulsa, 111-125.

Lebel, D., Langenberg, W., and Mountjoy, E.W., 1996, Structure of the central Canadian Cordilleran thrust-and-fold belt, Athabasca-Brazeau area, Alberta: a large, complex intercutaneous wedge: Bulletin of Canadian Petroleum Geology, 44, 282-298.

Liu, S., and Dixon, J.M., 1991, Centrifuge modeling of thrust faulting: structural variation along strike in fold-thrust belts: Tectonophysics, 188, 39-62.

Liu, S., Lawton, D.C., and Spratt, D.A., 1996, Three-dimensional geometry of the structural front between Berland River and Smoky River, central Alberta foothills: Bulletin of Canadian Petroleum Geology, 44, 299-312.

MacKay, P.A., 1991, A geometric, kinematic and dynamic analysis of the structural geology at Turner Valley, Alberta: Unpublished PhD. thesis, University of Calgary.

MacKay, P.A., 1996, The Highwood Structure: a tectonic wedge at the foreland edge of the southern Canadian Cordillera: Bulletin of Canadian Petroleum Geology, 44, 215-232.

May, B.T., and Hron, F., 1978, Synthetic seismic sections of typical petroleum traps: Geophysics, 43, 1119-1147.

Monger, J.W.H., Price, R.A., and Tempelman-Kluit, D.J., 1982, Tectonic accretion and the origin of the two major metamorphic and plutonic welts in the Canadian Cordillera: Geology, 10, 70-75.

Morse, P.F., Purnell, G.W., and Medwedeff, D.A., 1991, Seismic modeling of fault-related folds: in S.W. Fagin ed., Seismic modeling of geologic structures - applications to exploration problems: Geophysical Development Series, 2, Hoover, G.M., ed., Society of Exploration Geophysicists, Tulsa, 127-152.

Nicol, A., Watterson, J., Walsh, J.J., and Childs, C., 1996, The shapes, major axis orientations and displacement patterns of fault surfaces: Journal of Structural Geology, 18, 235-248.

Ollerenshaw, N.C., 1975, Geological compilation map, Rocky Mountain foothills and front ranges, Calgary region, 1:250,000: in H.J. H.J. Evers and J.E. Thorpe eds., Geology of the foothills between Savanna Creek and Panther River, southwestern Alberta, Canada, guidebook: Canadian Society of Petroleum Geologists and Canadian Society of Exploration Geophysicists, 64p.

Price, R.A., 1986, The southern Canadian Cordillera: Thrust faulting, tectonic wedging, and delamination of the lithosphere: Journal of Structural Geology, 8, 239-254.

Rudolph, K.W., and Greenlee, S.M., 1991, Seismic modeling of a pinnacle reef: An example from the Williston Basin: in S.W. Fagin ed., Seismic modeling of geologic structures - applications to exploration problems: Geophysical Development Series, 2, Hoover, G.M., ed., Society of Exploration Geophysicists, Tulsa, 197-208.

Sanderson, D.A., and Spratt, D.A., 1992, Triangle zone and displacement transfer structures in the eastern front ranges, southern Canadian Rocky Mountains: The American Association of Petroleum Geologists Bulletin, 76, 828-839.

Skeen, R.C., and Ray, R.R., 1983, Seismic models and interpretation of the Casper Arch Thrust: Application to Rocky Mountain Foreland structure: in J.D. Lowell ed., Rocky Mountain foreland basins and uplifts: Rocky Mountain Association of Geologists, Denver, 99-124.

Skuce, A.G., 1996, Frontal Foothills structures in central Alberta: the thin end of the intercutaneous wedge?: Bulletin of Canadian Petroleum Geology, 44, 153-164.

Slotboom, R.T., Lawton, D.C., and Spratt, D.A., 1996, Seismic interpretation of the triangle zone at Jumpingpound, Alberta: Bulletin of Canadian Petroleum Geology, 44, 233-243.

Soule, G.S., and Spratt, D.A., 1996, En echelon geometry and two-dimensional model of the triangle zone, Grease Creek Syncline area, Alberta: Bulletin of Canadian Petroleum Geology, 44, 244-257.

Spratt, D.A., Lawton, D.C., and MacKay, P.A., 1993, The triangle zone and Turner Valley structure west of Calgary: Geological Association of Canada, Mineralogical Association of Canada, Joint Annual Meeting 1993, Field Trip A-1 Guidebook, 41 p.

Stockmal, G.S., MacKay, P.A., Lawton, D.C., and Spratt, D.A., 1996, The Oldman River triangle zone: a complicated tectonic wedge delineated by new structural mapping and seismic interpretation: Bulletin of Canadian Petroleum Geology, 44, 202-214.

Zimmerman, L.J., 1991, Modeling the seismic response of geologic structures with physical models: in S.W. Fagin ed., Seismic modeling of geologic structures - applications to exploration problems: Geophysical Development Series, 2, Hoover, G.M., ed., Society of Exploration Geophysicists, Tulsa, 189-195.

TEST TARGET (QA-3)

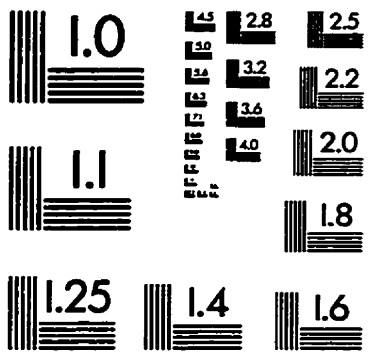

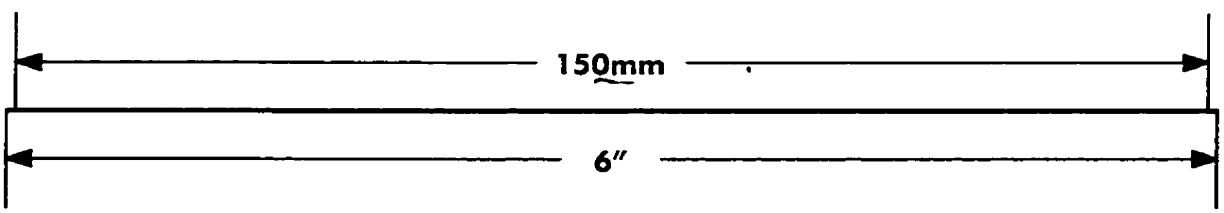

APPLIED IMAGE, Inc
1653 East Main Street
Rochester, NY 14609 USA
Phone: 716/482-0300
Fax: 716/288-5989